Intelligent Vehicle Drive Mode to Ameliorate the Engine Operating Conditions

by

Srikanth Kolachalama

A dissertation submitted in partial fulfillment
of the requirements for the degree of
Doctor of Philosophy
(Electrical and Computer Engineering)
at the University of Michigan – Dearborn
2023

Doctoral Committee:

Professor Hafiz Malik, Chair
Lecturer Randy Gene Boone
Lecturer Azeem Hafeez
Karthik Reddy Vemireddy, FKA GmbH
Hariharan Venkitachalam, IVECO group
Professor Weidong Xiang

Srikanth Kolachalama

skola@umich.edu

ORCID iD: 0000-0003-4428-6170

Dedication

To my daughter and parents

Advika “Parvathi” Kolachalama

Shyam Prasad Kolachalama

Acknowledgements

The last four years of working toward my doctoral degree have been a great experience, and I would like to thank all the people who have contributed to it. To begin with, the seeds of my research potential were sowed by Prof. Dr. Mukul Shukla and Prof. Dr. Madhava Krishna, who allowed me to work as a research intern at Motilal Nehru National Institute of Technology (MNNIT) - India and International Institute of Information Technology (IIIT) - India. After my bachelor's, I received an opportunity to undertake my master's at Rheinisch-Westfälische Technische Hochschule (RWTH) Aachen University, Germany, well known as the "Massachusetts Institute of Technology (MIT)" of Europe. My mentors, Dr. Ing Romie Augustino, Dr. Ing Sebastian Flock, and Prof. Dr. Ing Georg Jacobs, provided an eclectic ambiance that inculcated the natural good feel of pragmatic research and motivated me to enhance my efficacy in research. After graduating with my master's from RWTH Aachen, I entered the USA to work as an engineering consultant for the automotive original equipment manufacturers and suppliers in the field of driver assistance systems. After I began my work in 2017 at General Motors Inc., I encountered excellent benefits offered by the organization to support employees pursuing graduate studies. I immediately revived my plans of performing research and received an opportunity at the University of Michigan under the mentorship of Prof. Dr. Hafiz Malik, funded by William J. Clifford (Director) and Matt Schroeder (Executive Director) at General Motors Inc. My role as a Systems Engineer at General Motors Inc. had provided many insights regarding many features and functionalities of the automotive system. I was trained by Rajeev Ranjan, Engineering General Manager, and Tanzima Mushtarin, Lead Engineer, at General Motors Inc., and I appreciate their

understanding and assistance to pursue the graduate program in conjunction with my responsibilities as a Systems Engineer. I always enjoyed discussing eclectic ideas with my technical specialist Curtis L. Hay and received excellent feedback on my enthusiasm.

I had received substantial experience in real-time testing of vehicle systems at General Motors Inc., which triggered the core idea of feature development for my doctoral dissertation. To execute the proof of concept, I received all the approvals from William J. Clifford (Director) to retrieve vehicle data from Cadillac test vehicle segments. All the computational models developed in this thesis were validated by real-time datasets and I am overwhelmed by the assistance provided by Iqbal Surti (Systems Engineer) and Michael Mati (Vehicle Services Engineer) in real-time testing. I would like to thank my advisor Prof. Hafiz Malik, for his patience, excellent guidance, and support throughout the period. His compassion and perception toward working students are commendable and pursuing a graduate program under his supervision is the obvious choice for many employees. All the conversations I had during my studies were very productive, and I planned every element of my dissertation step-by-step, categorizing all the modules of my research. My committee Dr. Hariharan, Karthik Reddy, Dr. Weidong, Dr Randy, and Dr. Hafeez played a vital role in the sensitive phases of the thesis proposal by providing feedback and assisted me to shape up the scope of my work. I greatly appreciate the assistance provided by Geoffrey Hosker and Joel Seewald in proofreading my publications and shaping up my dissertation as per regulations. I would like to specially thank my spouse Ms. Annapurna Kuppa, for her support to pursue the challenge of doctoral studies in parallel with a full-time position and by taking care of an infant. Last and most importantly, I would like to thank my family and friends for their affection and continuous support throughout my career. It is to them that I dedicate this thesis.

Table of Contents

List of Tables

List of Figures

List of Equations

List of Appendices

Appendix

List of Abbreviations

ACC	Adaptive cruise control
ACCSSP	Adaptive cruise control set speed profile (MPH)
ACS	Air conditioning system
Area	Area under the curve
AVS	Allowable vehicle speeds (MPH)
AVC	Allowable vehicle cabin air temperatures (°F)
AWD	All-wheel drive mode
CAT	Cabin air temperature (°F)
CATOP	Cabin air temperature operating point
CATSP	Cabin air temperature set profile (°F)
DBV	Driver behavior vector
DL	Deep learning
EAT	External air temperature (°F)
ED	Euclidean distance—Ideal and predicted EOP
EOC	Engine operating conditions
EOP	Engine operating point
EOT	Engine oil temperature (°F)
ESC	Engine speed caliber

ETC	Engine torque caliber
FOD	First order derivative
GPS	Global positioning system
HVAC	Heating ventilation and air conditioning system
IAS	Initial ACC speed (MPH)
IBAQ	Instantaneous battery charge (Q)
IBAT	Instantaneous battery temperature (°F)
ICE	Internal combustion engines
ICAT	Initial cabin air temperature (°F)
IEE	Instantaneous engine efficiency (n_e)
IEM	Instantaneous engine map
IES	Instantaneous engine speed (rad.s^{-1})
IET	Instantaneous engine torque (Nm)
IFCR	Instantaneous fuel consumption rate (1E-8m^3s^{-1})
IINT	Instantaneous inverter temperature (°F)
IMOF	Instantaneous motor frequency (Hz)
IMOT	Instantaneous motor torque (Nm)
IMOP	Instantaneous motor power (kw)
IROT	Instantaneous rotor temperature (°F)
ISOT	Instantaneous stator temperature (°F)
ISB	Ideal steering behavior
IVDM	Intelligent Vehicle Drive Mode

LAT	Lateral acceleration (m.s^{-2})
LM	Levenberg-Marquardt backpropagation
LOT	Longitudinal acceleration (m.s^{-2})
LSTM	Long short-term memory
MPH	Miles per hour
NARX	Nonlinear Autoregressive network with exogenous inputs
RMSE	Root mean square error
RRC	Radius of road curvature (m)
SMV	Smoothness measure vector
SL	Speed limit (MPH)
SNR	Signal-to-noise ratio
SSE	Sum of squares error
TP	Tire pressure (kPa)
VEP	Vehicle engine performance
VLV	Vehicle-level vectors
YAR	Yaw rate (rad.s^{-1})

List of SI Units

°F	Fahrenheit
Hz	Hertz
kPa	Kilopascals (1000 N.m^{-2})
Kg	Kilogram
kg.m^{-3}	Kilogram per meter cube
Km	Kilometers
kWh	Kilowatt-hour
MJ	Million Joules
m	Meters
m^2	Meter square
m^3s^{-1}	Meter cube per second (volume rate flow)
m.s^{-2}	Meters per second square
ms	Milliseconds
Nm	Newton meter
N.m^{-2}	Newton meter square
PSI	Pounds per square inch
rad	Radians
rad.s^{-1}	Radians per second

s	Seconds
T_k	Time step
dT	Incremental time step (~10 ms or ~ 10m)

Abstract

The introduction of automobiles into the world inculcated innovation in many aspects of engineering, including design and manufacturing. Engineers worldwide continuously strive hard to develop cutting-edge technologies to augment the riders' comfort, optimize traffic behavior, enhance safety and reduce fuel consumption. In the current scenario, advanced features, which include forward collision, traction control, adaptive cruise control, and lane change, augment safety. Along with these features, vehicle drive modes play a dual role of enhancing safety (e.g., traction control drive mode) and reducing energy consumption (e.g., fuel economy drive mode) in real-time. But a feature that ameliorates engine performance and optimizes the trip time was not investigated by the researchers until now. In this dissertation, a novel drive mode, "Intelligent Vehicle Drive Mode" (IVDM), was proposed, which augments the vehicle engine performance (VEP) in real time.

In the current vehicle system, more than twenty drive modes are integrated that augment the safety and driver comfort, but none intervenes in the driver behavior vector (DBV). In this research, IVDM predicts the DBV, which optimizes the engine operating conditions (EOC). The metric of optimal EOC was defined using the vector engine operating point (EOP) and heating, ventilation, and air conditioning (HVAC) system. Deep learning (DL) models were developed by mapping the vehicle-level vectors (VLV) with EOP and HVAC parameters using real-time datasets obtained from the field tests performed using the Cadillac segment provided by General Motors Inc. The trained functions were utilized to predict the future states of DBV, reflecting augmented vehicle engine performance (VEP). An iterative analysis was performed by empirically estimating the

future states of VLV in the allowable range of DBV and was fed into the DL model to predict the performance vectors. The defined vehicle engine performance (VEP) metric was applied to the predicted vectors, and thus optimal DBV is the instantaneous output of the IVDM. Finally, the proposed concept was quantified by analyzing the instantaneous engine efficiency (IEE) and the smoothness measure of the instantaneous engine map (IEM).

Impact Statement: Real-time vehicle engine performance (VEP) is significantly affected by environmental conditions, HVAC systems, and the driver behavior vector (DBV). In this research, the featured vehicle drive mode that is integrated into the automotive system was the focus and can accommodate the user's input of either activation or deactivation. Vehicle drive modes were developed to augment the rider's comfort and safety and to reduce fuel consumption but not to intervene with the DBV, which is strictly the user's prerogative.

The proposed "Intelligent Vehicle Drive Mode" (IVDM) is embedded with the functionality of obliging the driver's command in all scenarios and predicting the driver behavior vector (DBV) to enhance the vehicle engine performance (VEP) without increasing the time of trip traversal. The IVDM accommodates two user inputs [range of speeds, range of cabin temperatures] which is utilized to predict the optimal DBV. Also, IVDM can be activated as a stand-alone application or in conjunction with any other drive modes, accommodating a vehicle speed > 25 MPH on a regular terrain profile under normal driving conditions. The IVDM, which possesses the unique capability of optimizing the [fuel consumption, trip time], could emerge as a new feature of the automotive system and is most applicable to vehicles with built-in advanced driver assistance, infotainment, and connectivity features.

Chapter 1 Introduction

1.1. Background — Automotive Features

The first commercial automobile developed by Karl Benz in 1886 consists of less than a hundred components and not more than ten features [1], whereas the advancement of vehicle technology in the year 2022 had reached the extent of integrating more than five thousand components supported by a hundred features [2]. All the features developed in the automotive system either enhance the efficiency of the vehicle (e.g., fuel economy drive mode, continuously variable transmissions) or augment the human driving experience (e.g., HVAC), which includes safety (e.g., adaptive cruise control (ACC), lane keep assist (LKA), and auto braking) [3].

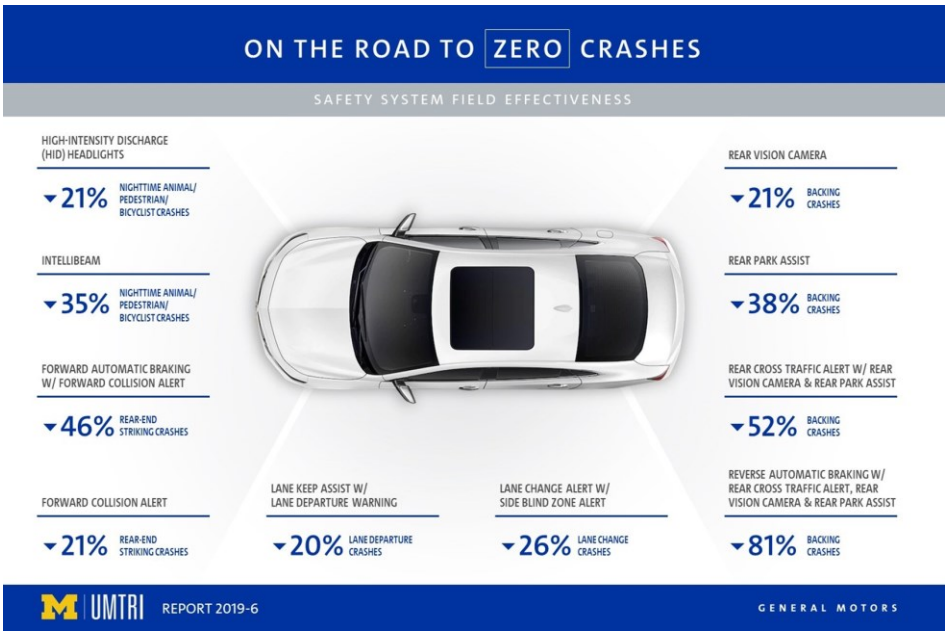

Figure 1: Feature safety statistics — Advanced driver assistance systems. [Source: General Motors Inc. and University of Michigan]

The advanced driver assistance systems (ADAS) integrated with vehicles have produced substantial positive results in reducing crashes, based on the recent study conducted in collaboration with the University of Michigan and General Motors Inc., which manifests the importance of these features, as shown in Figure 1.

1.2. Automotive Feature Types

The functionality of every feature is integrated into the system and is generally categorized into three aspects based on the type of user intervention and functionality.

1.2.1. No User Intervention

The first type would include features that function automatically without driver influence, e.g., automatic transmission, crankshaft, and spark ignition timing. Engineers have developed and integrated the functionalities of these elements into the automotive system.

1.2.2. Limited User Intervention

In the second category, the features are activated and deactivated upon the driver's command. The user interface (Figure 2) is provided by the system to the driver to trigger the features, e.g., driver assistance systems and vehicle drive modes [4]. Although the user triggers these features in the vehicle, the functionality, and the magnitudes of the parameters in real time are automated, e.g., the acceleration produced by the traction control, dynamics of drive modes, lateral dynamic control of the lane centering, and forward collision and auto braking while encountering a host in the proximity [5].

1.2.3. Bounded User Intervention

This feature is an extended version of limited user intervention with an additional degree of freedom to define the magnitudes of the parameters with boundary conditions. The simplest example includes the HVAC, where the user has the choice to activate the climate control and to

set cabin air temperature, e.g., CAT = [60 90] °F. A similar case would include activating the adaptive cruise control (ACC) feature and user-defined adaptive cruise control set speed profile (ACCSSP), e.g., [25 85] miles per hour (MPH).

Figure 2: 2021 Cadillac Escalade — User interface. [Source: General Motors Inc.]

Among these features, only a few functionalities were developed to enhance the driving behavior, of which the most popular one is the vehicle drive mode. All the integrated drive modes correspond to feature type 2, "Limited user intervention" (1.2.2), and in the current scope of this dissertation, all the concepts developed were focused on developing a new feature (drive mode) for the automotive system. To begin with, the following section 1.3 elaborates on the existent drive modes integrated into the vehicle system, and the scope of the dissertation is proposed in Section 1.4.

Vehicle Drive Mode	Functionality
All-wheel drive	The All-wheel drive mode provides torque to all four axles and assists traction control, suitable for snow driving. [Goodarzi and Esmailzadeh, 2007]
Baja	The Baja mode is activated explicitly during vehicle traversal over desert sand and can accommodate deflated tires to obtain more turnover stability.

	[Sharma et al., 2015]
Crab	The crab mode is activated for rear-steer vehicles to accommodate lateral shifts for speeds under < 25 MPH. [Cariou et al., 2008]
Custom	The custom mode is limited to the vehicles equipped to sense the terrain (e.g. Cadillac (V) and Corvette (Z)) and allow the user to input the desired behavior.
Economy/DFM/ AFM	The fuel economy mode is driven by controlled or reduced acceleration and deactivates the ignition for one or more cylinders to reduce the fuel consumption.
Fleet	The fleet mode is equipped with infotainment and connectivity features applicable to autonomous, connected vehicles. [Baldacci et al., 2008]
Hill descent	This mode is activated automatically when the vehicle encounters a downslope of more than 4% and provides controlled deceleration while traversing sudden slopes. [Paul et al., 2016]
Hold	The hold mode is more applicable to hybrid and electric vehicles (e.g., Chevy Volt), which retains the battery's state. This feature assists the vehicle to use the battery power optimally, especially when the battery charge is at a higher limit. [Chau C.K. et al., 2016]
Mountain	Mountain mode is similar to the hill descent mode, which provides stability and controlled acceleration on the contrast while climbing uphill (Slope > 14%). [Paul et al., 2016]
Off-road	The off-road mode is commonly used for rugged navigation, resulting in poor surface contact and low traction. [Taghavifar and Mardani, 2017]
Personal	The personal drive mode integrated into the vehicle system allows the driver to set the maximum allowable speed and teen driver limitations [Davis, 2019]
Power	The power mode produces higher torque by accommodating necessary changes in real-time, including reducing the ride height [Zhang and Mi, 2011]
Shuttle	Shuttle mode is most applicable to the transit vehicles used for delivery [Chen et al., 2019]
Snow/ Ice	This mode is activated in real-time to provide intelligent traction control for slippery roads and augments the safety of the vehicle system.
Sport	The sport mode provides higher torque and throttle response, robust suspension, and stiffer steering, which provides additional stability. [Melman et al., 2021]
Stealth	The stealth mode activation is not advisable for inexperienced and low confidence drivers. This mode reduces the level of interior illumination to assist night driving. [Zou et al., 2012]
Terrain/Crawl	The terrain mode is activated for uneven surfaces to improve traction and stability and to control vehicle traverse. [Taghavifar and Mardani, 2017]
Tour/Normal	The touring mode is activated under normal driving conditions, which can function with All-wheel drive and fuel economy modes to optimize the vehicle performance. [Lairenlakpam et al., 2018].
Tow/Haul	Haul mode is a customer choice used for logistical purposes for traversing

	heavy goods and towing. [Gao et al., 2015]
Track	The track mode is developed for circuits and tracks with known geometry, providing a more aggressive transmission shift pattern than the sport mode. [Onder and Geering, 1995]
Trailer	This mode is activated when a trailer is attached to the vehicle to control the entire system's longitudinal and lateral dynamics [Hac et al., 2008].

Table 1: Vehicle drive modes—Integrated vehicle system

1.3 Background—Vehicle Drive Modes

More than twenty drive modes that allow the user to activate them in real time have been installed in the latest vehicles in the current technological advances, shown in Table 1. The personal drive mode integrated into the vehicle system allows the driver to set the maximum allowable speed and teen driver limitations [6]. In contrast, the custom mode is limited to vehicles activated for specific terrains, e.g., mountain regions (Cadillac (V) and corvette (Z)). The touring mode is activated under normal driving conditions, functioning with all-wheel drive mode (AWD) [7] and fuel economy modes [8]. The AWD mode provides the torque to all four axles, suitable for snow driving, and the fuel economy mode is driven by controlled acceleration and cancels the ignition for one or more cylinders to save fuel. Also, to provide controlled traction, hill descent, snow, and mountain modes are available for the user to activate while traversing sudden slopes and uphill and slippery roads [9].

Three modes, namely power, sport, and track, are embedded into the vehicle to encourage racing enthusiasts [10]. When triggered, the sport mode provides higher torque and throttle response, robust suspension, and stiffer steering, whereas the power mode produces higher torque by accommodating necessary changes, including reducing the ride height [11]. Also, the track mode has been developed for circuits and tracks with known geometry, which provides a more

aggressive shift pattern of the transmission compared with sport mode. In these three modes, fuel efficiency is achieved by setting the threshold for the engine over speed [12].

(A) (B)

Figure 3: 2022 Electric Hummer: Drive mode — (A) Crab mode; (B) Baja mode

A challenge to vehicle navigation is driving on uneven terrain, for which the off-road, terrain/crawl, and Baja drive modes have been developed to assist the user's safety [13] (Figure 3). The off-road mode is commonly used for navigation of rugged terrain that results in poor surface contact and low traction. The surfaces could consist of any type of earthly materials like water, stones, and mud. In contrast, the terrain mode is activated for uneven surfaces to improve traction, stability and control. The Baja mode is activated explicitly during the vehicle's traversal over desert sand and can also accommodate deflated tires for obtaining more turnover stability [14]. Other miscellaneous drive modes include fleet mode, applicable to connected vehicles [15]; shuttle mode for delivery vehicles [16]; crab mode, activated for rear-steer vehicles to accommodate lateral shift [17]; haul mode while towing [18]; and trailer mode when a trailer is attached to the vehicle [19].

1.4 Dissertation Statement and Scope — IVDM

It is known from the existing literature that the driver behavior vector (DBV) holds more than a 30% share in affecting engine operating conditions (EOC) [20]. The existing drive modes do not

influence the DBV [speed, longitudinal acceleration (LOT), lateral acceleration (LAT), yaw rate (YAR), cabin air temperature (CAT)], which is the user's prerogative. Also, the functionality of these drive modes is embedded into the car, and the driver has limited control of activation or deactivation. Therefore, none of the drive modes augments the overall vehicle engine performance (VEP) and intervenes with the driver behavior vector (DBV).

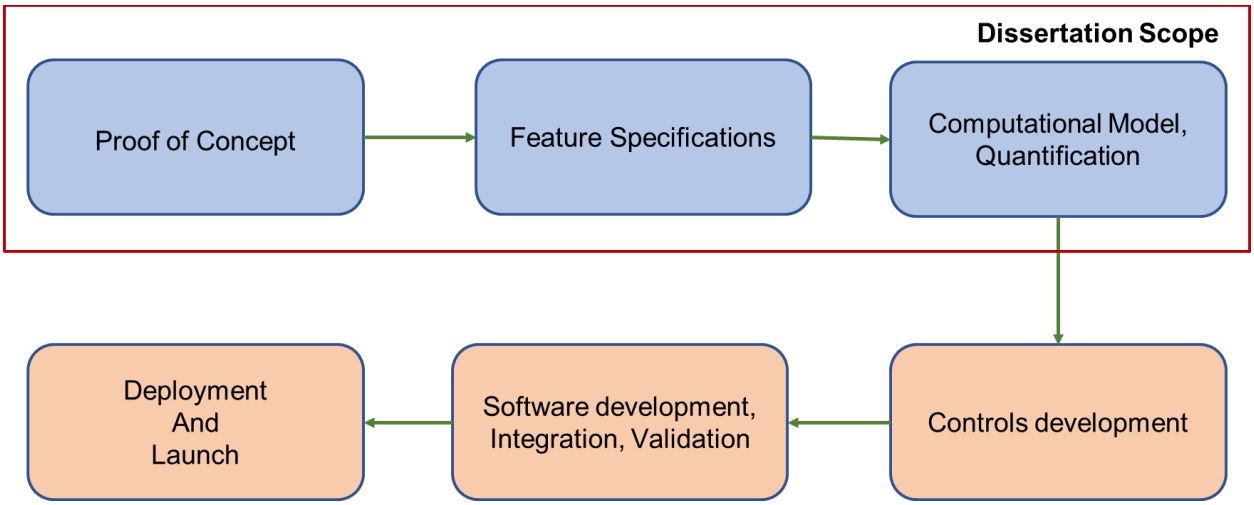

Figure 4: Dissertation scope and map — IVDM

Hence, in this dissertation, a multi-parametric optimization problem is addressed, and a novel "**Intelligent Vehicle Drive Mode**" is proposed for development. The IVDM predicts the driver behavior vector (DBV) for future time steps in real time by obliging the user's command to augment the vehicle engine performance (VEP). This new drive mode corresponds to the type 3 feature "**Bounded user intervention**" (1.2.3), resulting in optimal engine and HVAC operating conditions (e.g., lower [IFCR, Trip time, ACRFP], higher [IET, IES], optimal [EST]). In this dissertation, the scope of the research is limited to the development of the computational model and quantifying the concept with real-time test data (Figure 4).

1.5 Dissertation Outline

In this research, a computational model of the Intelligent Vehicle Drive Mode (IVDM) and its quantification is proposed. The current strategy aims to

- **Identify the functionality of the existing drive modes**. The integrated drive modes and their effect on driver behavior were investigated in the research. The latest General Motors Inc. Cadillac vehicle segment was considered in the analysis. The categorization was performed based on the effect on lateral and longitudinal dynamics along with interaction with multiple terrains.
- **Propose the core feature requirements of IVDM:** Feature development is a multistage process consisting of well-established protocols, in which defining the feature system requirements is the primary step. The requirements will define the parametric constraints and limitations to deploy the functionality effectively.
- **Identify the modeling parameters of IVDM:** The proposed concept of IVDM enhances the engine operating conditions for future time steps in real time and optimizes the lateral dynamics for low curvatures. Hence the relevant vehicle parameters to achieve the task were identified, and their real-time behavior was analyzed using experimental procedures adopting automotive industry protocols.
- **Develop the optimization criteria:** The Intelligent Vehicle Drive Mode (IVDM) was developed to ameliorate the engine operating conditions (EOC) and identify the real-time analytical methods corresponding to enhanced efficacy.
- **Develop the algorithm for resolving simultaneous equations:** The defined optimization criteria for EOC are not applicable for low curvatures. Hence, the concept of ISB was

utilized to develop the mathematical model relating the [Speed, radius of road curvature (RRC)].

- **Identify the optimal predictive model apt for the vehicle data.** The retrieved data were analyzed, and the optimally performing model needs to be identified among the many machine learning methods.
- **Develop the extended validation of the predictive model.** The efficacy of the developed deep learning (DL) model needs to be validated with the datasets of multiple vehicle lines to corroborate the prediction of the driver behavior vector (DBV).
- **Develop a fail-safe methodology algorithm.** In any real-time computational model, a fail-safe algorithm would enhance the safety of the system performance. Hence the predicted results of the driver behavior vector (DBV) in the defined range were evinced with the developed fail-safe algorithm.
- **Develop the test cases and validation model.** Validation and preparation of the applicable test cases are the final aspects of any research to conclude the implemented procedure. The novel feature was validated by selecting snippets of the real-time data and comparing the performance criteria for the two scenarios of predicted and constant driver behavior vector (DBV).
- **Develop the quantification model:** The performance vectors were estimated for the predicted and constant DBV and are quantified using a new approach by estimating the IEE and smoothness measure of IEM.

1.6 Dissertation Map

The entire dissertation is categorized into nine chapters detailing the procedures and assumptions adopted, as shown below.

Chapter 2 "Intelligent Vehicle Drive Mode." In this chapter, the basic functionality of the IVDM is discussed with relevant assumptions. The feature specifications of IVDM in the sense of system engineering perspective were defined along with the scope. Estimating the DBV by categorizing the road segments was discussed for two cases: Low curvatures at (1) Speeds = [15 25] MPH) and (2) Speeds > 25 MPH.

Chapter 3 "Modeling parameters." The IVDM predicts the DBV by optimizing the engine operating conditions. The parameters applicable to model the IVDM concept were identified in this chapter. The vehicle modeling parameters are categorized into three vectors [VLV, EOP, CATOP] for this project, and a real-time data retrieval procedure was adopted to develop the datasets applicable to predictive modeling. The experimental setup, path planning of test vehicles, utilizing the hardware and software to interface with the test vehicle, and methodology to retrieve selective data among the many recorded parameters applicable to the current research were discussed in this chapter.

Chapter 4 "Vehicle Engine Performance—Criteria." The criteria of optimal vehicle performance applicable to the modeling parameters of IVDM were defined in this chapter. The criteria includes the concepts of ideal steering behavior (ISB), engine operating point (EOP), HVAC, and smoothness measure vector (SMV).

Chapter 5 "Estimation of Speed for Low Curvatures." It is known from the existing literature that the effect of engine performance on low speeds is insignificant. Hence, the concept of ideal steering behavior (ISB) defined in Chapter 4 was applied to estimate the optimal speed for low

curvatures in the range [15 25] MPH. The non-linear simultaneous equations were solved using the known boundary values of the steering behavior vector (SBV) derived from the test cases. This chapter outlines the convex optimization and basic polynomial interpolation techniques used to estimate the desired speed.

Chapter 6 "Deep Learning Modeling." DL concepts have penetrated every aspect of engineering for the past decade, and multiple models have been developed to analyze the data. The current research focuses on supervised learning as the data retrieved is time-sensitive and readily available by real-time tests, as discussed in Chapter 4. However, identifying the apt predictive model for the vehicle data is required; hence, in this chapter, two deep learning (DL) models were developed using [NARX, LSTM] mapping [VLV, EOP, CATOP], and their performance was compared using standard statistical techniques.

Chapter 7 "Prediction of Driver Behavior Vector." In this chapter, the core concept of the proposed IVDM was developed computationally. The developed deep learning (DL) model (Chapter 6) was utilized to predict the future states of the engine performance parameters. This chapter applies vehicle engine performance (VEP) criteria to the predicted elements to estimate the optimal driver behavior vector (DBV) for future time steps.

Chapter 8 "Results and Quantification." The performance of predicted and constant driver behavior vector (DBV) is compared in this chapter by analyzing the resulting vehicle engine performance (VEP) criteria for two scenarios. An additional validation step is conducted to estimate the instantaneous engine efficiency (IEE) and smoothness measure vector (SMV) of the instantaneous engine map (IEM) to confirm the efficacy of the proposed approach.

Chapter 9 "Discussion." The performance analysis of the predicted and constant DBV was discussed categorically for each parameter, and for every test case, the explanation is provided in this Chapter to highlight the enhanced engine operating conditions (EOC) by IVDM.

Chapter 10 "Conclusion." All the steps implemented in this research were briefly outlined in this chapter, beginning with the functionality of Intelligent Vehicle Drive Mode (IVDM). This work utilizes many engineering concepts of automotive systems and data analytics. The methods and results were discussed in conjunction with the enhanced engine operating conditions (EOC) due to IVDM.

Chapter 11 "Future work." The proposed IVDM is novel and has not been integrated into automotive systems. However, the current dissertation is limited to developing a computational model for internal combustion engine (ICE)-driven vehicles with appropriate assumptions. Therefore, the final chapter of this dissertation discusses the ideas of potentially extending this research to pragmatically deploy the IVDM in real-time vehicles by overcoming the assumptions and its application to electric vehicle systems.

Chapter 2 Intelligent Vehicle Drive Mode

The core functionality of the Intelligent Vehicle Drive Mode (IVDM) is to predict the driver behavior vector (DBV) in real-time, reflecting optimal vehicle engine performance (VEP). The DBV is categorized into three main elements whose magnitudes are the user's choice: speeding behavior [Speed, longitudinal acceleration (LOT)], steering behavior [lateral acceleration (LAT), yaw rate (YAR)], and cabin air temperature (CAT), as shown in Figure 5. In this chapter, the feature requirements of IVDM were discussed.

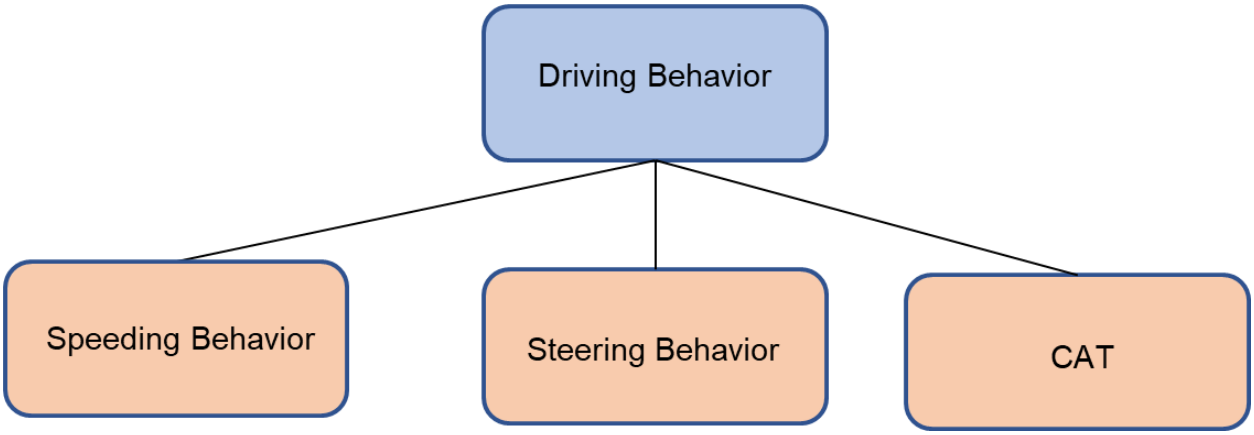

Figure 5: Driver behavior vector — IVDM

2.1 Properties of Intelligent Vehicle Drive Mode

- Intelligent Vehicle Drive Mode (IVDM) can be triggered as a stand-alone application or with any integrated drive mode.

- IVDM is not applicable to the scenarios with Speeds limits < 15 miles per hour (MPH), which include parking lots, critical zones, or traffic congestion. The critical zones include construction, accidents, or school areas.
- IVDM is not applicable to the arterial road segments with the speed limit zone of [15 25] MPH where the variation of engine operating point is insignificant and estimating the DBV for this scenario is not the scope of this dissertation.
- IVDM is applicable to the road segments with radius of road curvatures (RRC) = [8.34 42.57] m and with the range of allowable speeds [15 25] MPH.
- IVDM applies to Speeds > 25 MPH as per the categorization of road segments [connecting roads, state ways, freeways] discussed in the Table 25.
- IVDM is most applicable to any vehicle with built-in advanced driver assistance systems (ADAS) and advanced infotainment and connectivity (AICON) features (e.g., General Motors Inc. Cadillac vehicles with super and ultra-cruise features).
- IVDM estimates the direct correlation between [Speed, RRC] for low curvatures utilizing the concept of ideal steering behavior (ISB) defined in Section 4.
- IVDM activates the adaptive cruise control (ACC) feature for Speeds > 25 MPH to provide controlled longitudinal acceleration (LOT) and augmented safety to the vehicle.
- IVDM predicts [adaptive cruise control set speed profile (ACCSSP), cabin air temperature set profile (CATSP)] by optimizing [engine operating point (EOP), cabin air temperature operating point (CATOP)] and estimates [lateral acceleration (LAT), yaw rate (YAR)] by assuming ideal steering behavior (ISB). The details of optimal [EOP, CATOP] and ISB are discussed in Chapter 4.

- Finally, IVDM predicts the driver behavior vector (DBV) in real time to augment vehicle engine performance (VEP). The default time and range of predicting [ACCSSP, CATSP] = [10s, 1000 m] and details of [allowable vehicle speeds (AVS), allowable vehicle cabin air temperatures (AVC)], are discussed in Chapter 6.

2.2 Speeding Behavior

The proposed functionality states that Intelligent Vehicle Drive Mode (IVDM) activates the adaptive cruise control (ACC) feature in real-time; thus, the ACC controller automatically estimates the parameter longitudinal acceleration (LOT) based on the adaptive cruise control set speed profile (ACCSSP). Among the many features integrated into the vehicle, the ACC system developed by reference [21] plays a vital role in affecting safety and vehicle performance. The intricate concept of adaptive cruise control (ACC) is to produce controlled acceleration without disengaging the cruise control when encountering a host vehicle in the user-defined proximity and strictly following the user command of set speed [22]. Also, it is easy to conclude from the existing literature [23] that activation of ACC results in augmented vehicle engine performance (VEP) and can be done for any speed > 25 miles per hour (MPH). Thus, activating ACC is the core functionality of Intelligent Vehicle Drive Mode (IVDM), and predicting the optimal adaptive cruise control set speed profile (ACCSSP) based on the dynamic state of the vehicle and type of road segment is discussed in the following sections [24].

The road segments of either parking lots, low curvatures, or arterial roads have a speed limit (SL) = [15 25] MPH. The effect of engine performance at these speeds is insignificant, but for low-curvature segments, the concept of ideal steering behavior (ISB) was adopted to estimate the optimal speed for a definite radius of road curvature (RRC) = [8.34 42.57] m. The detailed analysis and mathematical models developed are described in Chapter 5.

2.3 Steering Behavior

The steering behavior consists of two elements, lateral acceleration (LAT) and yaw rate (YAR), and in real-time, these values are dependent on the radius of road curvature (RRC) obtained from the GPS coordinates and infotainment maps. To achieve optimal lateral dynamics, the authors of reference [25] extended the concept of estimating the driver behavior by introducing the concept of ideal steering behavior (ISB) in addition to hard braking and acceleration [26]. The ISB correlates the empirical parameter vehicle curvature ($\underline{AB} = R_{vt}$) and RRC ($\underline{AC} = R_{At}$), as shown in Figure 6. Therefore, the minimal curvature difference ($\underline{BC} = R_{dt}$) corresponds to ISB, and the relevant mathematical models in terms of the steering parameters [lateral acceleration (LAT), yaw rate (YAR), radius of road curvature (RRC)] models are defined in Chapter 4. Hence, Intelligent Vehicle Drive Mode (IVDM) would incorporate ISB, and the guidelines established by the US transportation authority to estimate the lateral acceleration (LAT) and yaw rate (YAR) for definite radius of road curvature (RRC) [27].

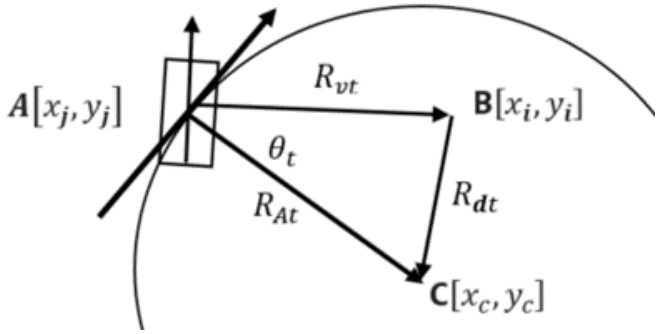

Figure 6: Driver behaviour vector — Steering behavior

2.4 Cabin Air Temperature

In an internal combustion engine (ICE) vehicle, the thermal energy produced by the fuel combustion is exchanged between the ambience, engine components, HVAC, lubrication oil, and

coolant [28]. Among the many integrated features of the vehicle, the HVAC is the only system that maintains the cabin air temperature (CAT). The set CAT inputted by the user, is maintained by extracting heat from the engine surface (EST) and transferring thermal energy to the Air conditioning system (ACRFP). The environmental conditions (EAT) also play a vital role in establishing thermal equilibrium between the four elements [Cabin, Engine, HVAC, Environment], as shown in Figure 7. The red colored connecting elements represent the heat exchange from higher to lower temperatures, while the blue connections represent the cooling of the component. Hence, Intelligent Vehicle Drive Mode (IVDM) proposes a model that can generate an optimal cabin air temperature set profile (CATSP), potentially augmenting the HVAC and engine performance, whose criteria are defined in Chapter 4 [29].

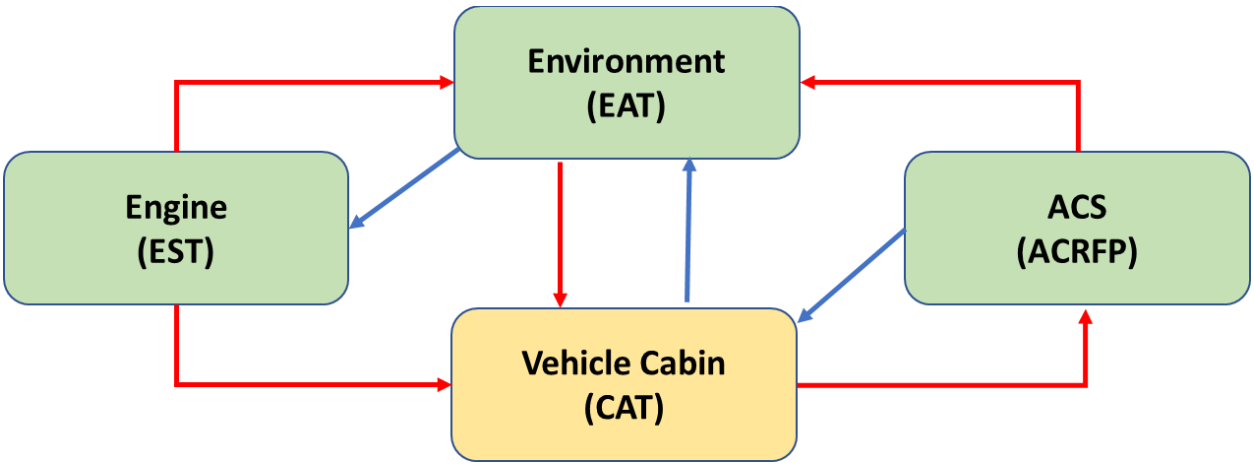

Figure 7: Heat exchange: Vehicle interactive elements—Combustion engine

Chapter 3 Intelligent Vehicle Drive Mode—Modeling Parameters

The feature specifications discussed in Chapter 2.1 state that the functionality of IVDM is applicable for two scenarios, (1) estimating the speed for low curvatures, which enhances the lateral dynamics, and (2) predicting the [Speed, CAT] by optimizing the engine operating conditions and HVAC parameters. In this chapter the applicable parameters of IVDM required for developing the mathematical and predictive models were identified, which are the intrinsic part of the optimization criteria (discussed in Chapter 4).

3.1 Vehicle-Level Vectors—VLV

The vehicle-level vectors (VLV) include three components, namely, body module, driver behavior, and environmental factors. The body module vector is embedded with the age of the vehicle [time step, odometer], tire pressure, Euler angles [Pitch, Roll], shape of the vehicle [aerodynamic drag], and load [trailer, passengers]. The tire pressure (TP) and external load affect the normal and traction forces exerted on the wheels, affecting the engine power requirement [30]. The body design influences aerodynamic resistance and, thereby, instantaneous fuel consumption rate (IFCR) [31]. Odometer value reflects the engine's age, and the driver behavior vector (DBV) consists of the elements discussed in Chapter 2 [Speed, longitudinal acceleration (LOT), lateral acceleration (LAT), yaw rate (YAR), cabin air temperature (CAT)]. The environmental factors consist of interactive vehicle elements in real time while traversing any terrain, including external air temperature (EAT), radius of road curvature (RRC), and gradient. The EAT (°F) influences the engine's thermal stress [32], whereas the terrain data (curvature and gradient) obtained from the

inbuilt infotainment maps and GPS coordinates affect the vehicle dynamics. Also, the gradient is proportional to the vehicle's Euler angles; hence, there is no loss of generality in considering pitch, roll, and yaw angles as inputs replacing the gradient [33]. The parameters steering angle, humidity (HUM—%rh), absolute wind velocity vector (WIND - $[W_x + W_y]$ m.s^{-1}) and atmospheric pressure (ATP—N.m^{-2}) were not included in this research as the variation of these parameters on engine operating conditions was observed to be insignificant. The real-time analysis was performed under normal driving conditions assuming no slip, i.e., the traction force generated at the wheels is proportional to the normal forces [34]. Thus, vehicle slip, and variation of rolling friction coefficient data are not applicable in this research.

3.2 Engine Operating Point—EOP

In an internal combustion engine (ICE)-driven vehicle, the only external input is the air-fuel mixture ignited to produce downward thrust onto the piston surface. The flame impingement produces engine torque and is transmitted to the engine components, which results in engine speed. It is a well-established industrial methodology to represent the engine's performance with the three parameters of instantaneous engine torque (IET), instantaneous engine speed (IES), and instantaneous fuel consumption rate (IFCR) projected as engine operating point (EOP) on the engine map generated for every vehicle [35]. Thus, optimal EOP was considered as the parameter representing the vehicle engine performance (VEP—Chapter 4).

3.3 HVAC Parameters—CATOP

In the existing literature, cabin thermal comfort was maintained by optimizing the air conditioning system (ACS), applying lower fuel or power consumption constraints. However, the experimental results show that the percentage of fuel saved per trip by adopting this procedure is < 1%. Hence, in this dissertation, two parameters [EST (°F), ACRFP (PSI)] that reflect HVAC performance are

identified, deviating from the traditional concept of optimizing fuel economy. The EST is maintained in a specific range by transferring heat to four main elements—engine oil, cabin, coolant, and external ambience—to maintain the optimal thermal stress on the engine components. The ACS is affected by multiple parameters, including ACRFP, compressor load, and energy consumed. However, variations of load and energy consumed are insignificant due to minor changes in cabin air temperature (CAT) (°F). Therefore, by analyzing the real-time testing data (Chapter 3.6), the ACRFP showed substantial variations based on changes in EAT (°F) and CAT (°F). Thus, in this dissertation, the vectors [EST, ACRFP] were empirically defined as cabin air temperature operating point (CATOP) representing the HVAC performance [29].

3.4 Data Retrieval

To understand the properties of the defined vectors [VLV, EOP, CATOP], it is necessary to retrieve the applicable data. In general, the data can be retrieved using two standard approaches: (1) generating synthetic data using software tools and (2) performing real-time experiments by traversing the test vehicle on predefined paths.

3.4.1 Synthetic Data Generation

It is a known industrial practice to test the developed algorithms by generating synthetic data using data analytic tools. The main two main advantages of adopting this procedure are (l) less time consuming, where the required data sets can be generated instantly with known properties, and (2) less expensive, as it requires only basic tools to implement without any copy right constraints. But it is impossible to recreate the real-time scenario of [terrain, environment, dynamic state of the vehicle] in a virtual simulation. Hence the best methodology to retrieve the data is to adopt real-time testing (approach 2).

3.4.2 Real-time Data Generation

To develop the concept of IVDM, the real-time vehicle data were retrieved by applying the principles of vehicle data architecture. To begin with, this research was performed by obtaining all the required approvals to utilize the Cadillac test vehicle segment provided by General Motors Inc. The details of the experimental procedure and test cases developed are discussed in the following Chapters 3.5 and 3.6.

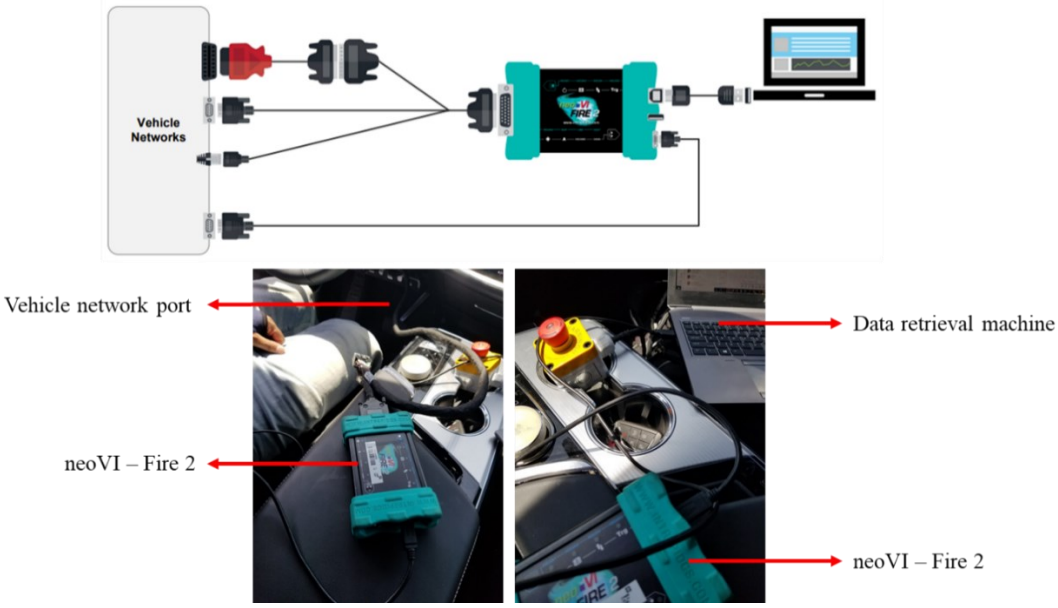

Figure 8: Hardware hookup diagram: neoVI — FIRE 2
[Source: Intrepid CS and General Motors Inc.]

3.5 Experimental Setup—Data Retrieval

A two-step procedure was employed to retrieve the data from the vehicle controller area network (CAN) bus [36]. The hardware neoVI - FIRE 2 was directly connected to the test vehicle (Figure 8), and the data retrieval was performed using the software Vehicle Spy (Figure 9). The software tool Vehicle Spy developed by Intrepid CS records data in real time [35] and allows the user to selectively retrieve the signal data required for analysis (Figure 9). The data retrieval was done by selecting a frequency of 10Hz for the elements vehicle-level vectors (VLV) and engine operating

point (EOP). The snippets of HVAC parameters were collected at a frequency of 10m (odometer reading), as CAN bus would require at least 300ms to record variations CAT (°F) during the steady state.

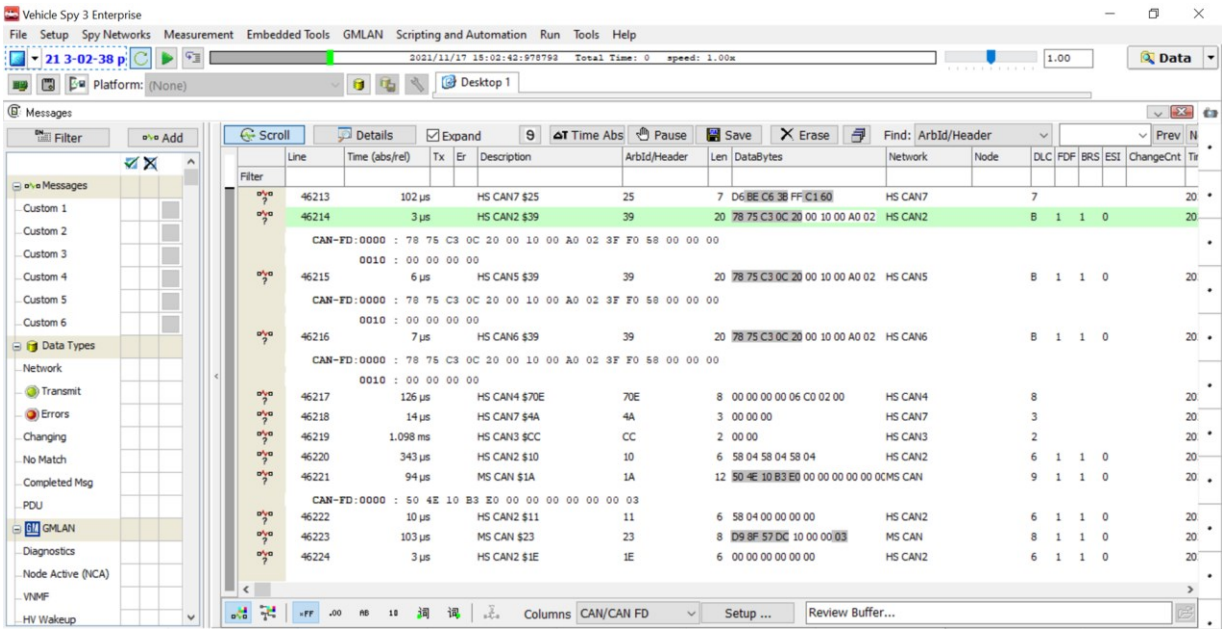

Figure 9: CAN data retrieval—Vehicle Spy graphical user interface
[Source: Intrepid CS and General Motors Inc.]

3.6 Real-time Testing

The test cases were developed for two scenarios, namely, (1) driving the vehicle on a constant curvature (Speed = [15 25] MPH, RRC = 18.4m) by multiple drivers and (2) by activating the adaptive cruise control (ACC) feature with the set speed in the range [25 75] miles per hour (MPH), targeting all the road segments shown in Table 25 and Figure 10. The test vehicle 2019 Cadillac Escalade was driven on a constant curvature (RRC = 18.4m) to retrieve the data for case (1), and details are discussed in Chapter 5.3. The second test (Speeds > 25 MPH) was conducted utilizing five vehicles, a 2020 Cadillac CT5, 2019 Cadillac XT6, 2021 Cadillac CT4, 2021 Cadillac Escalade ESV, and 2021 Cadillac Escalade AWD. The test cases were developed by driving the

vehicle under two external air temperature scenarios—EAT > 65 °F and EAT < 45 °F—and the properties of the data sets are shown in Tables 18–24.

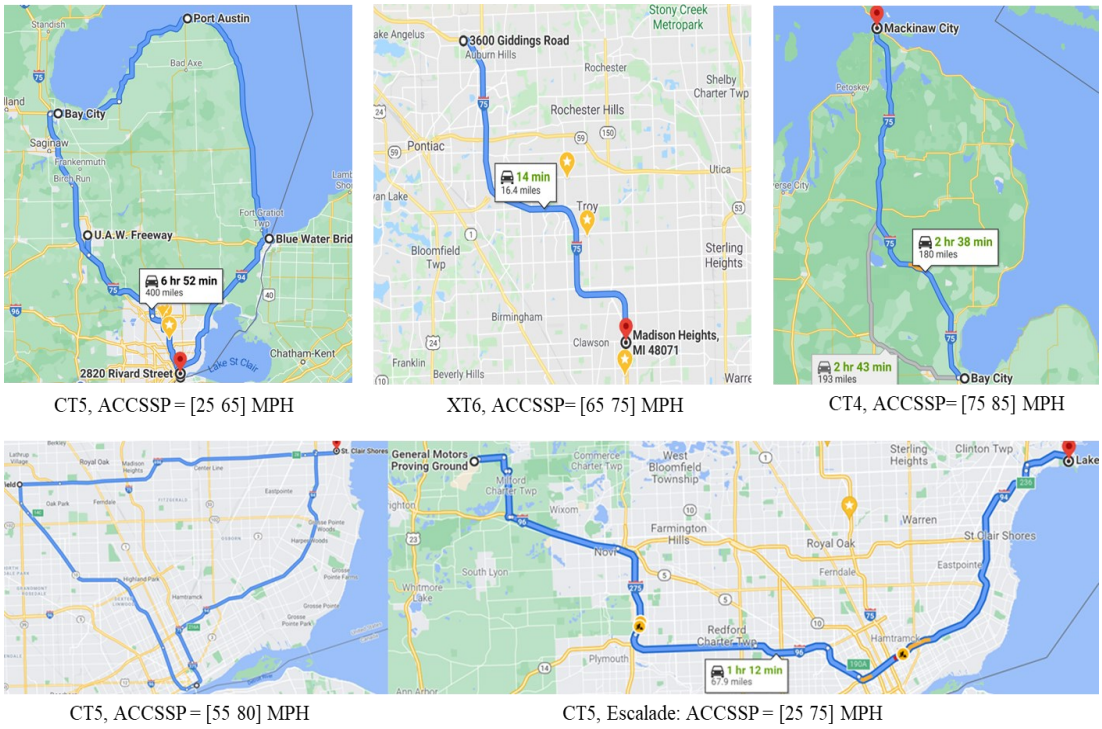

CT5, ACCSSP = [25 65] MPH

XT6, ACCSSP= [65 75] MPH

CT4, ACCSSP= [75 85] MPH

CT5, ACCSSP = [55 80] MPH

CT5, Escalade: ACCSSP = [25 75] MPH

Figure 10: Path traversed—Michigan, USA [Source: Google Maps]

Chapter 4 Engine Operating Conditions—Optimization Criteria

The engine operating conditions (EOC) are primarily defined by three main elements of the system: reliability, durability, and energy efficiency. In this dissertation, energy efficiency, which is enhanced with optimal engine and HVAC operating conditions, is focused on. The concept of ideal steering behavior (ISB) and constraints for optimal [engine operating point (EOP), cabin air temperature operating point (CATOP)] were defined in the following sections, reflecting augmented vehicle engine performance (VEP).

4.1 Ideal Steering Behavior

It is known from the existing literature that the effect of steering on engine performance is insignificant. As discussed in Chapter 2.3 the parameters [LAT (L_a), YAR (Y_a)] are an integral part of the driver behavior vector (DBV), and the concept of ISB was used to estimate these values. Extending the model developed by reference [25], equations (1) and (2) were defined, including all steering behavior parameters [V_s, L_a, Y_a, RRC] reflecting ISB. Resolving the simultaneous equations (quadratic and linear), it was observed that, [L_a, Y_a] = [0, 0] for high $RRC \sim \infty$, and it is easy to see that LOF (~ 0) has an infinite set of solutions that satisfy the constraint $RRC.Y_a^2 = L_a$. Hence, the parameters [LAT, YAR] can be estimated for definite RRC if the speed value (V_s) is known, and the detailed analysis is presented in Chapter 5-6 [27].

$$2RRC = \frac{V_s^2}{L_a} + \frac{V_s}{Y_a},\ V_s = \frac{-L_a + \sqrt{L_a^2 + 8RRC.L_a.Y_a^2}}{2.Y_a} \quad (1)$$

$$LOF = min\ [abs(Y_a.V_s - L_a)] \quad (2)$$

4.2 Euclidean Distance—Ideal EOP

In this research the metric for engine's capability was defined by three parameters, [engine torque caliber (ETC), engine speed caliber (ESC), Euclidean distance (ED)], directly related to vehicle engine performance (VEP). These parameters represent the torque produced per unit of fuel consumption [ETC], speed produced per unit torque [ESC], and the Euclidean distance [ED] of the operating engine operating point (EOP) from the ideal EOP under normal driving conditions [24]. Vehicles traversing arterial road segments with speed limits ranging [25 45] MPH have an operating EOP closer to the ideal EOP (lower ED), as shown in the engine map (Figure 11A). An engine map is a traditionally accepted convolute graph in the industry, plotted with operating EOPs calibrated at the manufacturing plant. The coordinate with the lowest instantaneous fuel consumption rate (IFCR) is assumed to be the ideal EOP, and the line segment conjoining the operating and ideal EOP is empirically defined as the engine performance vector. In Sections 5 and 6, the predictive model of [EOP, ACCSSP] is discussed, and Figure 11B is the pictorial representation of the instantaneous engine map (IEM), categorizing two ACCSSP profiles (predicted and constant). The magnitude of the engine performance vector represents the Euclidean distance (ED) (3), and instantaneous engine speed (IES) is ignored in estimating the Euclidean distance (ED), as higher IES is desired to reduce the trip time [Kolachalama and Malik, 2021].

$$\text{ED} = \sqrt{(IET_i - IET_k)^2 + (IFCR_i - IFCR_k)^2} \tag{3}$$

$$\text{ETC} = \frac{IET}{IFCR} \tag{4}$$

$$\text{ESC} = \frac{IES}{IET} \tag{5}$$

The vehicle speeds for freeways range [65 85] MPH, which correspond to higher IES and fluctuating [IET, IFCR], depending on the dynamic state of the vehicle. Also, the state ways with speed limit (SL) in the range [45 65] MPH are considered the green zone (low IFCR). Hence, the

generic criteria for augmented engine operating conditions (EOC) would be lower [ED, IFCR] and higher [IET, IES, ETC, ESC].

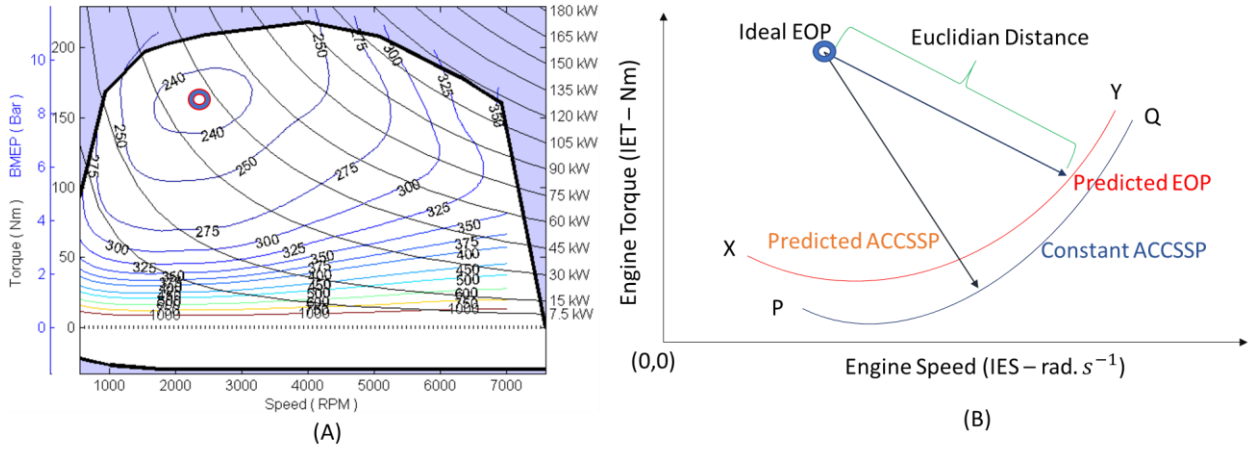

Figure 11: VEP Vector — (A) Engine Map: 2007 Toyota Camry 2.4L I4; (B) IEM

[Source: Ricardo baseline standard car engine: Tier 2 fuel. EPA ALPHA vehicle simulations. Version: June 20, 2016]. The engine map for the 2007 Toyota Camry 2.4L I4, who's ideal EOP = [170 Nm, 2400 RPM, 230 g/kwhr], is shown in Figure 11A. The conversion to SI units was performed assuming the fuel is gasoline [Calorific Value (C_v), Density (ρ_f)] = [45 MJ.Kg^{-1}, 750 Kg.m^{-3}], and thus the ideal EOP = [170 Nm, 251.33 rad.s^{-1}, 159 1E-8 $m^3 s^{-1}$]. A 2020 Cadillac CT5 test vehicle was utilized in the current research (Chapter 6), who's ideal EOP was assumed to be [250 Nm, 140 rad.s^{-1}, 180 1E-8 $m^3 s^{-1}$].

4.3 HVAC Criteria—CATOP

In this research, the parameters [EST (°F), ACRFP (PSI)] were defined as cabin air temperature operating point (CATOP). The optimal thermal stress on the engine components and engine oil viscosity result when EST (EST_i) = 194 °F [Borman and Nishiwaki, 1987]. The retrieved data shown in Tables 18–24 depict that the recorded EST ranges [165 220] °F. Also, the engine oil temperature (EOT) has a range of [192 196] °F, which is maintained by the coolant to maintain

the required viscosity. Hence, there is no loss of generality in assuming ideal engine surface temperature EST (EST_i) = 194 °F as the optimization criteria. The empirical parameters [A1, A2], shown in equations (6) and (7), represent the conformance between the operating EST (EST_o) and ideal EST (EST_i). Hence, minimum values of [A1, A2] are desired for optimal HVAC.

$$A1 = (EST_o - EST_i) \ , \ if \ EST_o > EST_i = 194 \ °F. \quad (6)$$

$$A2 = (EST_i - EST_o) \ , \ if \ EST_o \leq EST_i = 194 \ °F. \quad (7)$$

The refrigerant integrated into the air conditioning system (ACS) system of the General Motors Inc. Cadillac vehicle is assumed to be R134a, and augmented functionality of ACS was achieved by limiting the maximum value of operating ACRFP ($ACRFP_o$). The upper boundary limits of ACRFP ($ACRFP_h$) are defined in Table 27 in correlation with the EAT (°F), and the intermittent boundary values of ACRFP for EAT = [65 110] °F were estimated by basic linear interpolation.

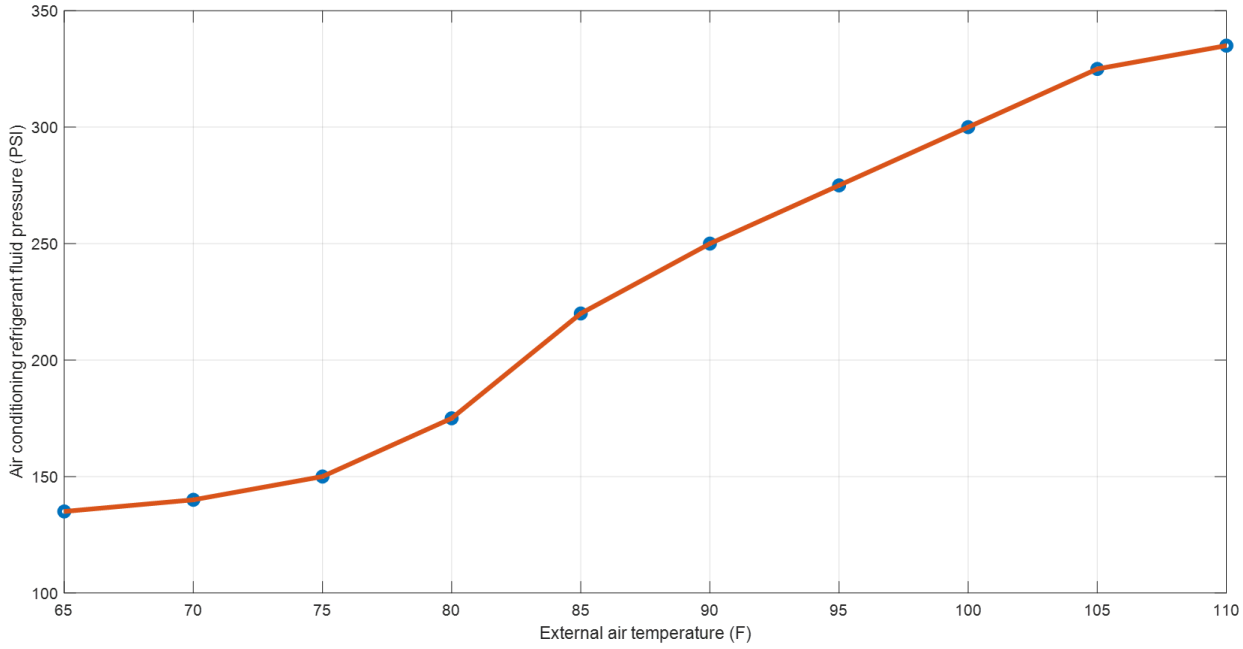

Figure 12: Linear interpolation: R134 ACS refrigerant — [EAT, ACRFP].

Therefore, minimum B defined in equations (8) and (9) was considered the optimal HVAC criterion corresponding to ACRFP [Kolachalama and Malik, 2021]. Thus, B is always non-negative when EAT ≥ 65 °F, but when EAT < 65 °F, the parameter B is not significant in our analysis [29].

$$B = (ACRFP_o - ACRFP_h), if\ ACRFP_o > ACRFP_h \text{ (PSI)} \quad (8)$$

$$B = 0, if\ ACRFP_o \leq ACRFP_h \text{ or EAT} < 65\ °F \quad (9)$$

4.4 Smoothness Measure Vector

The combustion of fuel and the flame impingement phenomena in the engine produces torque with fluctuating magnitudes. Engineers developed multiple techniques to minimize the torque fluctuations by introducing the flywheel and generator [38] and optimizing the spark ignition timing and camshaft mechanism [39]. The parameter instantaneous engine speed (IES) follows a smooth curve, whereas instantaneous fuel consumption rate (IFCR) and instantaneous engine torque (IET) have oscillating behavior. Therefore, the smoothness measure vector (SMV) of the parameters [engine operating point (EOP), cabin air temperature operating point (CATOP)] and [Euclidean distance (ED), engine torque caliber (ETC), engine speed caliber (ESC)] was considered in our analysis, and the vehicle engine performance (VEP) criteria are shown in Table 28 [Kolachalama and Malik, 2021]. The smoothness measure vector (SMV) was estimated using the built-in toolboxes of MATLAB, and the spline function was utilized to fit the data points [24] [29]. The SMV was defined using the traditional statistical techniques R^2/Adjusted R^2 and SSE/RMSE, represented by equation (10).

$$\text{SMV} = [R^2, \text{Adjusted } R^2, \text{SSE, RMSE}] \quad (10)$$

$R^2$is a statistical measure of how close the data are to the fitted regression line, whereas Adjusted R^2 is a modified version of R^2 adjusted for the number of predictors in the model, which is always

lower than R^2. The mathematical model below derives the expression of the technique R^2/Adjusted R^2. Assuming that the marked value is y_i and the fitted value is f_i, the mean value is derived by equation (11); thus, the sum of squares of residuals (SS_{res}) and the total sum of squares (SS_{tot}) are estimated by equations (12) and (13). Therefore, R^2/Adjusted R^2 is determined by equations (14) and (15) for the sample size and explanatory variable size [n, p].

$$\underline{y} = \frac{\sum_{i=1}^{n} y_i}{n} \tag{11}$$

$$SS_{tot} = \sum_{i=1}^{n} (y_i - \underline{y})^2 \tag{12}$$

$$SS_{res} = \sum_{i=1}^{n} (y_i - f_i)^2 \tag{13}$$

$$R^2 = 1 - \frac{SS_{res}}{SS_{tot}} \tag{14}$$

$$Adjusted\ R^2 = 1 - (1 - R^2)\ \frac{n-1}{n-p-1} \tag{15}$$

Sum of squares error (SSE) is the residual sum of squares of the conformance between the predicted and fitted curves, and the square root of the mean SSE represents RMSE. Higher values of R^2/Adjusted R^2 and lower SSE/RMSE are considered a good fit for the curve [24] [29]. R^2/Adjusted R^2 values range between [0 1], representing the percentage of match, whereas SSE/RMSE have the same units of the parameters, as shown in equation (16).

$$RMSE = \sqrt{\frac{SS_{res}}{n}} \tag{16}$$

Chapter 5 Estimation of Vehicle Speed: Low Curvatures

Vehicle speed is the primary factor that influences the automotive system's safe traversal for low curvatures. [Chen et. al and Chowdhury et.al] have developed many techniques to estimate the optimal speed [40] and speed range [41] for traversing such curvatures. These values are estimated by considering the factors of steering behavior [42] and terrain data [43]. [Merrit et. al and Bonneson et.al] describe the technique to estimate the maximum safe speed using the ball bank indicator method, which has been traditionally accepted in the automotive industry for a century. In this method, an empirical relationship is developed between curvature speed and the deflection of the indicator device. [Bonneson et. al and Carlson et.al] challenge the existing ball bank indicator method by estimating the speed using curvature information provided by the GPS/compass. [Carlson et.al] correlates the results between the ball bank indicator and accelerometer methods for multiple curvatures. In contrast, [Lusetti et.al, Glaser et.al, and Wang et.al] proposed a methodology to estimate the safe speed by including radius of road curvature (RRC), friction factor (f), and elevation coefficient (e).

The guidelines established by the US transportation authority recommend the range of speed for a definite radius of road curvature (RRC) [52]. In this dissertation, a challenging problem was addressed that estimates a unique speed for a definite radius of road curvature (RRC). Also, it is interesting to investigate a mathematical model connecting all the steering parameters to generate a unique speed for low curvatures by analyzing the retrieved vehicle data. [Kolachalama et.al] developed a deep learning (DL) model to predict the engine operating point (EOP) mapping the

vehicle-level vectors (VLV). However, deep learning (DL) models may not be apt for estimating optimal curvature speed because the variations in EOP are insignificant for low speeds [15 25] MPH. Hence, in this chapter a unique vehicle speed for a definite radius of road curvature (RRC) was estimated utilizing the ideal steering behavior (ISB) model defined in Chapter 4. The ISB model was developed by assuming no change in the parameters of vehicle posture [35] and slip [36], which directly affect the traction for low speeds. Also, the range of the steering parameters was obtained by real-time vehicle testing of 2019 Cadillac Escalade on a constant curvature (RRC=18.4m) by four human drivers (adapting "human-like" driving behavior) under normal driving conditions.

5.1 Existing State of Art

The concept of ideal steering behavior (ISB) relating all steering parameters [$V_s,\ Y_a, L_a, RRC$] was shown in Chapter 4 and Section 5.3. The existing methodologies that gained importance to estimate the curvature speed and their limitations are discussed in this section.

5.1.1 Linear Method

In this method, the vehicle speed for low curvatures is estimated by the ratio of $[L_a]$ and $[Y_a]$. This ratio is integrated into the LOF, (2) and therefore, it does not consider the effect of radius of road curvature (RRC).

$$V_s = \frac{L_a}{Y_a} \tag{17}$$

5.1.2 Accelerometer Method

The accelerometer method is a well-known technique used to determine speed by measuring the lateral acceleration (LAT). This approach produces satisfactory results but does not consider the parameter yaw rate (YAR).

$$V_s^2 = L_a . RRC \tag{18}$$

5.1.3 Geometric Design Method

The geometric design technique is commonly adopted for curvatures and considers elevation (e) and friction factor (f) coefficients in estimation, as shown in the following empirical relation (19). However, this method does not consider the effect of steering behavior parameters.

$$V_s^2 = 15(0.01. e + f)L_a . RRC \tag{19}$$

5.1.4 Ball Bank Indicator Method

The ball-bank indicator consists of a curved glass tube with a floating weighted ball filled with a liquid. The ball-bank indicator is mounted, and as the vehicle travels around a curve, the ball floats outward in the curved glass tube due to the centrifugal force exerted in the driver reference frame, e.g., 16 degrees of deflection for speeds of 20 MPH or less. In this method, the range of speeds is estimated by an empirical relation consisting of the deflection of the instrumental angle, which does not include accurate mathematical models and steering parameters.

5.1.5 Global Positioning System/Compass Method

This method is implemented based on a compass heading and curve length measurements taken at the critical portion of the curve. The major limitation to this method is the deflection of the compass measured by the instrument, which has low precision and does not consider steering

behavior. Also, a range of speeds might result in similar deflections, and thus this method cannot estimate a unique speed.

Hence, in this work, equations (1) and (2) defined in the Chapter 4 were assumed to be appropriate models that include all the steering parameters. The iterative analysis of these parameters based on the boundary values of the retrieved data quantifies the developed function as shown in the following sections.

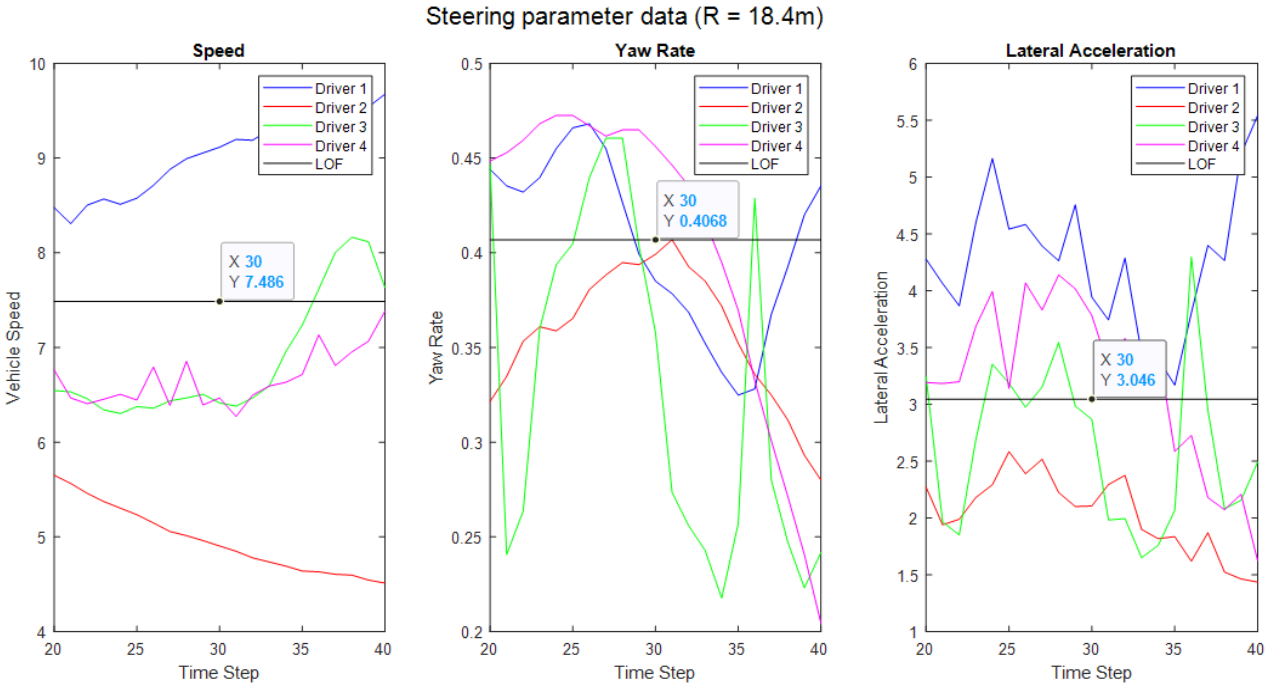

Figure 13: Low curvatures: Driver data—Steering parameters

5.2 Data Retrieval—Analysis

In this project, the integrated advanced data architecture in the vehicle was utilized to perform the analysis as described in Chapter 3.4. The test vehicle, 2019 Cadillac Escalade, provided by General Motors Inc., was utilized and four drivers were selected to traverse the vehicle on the track with RRC=18.4m. The sensorial data of steering behavior vector (SBV) was retrieved using the integrated controller area network, which directly provide the magnitudes in real time. The

steering parameter data retrieved from four drivers is shown in Figure 13, and hence the boundary values of [V_s, L_a, Y_a] for RRC= 18.4m were estimated. The iterative analysis was performed by utilizing the derived boundary conditions and adapting the ideal steering behavior (ISB), whose results were discussed in Chapter 5.4.

5.3 Iterative Analysis

The boundary values of the steering parameters were known from Figure 13, and the range of yaw rate (Y_a) for all four drivers is [0.325 0.472] rad.s^{-1} for RRC = 18.4m, whereas speed (V_s) and lateral acceleration (L_a) have the range of [4.6 9.8] m.s^{-1} and [1.5 5.5] m.s^{-2}. The iterative analysis was performed by varying [Y_a, L_a] in the estimated range, and V_s is derived by inputting these values in equation (1). Figure 14 shows the surface plot of the iterative analysis but does not correlate the unique magnitudes of [V_s, L_a, Y_a] for definite RRC. Hence, basic statistical methods were adopted to estimate the steering parameters by appropriate assumptions of the boundary values, as shown in Table 2.

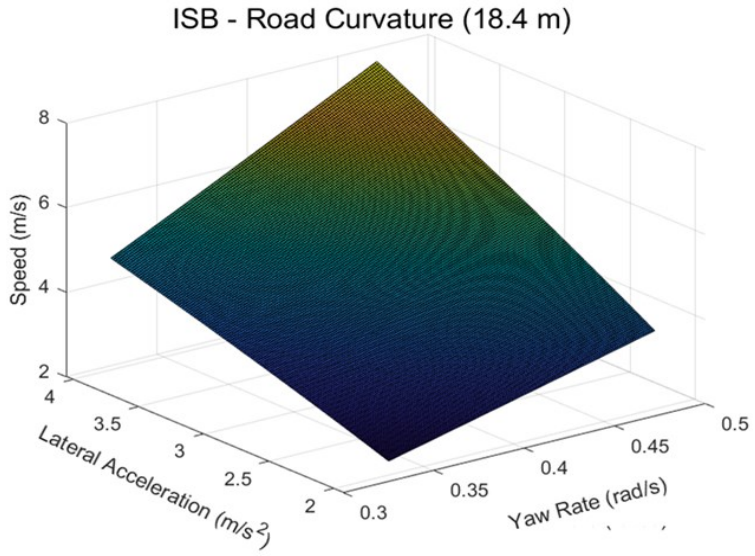

Figure 14: Low curvatures: Iterative analysis [Speed, LAT, YAR] — ISB.

RRC (m)	Speed ($m.s^{-1}$)	Lateral acceleration (LAT) ($m.s^{-2}$)	Yaw rate (YAR) ($rad.s^{-1}$)
8.34	[3.88 9.08]	[3.89 7.89]	[0.72 0.87]
10	[3.98 9.18]	[3.13 7.13]	[0.59 0.74]
15	[4.35 9.55]	[1.94 5.94]	[0.39 0.54]
18.4	[4.60 9.80]	[1.50 5.50]	[0.32 0.47]
20	[4.83 10.03]	[1.43 5.43]	[0.29 0.44]
25	[5.41 10.61]	[1.21 5.21]	[0.24 0.39]
30	[6.09 11.29]	[1.15 5.15]	[0.21 0.36]
35	[6.87 12.07]	[1.19 5.19]	[0.19 0.34]
40	[7.75 12.95]	[1.30 5.30]	[0.18 0.33]
42.57	[8.25 13.45]	[1.38 5.38]	[0.17 0.32]

Table 2: Low curvatures: Range of values—Steering behavior vector

5.4 Implementation

To resolve the simultaneous equations (1) and (2) [Chapter 4.1] with three variables [V_s, L_a, Y_a], the following two methods were adopted to estimate a unique speed for definite radius of road curvature (RRC) using the boundary values defined in Table 2.

5.4.1 Convex Optimization

Method 1: The two equations defined representing ISB, consists of three unknown variables [V_s, L_a, Y_a], with known boundary values. Hence, a unique set of [V_s, L_a, Y_a] for definite RRC, could be derived using known numerical techniques in the existing literature. But to reduce the complexity, in this method, the built-in convex optimization functions (solve) of MATLAB were adopted in the range of recorded values of [Speed, LAT, YAR]. The detailed mathematical models is the not scope of this thesis, but the solutions obtained by adopting this technique are dependent on the initial values, and the results for different initial coordinates produced similar results for RRC = 18.4 m as shown in Table 3. Thus, a similar approach was adopted for RRC = [8.34 42.57] m by assuming an acceptable range of values (Table 2), results of which are presented in Table 4.

Figure 15 was plotted with the resulting values of [RRC, Speed (V_s)], and it was observed that quadratic fit is the most applicable correlation. Thus, the following empirical relation (20) was developed, which achieved more than 99% confidence in estimating the speed in comparison with the adopted convex optimization technique.

$$V_s = 0.001.(2.1\,RRC^2 + 22RRC) + 6.37 \quad (20)$$

Convex optimization			
Initial Coordinate X_o= [V_s, Y_a, L_a]	Speed (m.s^{-1})	Yaw rate (rad.s^{-1})	Lateral acceleration (m.s^{-2})
[4.6, 0.32, 1.5]	7.412	0.4028	2.985
[7.2, 0.39, 3.5]	7.415	0.4030	2.988
[9.8, 0.47, 5.5]	7.413	0.4029	2.986

Table 3: Low curvatures: Steering parameters—Estimation of speed (RRC = 18.4 m)

	Polynomial	**Convex optimization**		
RRC (m)	Speed (m.s^{-1})	Speed (m.s^{-1})	Lateral acceleration (m.s^{-2})	Yaw rate (rad.s^{-1})
8.34	6.699	6.699	5.381	0.803
10	6.799	6.797	4.620	0.679
15	7.169	7.176	3.433	0.478
18.4	7.481	7.477	3.039	0.406
20	7.644	7.642	2.920	0.382
25	8.223	8.222	2.704	0.328
30	8.906	8.906	2.644	0.296
35	9.693	9.696	2.686	0.277
40	10.585	10.585	2.801	0.264
42.57	11.084	11.083	2.885	0.260

Table 4: Low curvatures: Convex optimization—Steering parameters.

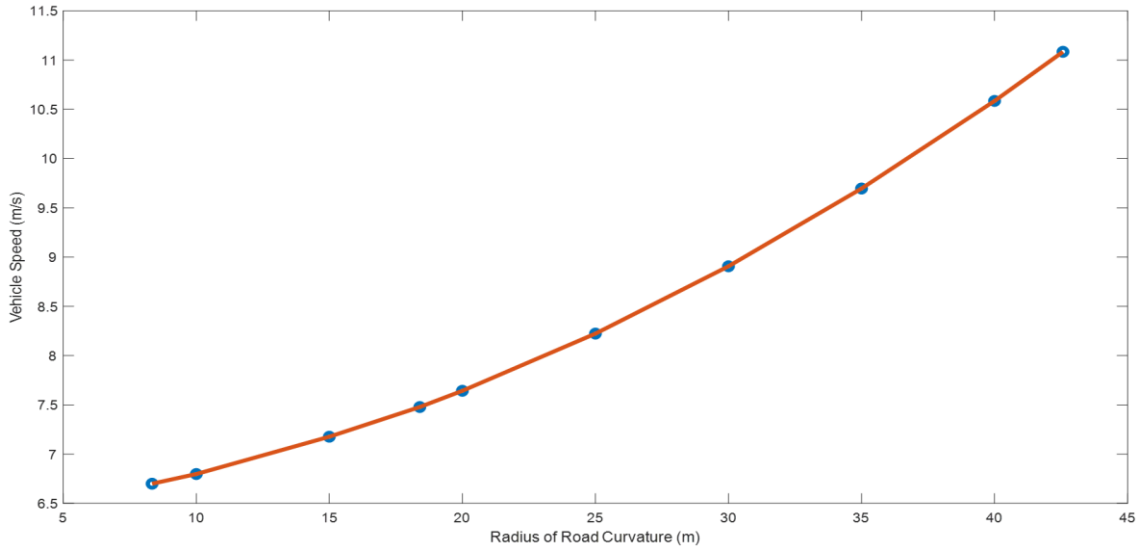

Figure 15: Low curvatures: Ideal steering behavior (ISB) — Convex optimization

5.4.2 Polynomial Interpolation

Method 2: In this method a simple technique of quadratic polynomial interpolation was adopted by assuming the mean value of yaw rate from the test case as the desired yaw rate. Hence Y_a = 0.406 rad.s^{-1} for RRC = 18.4 m was inputted into the constraint $RRC.Y_a^2 = L_a$ and equation 2 to obtain [V_s, L_a , Y_a] = [7.485 m.s^{-1}, 3.045 m.s^{-2}, 0.406 rad.s^{-1}]. As a next step, two other boundary coordinates were obtained assuming the recommended maximum allowable speeds for the curvatures, i.e., 15 MPH (6.7 m.s^{-1}) for RRC = 8.34 m and 25 MPH (11.07 m.s^{-1}) for RRC = 42.57 m. Thus, the required three coordinates for quadratic interpolation are framed in Table 5, and the results for the range RRC = [8.34 42.57] m are shown in Table 6 and Figure 16. Similar to the previous method, a correlation between the two parameters [RRC, Speed (V_s)] was developed as shown in the following equation (21).

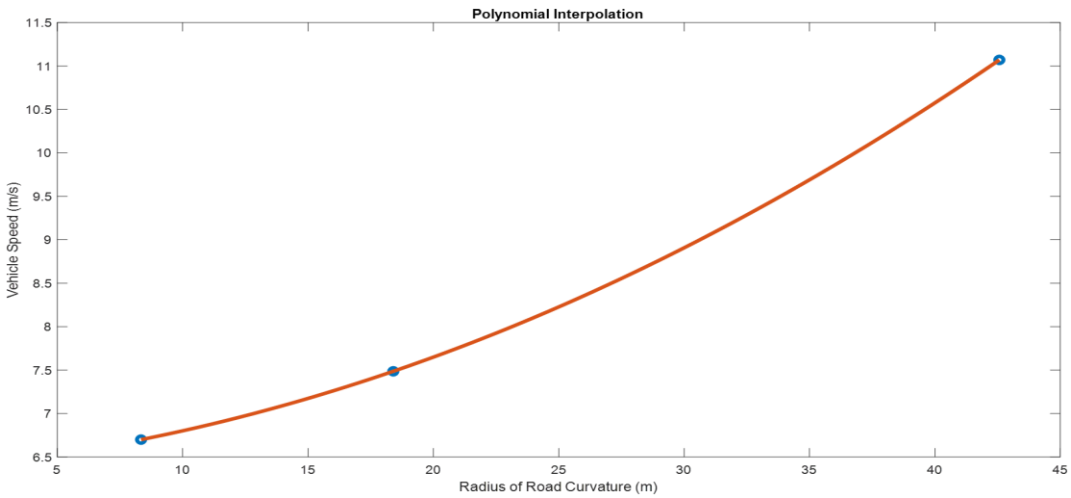

Figure 16: Low curvatures: Ideal steering behavior (ISB) — Polynomial interpolation

$$V_s = 0.001.(2\,RRC^2 + 23.4RRC) + 6.36 \quad (21)$$

Quadratic Interpolation		
Segment	RRC (m)	Speed (m.s^{-1})
U-Turn	8.34	6.699
Roundabout	18.4	7.48
Cloverleaf	42.57	11.069

Table 5: Low curvatures: Coordinates—Estimation of speed

	Quadratic interpolation		
RRC (m)	Speed (m.s^{-1})	Lateral acceleration (m.s^{-2})	Yaw rate (rad.s^{-1})
8.34	6.699	5.381	0.803
10	6.800	4.624	0.680
15	7.173	3.431	0.478
18.4	7.485	3.045	0.406
20	7.649	2.926	0.382
25	8.227	2.707	0.329
30	8.907	2.644	0.297
35	9.689	2.683	0.277
40	10.574	2.796	0.264
42.57	11.069	2.877	0.260

Table 6: Low curvatures: Polynomial interpolation—Steering parameters

5.5 Validation—Speed Profile

Investigating the results, method 1 (convex optimization) and method 2 (mean value for yaw rate) produced similar values for the speed profile. The quadratic correlation between the [RRC, Speed] was established in equations (20) and (21), which have equivalent coefficients, and thus, the core concept of estimating a unique speed for a definite RRC was projected. This research was performed with a limitation of single curvature test data (four drivers), and hence there is no loss of generality to assume that method 1 (convex optimization) is more accurate than method 2. The resulting steering behavior vector (SBV) was quantified by comparing it with the real-time data retrieved for the four test cases and estimating the performance parameters of vehicle curvature (V_c), roll coefficient (R_c), and slip coefficient (S_c). The test vehicle 2019 Cadillac Escalade dimensions are presented in Table 7, and equations (22), (23), and (24) reflect the performance parameters [V_c, R_c, S_c].

Cadillac Escalade - Parameters		
Symbol	Parameter	Magnitude
g	Gravity	9.81 m.s^{-2}
μ	Friction	0.15
[H, W]	Height, Width	[76.7, 81.1] Inches

Table 7: Low curvatures: Parameters—Validation of the speed profile

$$R_C = \frac{V_s^2 H}{gWR} \tag{22}$$

$$S_C = \frac{V_s^2}{g\mu R} \tag{23}$$

$$2V_C = \frac{V_s^2}{L_a} + \frac{V_s}{Y_a} \tag{24}$$

The plots of the parameters [V_c, R_c, S_c] are depicted in Figure 17, and the roll and slip coefficients for the optimal speed were R_C = 0.330 and S_C = 2.33 for RRC = 18.4m. The V_c matches the RRC for the optimal speed V_s= 7.48 m.s^{-1}, i.e., V_c= RRC = 18.4m reflecting ideal steering behavior

(ISB). The estimated values of $[V_s, L_a, Y_a] = [7.485\ \text{m}.s^{-1}, 3.045\ \text{m}.s^{-2}, 0.406\ \text{rad}.s^{-1}]$ for RRC = 18.4m falls within the range of the acceptable limit for safe traverse. Thus, adopting the proposed technique for estimating the speeds for low curvatures would augment the driving behavior, and the results were assumed to be satisfactory.

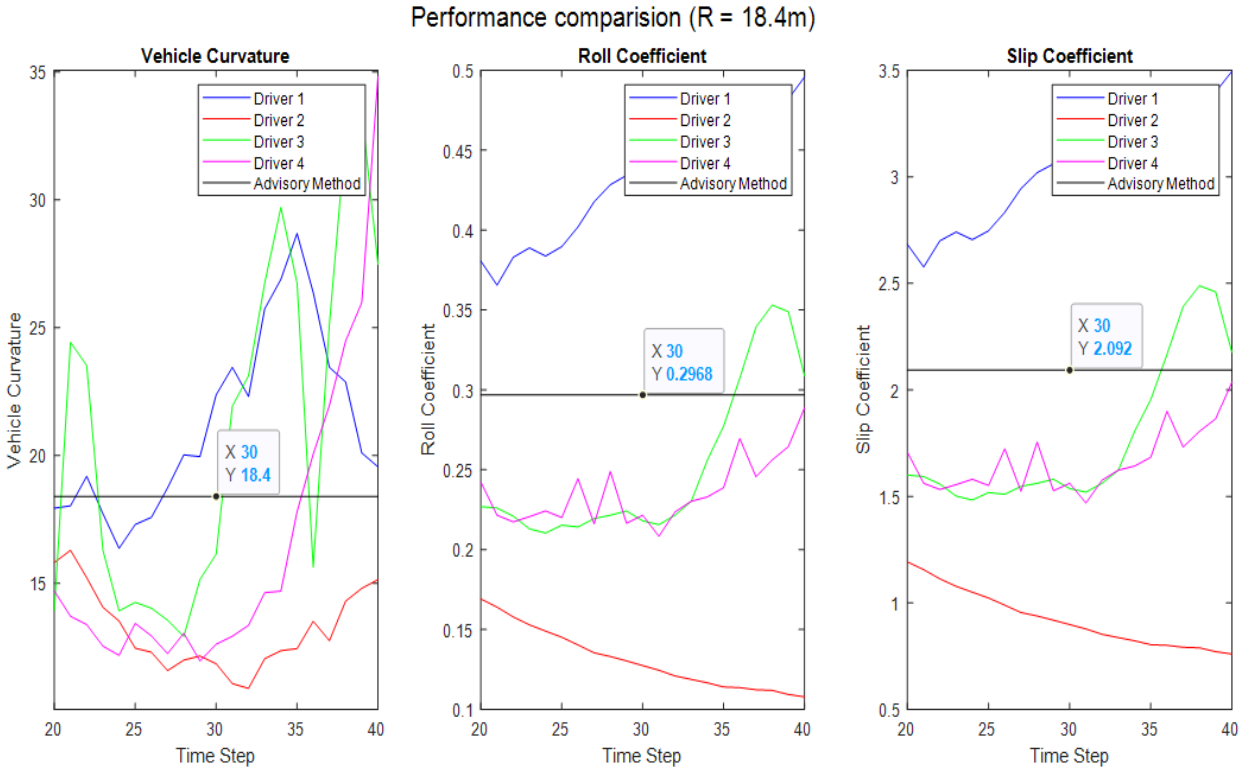

Figure 17: Low curvatures: Performance comparison—Driving behavior.

5.6 Speed Profile for IVDM — Low Curvatures

In this chapter, an empirical model to estimate a unique speed for low curvatures was proposed as one of the functionalities of IVDM. The constraint of ideal steering behavior (ISB) and basic statistical techniques were applied on the data retrieved, which resulted in a unique speed value of 7.48 $\text{m}.s^{-1}$ for RRC = 18.4 m. The convex optimization and polynomial interpolation methods were adopted, and the speed estimated for every curvature (Table 4 and 6) falls in the range of the

allowable speed limits of [15 25] MPH recommended by the US Department of Transportation. The mathematical constraint $RRC.Y_a^2 = L_a$ and the empirically developed quadratic relationship [$V_s = 0.001.(2.1\,RRC^2 + 22RRC) + 6.37$] between [RRC, Speed (V_s)] is novel and produced acceptable results. The validation of the estimated speed was performed by comparing the performance parameters of vehicle curvature, roll, and slip coefficients for all the test cases.

The estimated speed for a definite RRC (retrieved from infotainment maps), and the mathematical model could serve as a measure of driver behavior and feedback to the steering and powertrain controller for level 3+ autonomous vehicles, resulting in optimal lateral dynamics. In the current scenario, this research has limited data availability for a single curvature test, driven under normal driving conditions (no elevation and banking angle), no-slip (lateral and longitudinal), and no traffic congestion. Therefore, the proposed approach can be further validated with extensive testing using multiple drivers traversing different curvatures, considering all the critical scenarios, and the proposed concept could be extended for high curvatures RRC > 42.57 m.

Chapter 6 Deep Learning Models

The automotive industry's evolution has influenced every aspect of engineering, including materials science, thermal engineering, and control theory [54]. In the past two decades, the emergence of the new field of data science has opened the doors to many unsolved problems, and the analytical methods (machine learning) have intruded into every field of engineering. Machine learning techniques have been widely applied in the automotive industry to enhance overall vehicle performance [55]. Supervised deep learning (DL) models are commonly used to optimize engine control [56] and for calibration to enhance engine performance [57]. As mentioned in the previous chapters, this dissertation focuses on engine and HVAC, a core element of the automotive system whose efficiency is directly proportional to vehicle performance.

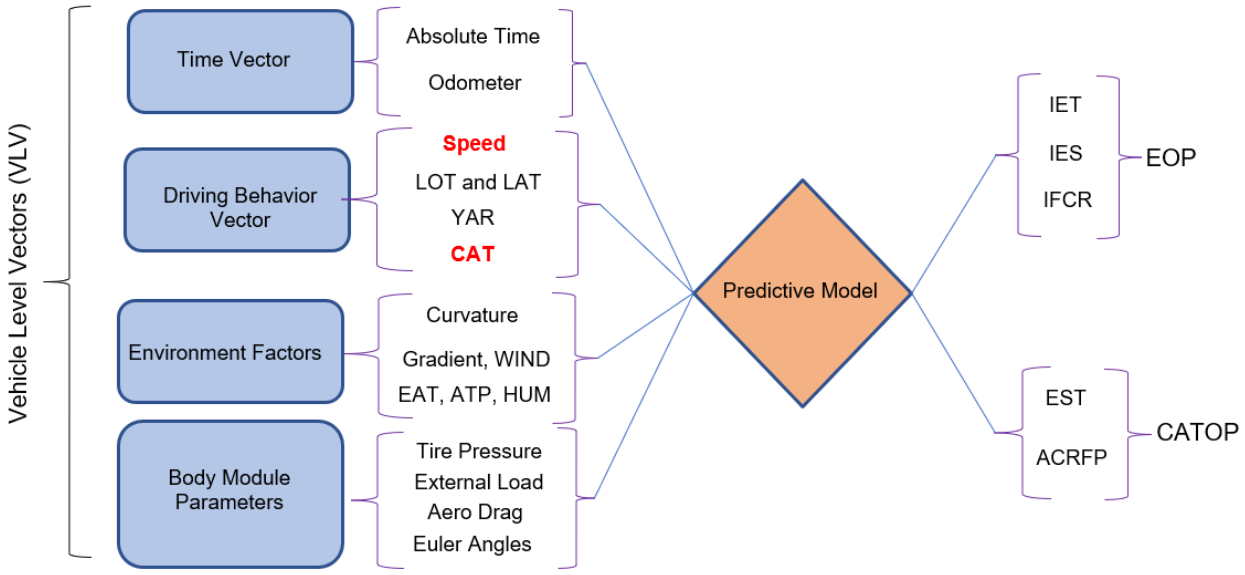

Figure 18: Predictive model — Inputs [VLV] and outputs [EOP, CATOP]

The proposed IVDM predicts driver behavior vector (DBV) by optimizing the [EOP, CATOP] for future time steps. In this chapter, two predictive models are developed by mapping the vehicle-level vectors (VLV) with the vectors [EOP, CATOP] using the retrieved vehicle data obtained from real-time testing (Chapter 3), based on Figure 18.

To summarize the existing literature, [Malikopoulos et.al] was the first to develop data-driven techniques using driving behavior and spark ignition timing to predict fuel consumption. [Shayler et.al and Turkson et.al] used deep learning (DL) models to optimize calibratable parameters such as fuel injection, crankshaft timing, etc., resulting in enhanced engine performance. To predict the brake-specific instantaneous fuel consumption rate (IFCR) and exhaust temperature, [Parlak et.al] developed a deep learning (DL) algorithm using engine speed, mean effective brake pressure, and injection timing. [Togun et.al] explored the relationship between ignition timing, throttle position, and engine speed using the backpropagation neural network function to predict instantaneous fuel consumption rate (IFCR) and engine torque. [Rahimi-Ajdadi et.al] integrated multiple regression models into a neural network to improve the accuracy of predicting fuel consumption as a function of speed, load, and vehicle type. [Wu et.al] developed a forecasting system to estimate the fuel intake based on static vehicle model parameters such as engine type, vehicle type/model, transmission type, and vehicle load but did not use dynamic vehicle parameters. [Liu et.al] used driver behavior and dynamic traffic information to predict IFCR and torque and subsequently deduced the desired control model. [Song et.al] adopted vector quantization techniques of driving patterns to develop a predictive model for energy management of fuel cell vehicles. References [68]–[74] predicted engine torque and engine speed using multivariate inputs.

6.1 Predictive Model

The deep learning (DL) models developed by the researchers predict only one or two elements of the [engine operating point (EOP), cabin air temperature operating point (CATOP)] but not all five. The concept of IVDM was developed to predict the DBV by optimizing all five of the elements [IET, IES, IFCR] and [EST, ACRFP] which play a prominent role in effecting engine performance. More importantly, prior works utilize only a limited number of inputs to obtain results, unlike in our work. Our input vector consists of all factors that impact the [EOP, CATOP] at the vehicle level, especially dynamic factors such as driver behavior vector (DBV), environment, and body module parameters, as shown in Figure 18. When activated, the proposed Intelligent Vehicle Drive Mode (IVDM) predicts the DBV elements [adaptive cruise control set speed profile (ACCSSP), cabin air temperature set profile (CATSP)] by optimizing the vectors [EOP, CATOP] and estimates [yaw rate (YAR), lateral acceleration (LAT)] utilizing ideal steering behavior (ISB). In this section, individual supervised predictive models were developed for five Cadillac vehicle lines [CT4, CT5, Escalade AWD, Escalade ESV, XT6] by mapping the vehicle-level vectors (VLV) with the elements [EOP, CATOP], as shown in Figure 18. The retrieved data were analyzed as time-sensitive; thus, a Nonlinear autoregressive network with exogenous inputs (NARX) and Long short-term memory (LSTM) DL methods were the obvious choices of the current research [Kolachalama et al., 2021]. Hence, the apt deep learning (DL) model for vehicle data is identified in the following chapters, and performance analysis was conducted using a traditional statistical measure vector (STMV). The ARIMA DL model, shall function based on the weighted moving average of the input vector to predict the state of the output, which is not applicable to real-time automotive data as the magnitudes of most of the parameters depend on their previous states. Also, ARIMA models has a

limitation on the input vector size and thus in this research only the performance of [NARX, LSTM] was compared identify the apt technique.

6.2 Properties of DL Models—NARX and LSTM

The default properties built into MATLAB were utilized to initialize the process, as shown in Table 29, and deep learning (DL) models were developed using m-script, the details of which are provided in the following subchapters 6.3.1 and 6.3.2.

6.2.1 NARX

The Nonlinear autoregressive network with exogenous inputs (NARX) is a recurrent dynamic network with feedback connections enclosing several network layers. This model is based on the linear autoregressive method with additional input (ARX) model, which is commonly used in time-series modeling. The future state of the output signal is regressed on previous values of the output signal and previous values of an independent (exogenous) input signal, which is implemented using a feedforward neural network. The NARX method produces the best results for non-linear dynamic systems, with two forms of open and closed-loop transformation.

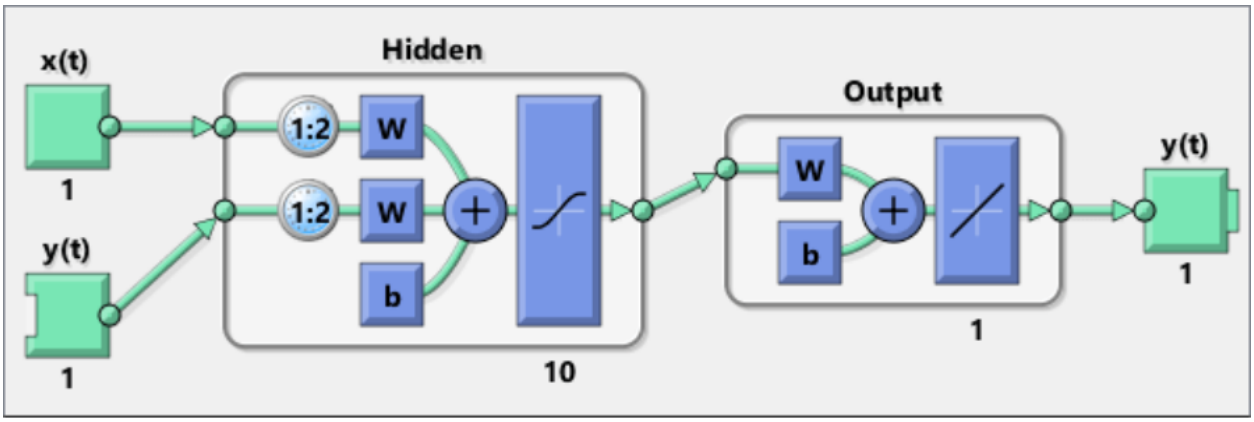

Figure 19: NARX DL model—Open-loop network diagram

The closed loop can predict multiple future states and is generally adopted by internal feedback when an external feedback vector is not available. In the current work, the vehicle is equipped with controller area network (CAN) architecture that provides the instantaneous magnitudes of the vectors [vehicle-level vectors (VLV), engine operating point (EOP), cabin air temperature operating point (CATOP)]. Thus, an open-loop network was implemented to develop the model, as shown in Figure 19, which is the default property of built-in MATLAB functionality [Kolachalama et al., 2021].

The Nonlinear autoregressive network with exogenous inputs (NARX) method was adopted using the default training options with two input and feedback delays and a fixed hidden layer with ten neurons. The Levenberg-Marquardt backpropagation (LM) training function was chosen from among the available list of options, and its performance was validated by the traditional statistical technique root mean square error (RMSE) (Equation 16) [MATLAB 2021a]. The LM is the default supervised algorithm in MATLAB, as it is the optimal and fastest backpropagation algorithm in the toolbox. A detailed analytical model of LM is not within the scope of this dissertation, but the mathematical model of the Nonlinear autoregressive network with exogenous inputs (NARX) method is outlined in Chapter 6.5.

6.2.2 LSTM

Long short-term memory (LSTM) predicts the output by considering the long-term dependencies of the entire set of inputs and possesses the properties of artificial recurrent neural networks (RNN) [87] [Kolachalama et al., 2021]. The core components of an LSTM network are the sequence input layer and LSTM layer, implemented for classification and regression tasks since there can be lags of unknown duration between actual events in a time series. In the current work, the prediction of

future states applies to the regression task where the network ends with a fully connected layer and a regression output layer, as shown in Figure 20.

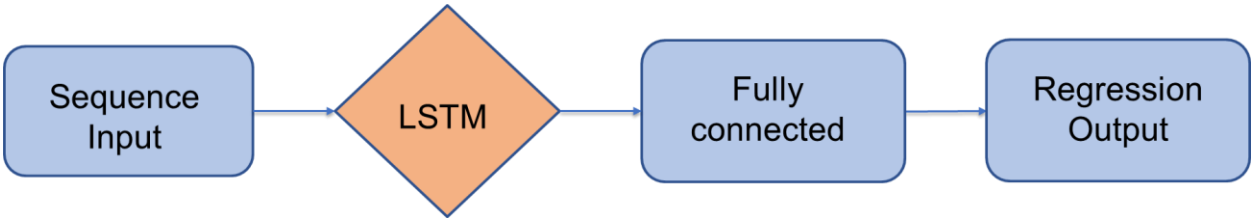

Figure 20: LSTM DL model — Architectural diagram

Similar to the previous section, the default properties of Long short-term memory (LSTM) include the training function stochastic gradient descent with momentum optimizer (SGD), with unit gradient threshold and two hundred (200) hidden units. Further details of the intrinsic properties of the mathematical model are out of the scope of this dissertation; implementation of the deep learning (DL) models using the datasets retrieved is discussed in Chapter 6.4.

6.3 Validation of Results—NARX and LSTM Modeling

Long short-term memory (LSTM) produced the best results for classification and regression of biological data (e.g., antibody sequencing) in the existing literature and Nonlinear autoregressive network with exogenous inputs (NARX) was preferred for data with non-linear behavior dependent on previous time step. The performance analysis of the predictive model of engine operating point (EOP) using [NARX, LSTM] deep learning (DL) methods was done by varying the parameters [training size, test size, hidden layers/units], and it was proven that the NARX method outperformed LSTM for adaptive cruise control (ACC)-activated and deactivated datasets [Kolachalama et al., 2021]. In this section, extended validation is performed using a similar methodology for the five Cadillac test vehicle datasets depicted in Tables 18–24 to predict the

vectors [EOP, CATOP] by mapping vehicle-level vectors (VLV). The available data sets were categorized into training (70% of data) and validation (30% of data). As is typically done for improved performance, the data were normalized to have zero mean and unit variance.

The resulting plots compare the retrieved data (blue) and predicted values (orange) using [Nonlinear autoregressive network with exogenous inputs (NARX), Long short-term memory (LSTM)] methods for randomly selected snippets, as shown in Figures 31–35 (NARX) and Figures 37–42 (LSTM). The first row of the figure represents the three elements of EOP, and the units of [instantaneous engine torque (IET), instantaneous engine speed (IES)] are Nm and rad.s^{-1}, whereas instantaneous fuel consumption rate (IFCR) was recorded on a scale of 1E-8 $m^3 s^{-1}$. The second row consists of the cabin air temperature operating point (CATOP) vector [EST, ACRFP], measured in [°F, PSI]. The numerical performance of the developed deep learning (DL) models were validated by adopting traditional statistical measure vector (STMV) = [root mean square error (RMSE), first order derivative (FOD), signal-to-noise ratio (SNR)] on the conformance between actual and predicted values, as shown in Tables 30–31.

The NARX method produced a maximum RMSE IET = 2.465 (CT4—Set 1), whereas the LSTM network produced a minimum RMSE IET = 18.515 (XT6—Set 2). The element IES was predicted with equal competence by NARX (FOD <1.129) and LSTM (FOD <1.42), but LSTM lacked the required consistency savvy (mean IFCR FOD = 11.9) to match the NARX output (mean IFCR FOD = 10.22) for all the datasets. Similarly, the NARX prediction had 75% lower RMSE EST and 18% lower FOD ACRFP when compared to LSTM output. It is easy to see that despite the stochastic variation, the predicted curves aligned to the actual values, and by visualizing, the fit of NARX prediction is smoother when compared with LSTM graphs and thus the signal-to-noise ratio (SNR) results play a low-priority role. Also, the average computational time required for

developing the NARX training function was 71.195s, whereas Long short-term memory (LSTM) required 125.83s. Hence, the developed NARX DL model can predict the [EOP, CATOP] vector with enhanced accuracy, and the results for the test cases were assumed to be satisfactory.

In this research, the scope was limited to a single-vehicle test case for developing the computational model for Intelligent Vehicle Drive Mode (IVDM) leveraging the 2020 Cadillac CT5 datasets (Tables 21-24). Hence, specific snippets of data with adaptive cruise control set speed profile (ACCSSP) = [30 75] miles per hour (MPH) (Table 32) were selected, and another validation check was performed for the developed nonlinear autoregressive network with exogenous inputs (NARX) DL model. The plots of predicted [EOP, CATOP], comparing the actual values, were shown individually in the Figures 43–47, Figures 48–52 (EAT > 65 °F), and Figures 53–57 (EAT < 45 °F). The computational efficacy of prediction was projected using the statistical measure vector (STMV), as shown in Tables 33-35. The IET RMSE values were <1.7, and IES FOD was < 0.27 for all the datasets, whereas the IFCR SNR has an acceptable range of [6.36 985.73]. Similarly, the EST RMSE < 2.3 (EAT > 65 °F) and < 0.9 (EAT < 45 °F), whereas ACRFP SNR has a range of [2.2 16.1]. Therefore, the efficacy of the NARX deep learning (DL) model was proven, and the results were assumed to be satisfactory. Also, an increased number of datasets and enhanced validation would enrich prediction precision.

However, in any scenario, adopting deep learning (DL) techniques for engineering purposes is a complete black box methodology, and the results of these algorithms may not be reproducible or deterministic. Nevertheless, the DL model may produce different outputs at multiple instances of time for the same input. Hence, an intelligent engineering solution would require describing the mathematical model of the Nonlinear autoregressive network with exogenous inputs (NARX) DL method analytically and conceptually. Also, the proposed concept of Intelligent Vehicle Drive

Mode (IVDM) would affect the critical safety functionality of the lateral and longitudinal dynamics of the automotive system. Therefore, to resolve this issue, a fail-safe algorithm was developed (Chapter 7.7), and a brief description of the mathematical model adopted for the NARX DL method is presented in Chapter 6.5.

6.4 NARX DL Method—Mathematical Modeling

The NARX deep learning (DL) model is the simplest among all techniques considering previous states (e.g., last three states) to predict the future state. This model is the linear representation of the dynamic system in discrete-time and can accommodate multiple exogenous inputs. The model relates the current value of a time series to the past values of the same vector and the current and past values of the driving (exogenous) series. The following equation (25) represents the linear model of NARX [MATLAB 2021a].

$$Y_{k+1} = \sum_{i=1}^{n_a} a_i Y_{k-i+1} + \sum_{i=1}^{n_b} b_i U_{k-i+1} \quad (25)$$

$[a_i, b_i]$—Derived coefficients for the outputs and exogenous inputs.

$[n_a, n_b]$—The length of the previous states of vector: outputs and inputs.

$[Y_k, U_k]$—The magnitude of the output and input vector at the time step k.

However, in the current scope of this dissertation, the focus was to develop the feature requirements and computational model of Intelligent Vehicle Drive Mode (IVDM) along with extensive validation. Hence the detailed, customized algorithm of the nonlinear autoregressive network with exogenous inputs (NARX) DL model for the vehicle data is planned as future work. In the current work, built-in functions of MATLAB with default properties were utilized to develop the core concept of IVDM, and further elements of the research are pursued in Chapters 7–9.

Chapter 7 Prediction of Driver Behavior Vector

To reiterate the proposed concept, when triggered, Intelligent Vehicle Drive Mode (IVDM) predicts the driver behavior vector (DBV) elements [adaptive cruise control set speed profile (ACCSSP), cabin air temperature set profile (CATSP)] by optimizing [EOP, CATOP] in real time and estimates [yaw rate (YAR), lateral acceleration (LAT)] utilizing the concept of ideal steering behavior (ISB). In this chapter, the detailed procedure adopted, and relevant assumptions incorporated are discussed.

7.1 Background—Prediction of CATSP

It is known from the existing literature [78] that the cabin air temperature (CAT) is reduced by the air conditioning system (ACS) [75] and increased by extracting heat from the engine surface [76–77]. [Khayyam et.al] adopted an adaptive control technique to alter the functioning of the ACS based on environmental conditions and driver behavior. This method produced simulation results that project 1% more energy-saving than the conventional fuzzy logic control used by [Nasution et.al]. The fuzzy logic control developed in [80] contained an iterative analysis of cabin air temperature (CAT) and the ACS compressor load to evaluate the system's performance, including reduced energy consumption [80]. [Khayyam et.al] developed an ACS to produce a desirable cabin air temperature (CAT) and maintain the air quality in conjunction with the engine controller by activating cruise control. [Khayyam et.al and Huang et.al] investigated the parameters of the mass flow rate of the air by dynamically adjusting the blower speed and air-gates opening under various thermal loads, which resulted in reduced energy consumption. [Fayabakhsh et.al] developed a heat

balance method for estimating the thermal load encountered by the cabin using a predictive model mapping the driving conditions. This method could potentially predict thermal comfort in real-time and thus reduce the power consumption of the air conditioning system (ACS). Finally, [Cvok et.al] developed an optimized control model for three stages to enhance the efficiency of the ACS. These stages include optimizing the ACS operating point based on the control inputs and relevant actuators.

7.2 Background—Prediction of ACCSSP

Identifying the optimal adaptive cruise control set speed profile (ACCSSP) by considering the dynamic state of the vehicle for a definite coordinate on the terrain is an unsolved, challenging task for engineers. In the existing literature, researchers have performed the parametric optimization of adaptive cruise control (ACC) output by analyzing the real-time data of driver behavior, traffic congestion, terrain, and environmental factors. References [88] – [93] considered driver behavior as the key input to develop the control algorithm using analytical techniques and to tune the outputs of the ACC system. The enhancements of vehicle connectivity opened doors to obtain real-time traffic congestion information. References [94] – [98] adopted deep learning (DL) models to estimate the ACCSSP and desired acceleration based on traffic congestion data retrieved in real time. References [99] – [107] adopted terrain data to estimate the ACC control parameters to reduce instantaneous fuel consumption rate (IFCR) using the known mathematical models.

7.3 Prediction of Driver Behavior Vector — [ACCSSP, CATSP]

The steps applicable to Intelligent Vehicle Drive Mode (IVDM) prediction of driver behavior vector (DBV) utilizing the functionality (Chapter 2), datasets (Chapter 3), criteria (Chapter 4), and deep learning (DL) models (Chapter 6) are defined in this section. The prediction of DBV elements [ACCSSP (MPH), CAT (°F)] was made by the four-step process described in Figure 21, and the

applicable equation sets are shown in Table 8. The ACCSSP (> 25 MPH) was predicted by optimizing the engine operating point (EOP) assuming CAT (°F). Similarly, the CATSP (°F) was predicted by optimizing the cabin air temperature operating point (CATOP) and ACCSSP resulting from the previous step [Kolachalama and Malik, 2021].

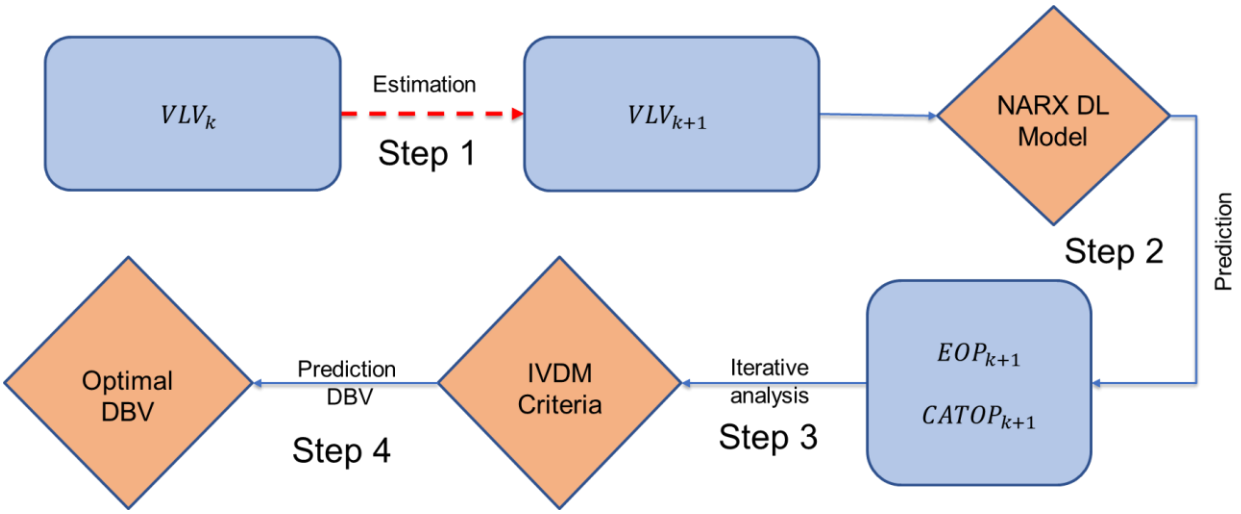

Figure 21: Prediction of driver behavior vector — IVDM process

The default range of [allowable vehicle speeds (AVS), allowable vehicle cabin air temperatures (AVC)] to predict [ACCSSP, CATSP] was estimated by relations (26) and (27), assuming [$DCAT$, EAT_o] = [70, 65] °F. The speed limit (SL) of the road segment in real-time could be retrieved from the built-in advanced infotainment and connectivity (AICON) features of the vehicle system, and the functionality of the Signum function—Sign of the real number (SIGN) mathematical model was utilized to estimate AVC = [65 70] °F (EAT $\geq$ EAT_o °F) or [70 75] °F (EAT $<$ EAT_o °F).

$$\text{AVS} = [\text{SL-5, SL+5}]\ \text{MPH} \tag{26}$$

$$\text{AVC} = [MinCAT, MaxCAT]\ °\text{F} \tag{27}$$

$$MinCAT = min\ [DCAT - 5x;\ DCAT + 5x];$$

$$MaxCAT = max\ [DCAT - 5x;\ DCAT + 5x]$$

$$x\ = SIGN\ (EAT - EAT_o);$$

7.4 Estimation of Future Input States

Step 1: The empirical relations defined in Table 8 were utilized to estimate the future input values (VLV_{k+1}) of the deep learning (DL) model relative to the current state of the vehicle (VLV_k) (Figure 21). The speed (S_{k+1}) was varied in the default range of allowable vehicle speeds (AVS), and the odometer parameter (O_{k+1}) was calculated by basic linear interpolation using [S_{k+1}, $L_{o(k+1)}$], assuming a constant time step.

$T_{k+1} = T_k + dT$ $EAT_{k+1} = EAT_k$	$2RRC_{k+1} = \frac{S_{k+1}^2}{L_{a(k+1)}} + \frac{S_{k+1}}{Y_{a(k+1)}}$, $min\ [abs(Y_{a(k+1)}.S_{k+1} - L_{a(k+1)})]$	$W_y \approx 0$ m.s^{-1} Wind velocity
$O_{k+1} = O_k + S_k.dT$ $TP_{k+1} = TP_k$	$L_{o(k+1)} = g\mu_r + gsin(\theta_{g(k+1)}) + \frac{\rho_a C_d.A_c}{2.(M_c+M_L)}.(S_{k+1} + W_y)^2$	ρ_a = 1.225 kg.m^{-3} Density of air
$S_{k+1} = [SL - 5, SL + 5]$ MPH	$CAT_{k+1} = CAT_k\ or$ [65 70] °F or [70 75] °F	g = 9.81 m.s^{-2} Gravity
C_d= 0.31. Drag coefficient	Mass of the Vehicle M_c=1769.69 kg, Mass of the external load M_L=78.7 kg ; Area of cross section A_c = 1.71 m^2	μ_r= 0.013 Rolling coefficient

Table 8: Equation set—Prediction of DBV.

The magnitude of LOT ($L_{o(k+1)}$) was estimated by calculating the force required to overcome the resistance [rolling, gradient, aerodynamics] for maintaining the adaptive cruise control set speed profile (ACCSSP), while the yaw rate (YAR) ($Y_{a(k+1)}$) and LAT ($L_{a(k+1)}$) were estimated assuming ideal steering behavior (ISB). The CAT_{k+1} was varied in the default range of allowable vehicle cabin air temperatures (AVC), whereas TP_{k+1} was assumed to be the same as in the

previous time step. The General Motors Inc. Cadillac is equipped with advanced driver assistance systems (ADAS) and advanced infotainment and connectivity (AICON) features (super and ultra-cruise), which would generate the vectors RRC (RRC_{k+1}), gradient (θ_{k+1}), and EAT_{k+1} based on the GPS coordinates. An example of an estimated VLV_{k+1} is shown in Table 9.

Time Step	Odometer (Miles)	Speed (MPH)	RRC (m)	YAR (rad/s)	LAT (m.s^{-2})	LOT (m.s^{-2})	EAT (°F)	CAT (°F)
T_0	1000.000	[65 75]	8304.140	0.216	0.118	0.438	[78.3], [40.1]	[65 70], [70 75]
dT_1	1000.002	[65 75]	8304.140	0.216	0.118	0.375	[78.3], [40.1]	[65 70], [70 75]
dT_2	1000.004	[65 75]	8304.140	0.216	0.118	0.313	[78.3], [40.1]	[65 70], [70 75]
dT_3	1000.006	[65 75]	9342.158	0.192	0.105	-0.125	[78.3], [40.1]	[65 70], [70 75]
dT_4	1000.008	[65 75]	24912.420	0.072	0.039	-0.188	[78.3], [40.1]	[65 70], [70 75]
dT_5	1000.010	[65 75]	74737.261	0.024	0.013	-0.063	[78.3], [40.1]	[65 70], [70 75]
dT_6	1000.012	[65 75]	74737.261	0.024	0.013	0.250	[78.3], [40.1]	[65 70], [70 75]
dT_7	1000.014	[65 75]	37368.631	0.048	0.026	0.250	[78.3], [40.1]	[65 70], [70 75]
dT_8	1000.016	[65 75]	24912.420	0.072	0.039	0.188	[78.3], [40.1]	[65 70], [70 75]
dT_9	1000.018	[65 75]	24912.420	0.072	0.039	0.188	[78.3], [40.1]	[65 70], [70 75]
T_1	1000.019	[65 75]	9342.158	0.192	0.105	0.313	[78.3], [40.1]	[65 70], [70 75]

Table 9: Estimated inputs—Deep learning model (10 Time steps = 1 s)

7.5 Prediction of Output States—DL Model

Step 2: The input sets VLV_{k+1} were estimated for all the values of allowable vehicle speeds (AVS) range (e.g., [65, 75] MPH), and thus eleven sets of inputs were generated. These matrices were fed into the developed NARX deep learning (DL) model, and therefore a corresponding eleven sets of EOP_{k+1} were predicted. Similarly, six sets of $CATOP_{k+1}$ were predicted by varying the cabin air temperature (CAT) in the allowable vehicle cabin air temperatures (AVC) = [65 70] °F.

7.6 Implementation of VEP Criteria

Step 3: The vehicle engine performance (VEP) criteria defined in Chapter 4 were applied to the predicted vectors [$EOP_{k+1}, CATOP_{k+1}$], and the results for ten time-steps are shown in Tables 10–11. The six top-performing optimal ACC speeds and CAT's were selected for each VEP criteria, as shown in Tables 12–13. Among these values, the top three modes were selected as the eligible

vehicle speeds (EVS) ([71, 70, 69] MPH) and eligible vehicle cabin air temperatures (EVC) ([68, 70, 67] °F or [72, 71, 70] °F) for the time step T_{k+1}. A similar process was implemented for one-hundred-time steps, and therefore the [ACC, CAT] matrix was framed as shown in Table 14.

Data	**ACC Speed—Iterative Analysis**											
EOP	Speed	65	66	67	68	69	70	71	72	73	74	75
IET	Dist	1.6E+04	3.1E+04	4.7E+04	6.2E+04	7.8E+04	9.4E+04	1.1E+05	1.2E+05	1.4E+05	1.6E+05	1.7E+05
	R^2	0.76	0.83	0.77	0.74	0.77	0.77	0.75	0.77	0.75	0.78	0.76
	Adj R^2	0.4	0.57	0.43	0.36	0.44	0.43	0.39	0.44	0.37	0.44	0.4
	SSE	6.26	4.47	5.94	6.69	5.82	5.94	6.34	5.76	6.49	5.72	6.16
	RMS	0.4	0.33	0.39	0.41	0.38	0.38	0.4	0.38	0.4	0.38	0.39
IES	Area	1.8E+04	3.5E+04	5.3E+04	7.1E+04	8.9E+04	1.1E+05	1.2E+05	1.4E+05	1.6E+05	1.8E+05	2.0E+05
	R^2	1	1	1	1	1	1	1	1	1	1	1
	Adj R^2	0.99	0.99	0.99	0.99	0.99	0.99	0.99	0.99	1	0.99	0.99
	SSE	0.003	0.002	0.003	0.003	0.003	0.003	0.002	0.001	0.001	0.001	0.001
	RMS	0.009	0.007	0.008	0.008	0.009	0.008	0.007	0.006	0.005	0.006	0.006
IFCR	Area	2.8E+04	5.6E+04	8.4E+04	1.1E+05	1.4E+05	1.7E+05	1.9E+05	2.2E+05	2.5E+05	2.7E+05	3.0E+05
	R^2	0.78	0.78	0.72	0.74	0.8	0.75	0.81	0.74	0.76	0.68	0.67
	Adj R^2	0.46	0.45	0.31	0.35	0.5	0.37	0.53	0.36	0.4	0.22	0.17
	SSE	4913.31	4737.99	5613.29	4967.08	3726.95	4633.05	3429.65	4679.59	4418.54	5766.31	6140.52
	RMS	11.19	10.99	11.97	11.26	9.75	10.85	9.35	10.92	10.62	12.13	12.52
ETC	Area	5.4E+01	1.1E+02	1.6E+02	2.2E+02	2.8E+02	3.3E+02	3.9E+02	4.5E+02	5.0E+02	5.6E+02	6.2E+02
	R^2	0.788	0.781	0.724	0.739	0.802	0.751	0.814	0.745	0.759	0.689	0.671
	Adj R^2	0.469	0.452	0.309	0.348	0.504	0.377	0.535	0.362	0.398	0.222	0.176
	SSE	0.02	0.02	0.025	0.023	0.017	0.022	0.016	0.023	0.022	0.03	0.033
	RMS	0.022	0.023	0.025	0.024	0.021	0.023	0.02	0.024	0.024	0.028	0.029
ESC	Area	1.1E+02	2.2E+02	3.3E+02	4.5E+02	5.6E+02	6.7E+02	7.8E+02	9.0E+02	1.0E+03	1.1E+03	1.2E+03
	R^2	0.822	0.869	0.824	0.801	0.826	0.817	0.799	0.812	0.783	0.807	0.792
	Adj R^2	0.554	0.672	0.56	0.503	0.565	0.542	0.497	0.529	0.457	0.517	0.479
	SSE	0	0	0	0	0	0	0	0	0	0	0
	RMS	0.003	0.002	0.003	0.003	0.003	0.003	0.003	0.003	0.003	0.003	0.003
ED	Area	1.9E+04	3.7E+04	5.5E+04	7.2E+04	9.0E+04	1.1E+05	1.2E+05	1.4E+05	1.6E+05	1.7E+05	1.9E+05
	R^2	0.787	0.783	0.725	0.743	0.802	0.751	0.815	0.747	0.761	0.689	0.671
	Adj R^2	0.467	0.457	0.311	0.358	0.504	0.378	0.538	0.368	0.402	0.222	0.176
	SSE	4896.87	4721.42	5595.32	4950.75	3716.68	4620.39	3421.22	4665.06	4404.92	5749.95	6123.26
	RMS	11.18	10.978	11.951	11.241	9.74	10.86	9.345	10.912	10.604	12.115	12.502

Table 10: VEP criteria—Iteration of AVS (10 Time steps = 1 s)

CAT	A1					A2					B				
Area	R^2	**Adj** R^2	**SSE**	**RMS**	**Area**	R^2	**Adj** R^2	**SSE**	**RMS**	**Area**	R^2	**Adj** R^2	**SSE**	**RMS**	**Area**
ACCSSP = 70 MPH; EAT = 78.75 °F															
65	114.5	0.994	0.986	1.495	0.194	1931	0.998	0.994	61.03	1.242	2252	0.995	0.989	158.9	2.004
66	175.2	0.995	0.987	2.749	0.264	1994	0.998	0.994	64.36	1.275	2365	0.996	0.989	167.8	2.059
67	216.5	0.992	0.979	6.555	0.407	2020	0.998	0.994	67.47	1.306	2379	0.996	0.990	149.4	1.943
68	203.8	0.992	0.981	5.391	0.369	1872	0.997	0.993	67.63	1.307	2399	0.996	0.990	155.5	1.983
69	178.2	0.993	0.982	3.933	0.315	1688	0.997	0.993	52.16	1.148	2402	0.996	0.990	167.6	2.058
70	201.9	0.995	0.986	3.773	0.309	1612	0.998	0.994	44.56	1.061	2416	0.996	0.990	162.6	2.027
ACCSSP = 70 MPH; EAT = 38.3 °F															
70	47.069	0.990	0.976	0.551	0.118	40.095	0.987	0.968	0.938	0.154	0.000	0.000	0.000	0.000	0.000
71	45.876	0.990	0.975	0.557	0.119	40.662	0.987	0.968	0.961	0.156	0.000	0.000	0.000	0.000	0.000
72	45.408	0.990	0.975	0.561	0.119	41.013	0.987	0.968	0.978	0.157	0.000	0.000	0.000	0.000	0.000
73	45.575	0.990	0.975	0.566	0.120	41.169	0.987	0.968	0.988	0.158	0.000	0.000	0.000	0.000	0.000
74	46.270	0.990	0.975	0.569	0.120	41.162	0.987	0.968	0.993	0.158	0.000	0.000	0.000	0.000	0.000
75	47.368	0.990	0.975	0.572	0.120	41.026	0.987	0.967	0.993	0.158	0.000	0.000	0.000	0.000	0.000

Table 11: VEP criteria—Iteration of AVC (10-time steps = 100 m)

Area	R^2	**Adj** R^2	**SSE**	**RMS**	**Area**	R^2	**Adj** R^2	**SSE**	**RMS**	**Area**	R^2	**Adj** R^2	**SSE**	**RMS**
IET					**IES**					**IFCR**				
75	69	69	70	70	75	68	68	75	75	65	66	66	75	75
74	70	70	69	69	74	71	71	71	71	66	69	69	66	66
73	65	65	71	71	73	70	70	68	68	67	75	75	69	69
72	68	68	72	72	72	69	69	70	70	68	65	65	65	65
71	71	71	68	68	71	67	67	72	72	69	70	70	70	70
70	73	73	73	73	70	72	72	74	74	70	67	67	72	72
ETC					**ESC**					**ED**				
75	66	66	66	66	75	69	69	70	70	65	66	66	75	75
74	69	69	65	65	74	70	70	69	69	66	69	69	66	66
73	75	75	69	69	73	68	68	71	71	67	75	75	69	69
72	65	65	75	75	72	65	65	72	72	68	65	65	70	70
71	70	70	70	70	71	71	71	73	73	69	70	70	65	65
70	67	67	67	67	70	66	66	68	68	70	67	67	72	72

Table 12: VEP criteria — Optimal ACC speeds (10 Time steps = 1 s)

A1					A2					B				
Area	R^2	**Adj** R^2	**SSE**	**RMS**	**Area**	R^2	**Adj** R^2	**SSE**	**RMS**	**Area**	R^2	**Adj** R^2	**SSE**	**RMS**
EAT = 78.75 °F														
65	66	66	65	65	70	66	66	70	70	70	67	67	67	67
66	70	70	66	66	69	65	65	69	69	69	68	68	68	68
69	65	65	70	70	68	67	67	65	65	68	70	70	65	65
EAT = 38.3 °F														
72	70	70	70	70	70	71	71	70	70	70	70	70	70	70
73	71	71	71	71	71	70	70	71	71	71	71	71	71	71
71	72	72	72	72	72	72	72	72	72	72	72	72	72	72

Table 13: VEP criteria — Optimal CAT values (10 Time steps = 100 m)

ACC Speed Matrix (10 seconds)										CAT Matrix (1000 m)									
T_1	T_2	T_3	T_4	T_5	T_6	T_7	T_8	T_9	T_{10}	dT_1	dT_2	dT_3	dT_4	dT_5	dT_6	dT_7	dT_8	dT_9	dT_{10}
69	68	66	75	74	67	67	75	67	75	67	70	67	65	66	65	68	67	65	69
71	70	65	68	72	71	72	66	75	71	65	67	70	69	67	70	65	69	66	68
68	71	67	65	65	74	73	68	73	65	70	68	68	67	65	69	66	65	68	67

Table 14: Optimal ACC Speed (10s) and CAT Matrix (1000 m)—100-time steps

7.7 Algorithm—Generation of [ACCSSP, CATSP]

Step 4A: *Estimation of ACCSSP*

The ACC matrix has three speed values for each second. Thus, a maximum of 3^{10} ACCSSPs are possible for 10 seconds, and the following conditions were defined to identify a unique ACCSSP [24].

1. Assuming the ACC speed at T_k is S_k, and if the eligible vehicle speeds (EVS) at $T_{k+1}$are either S_k+1, S_k, or S_k-1, then S_{k+1} = S_k+1.
2. If the EVS at T_{k+1} is neither S_k+1, S_k, nor S_k-1, then $S_{k+1} = S_k$.
3. If $S_{k+1} = S_k$ for more than a hundred-time steps, S_{k+1}= S_k+1 if S_k+1 ≤ SL+5 or S_{k+1}= S_k- 1 if S_k= SL+5.

Step 4B: *Estimation of CATSP*

Similarly, the cabin air temperature (CAT) matrix has three eligible values for 100 m. The CATSP for 1000m was predicted using the following conditions defined based on external air temperature (EAT) [29].

1. Assuming the CAT at dT_k is C_k, if the eligible vehicle cabin air temperature (EVC) at dT_{k+1} is either C_k+1, C_k, or C_k-1.

   Case 1: $EAT_k \geq EAT_o$ °F, then C_{k+1} = C_k+1 (C_k+1 ≤ $maxCAT$ °F).

   Case 2: $EAT_k < EAT_o$ °F, then C_{k+1} = C_k-1 (C_k-1 ≥ $minCAT$ °F).

2. If the EVC at dT_{k+1} is neither C_k+1, C_k, nor C_k-1, then $C_{k+1} = C_k$ ($minCAT$ °F $\leq C_k \leq$ $maxCAT$ °F).

3. If $C_{k+1} = C_k$ for more than a hundred-time steps, then

   Case 1: $EAT_k \geq EAT_o$ °F, then $C_{k+1} = C_k$+1, if C_k+1$\leq maxCAT$ °F or $C_{k+1} = C_k$- 1, if $C_k = maxCAT$ °F.

   Case 2: $EAT_k < EAT_o$ °F, then $C_{k+1} = C_k$-1, if C_k-1$\geq minCAT$ °F or $C_{k+1} = C_k$+ 1, if $C_k = minCAT$ °F.

   The algorithm proposed in Step [4A, 4B] was implemented on the [ACC, CAT] matrices (Table 14) by a unit step increment of $[S_0, C_0]$ in the range of [allowable vehicle speeds (AVS), allowable vehicle cabin air temperatures (AVC)]. The possible [ACCSSPs, CATSPs] are shown in Figures 22–23, and a unique [ACCSSP, CATSP] was obtained by assuming [initial ACC speed (IAS) (S_0), initial cabin air temperature (ICAT) (C_0)] = [70 MPH, 65°F], as shown in Figures 24–25.

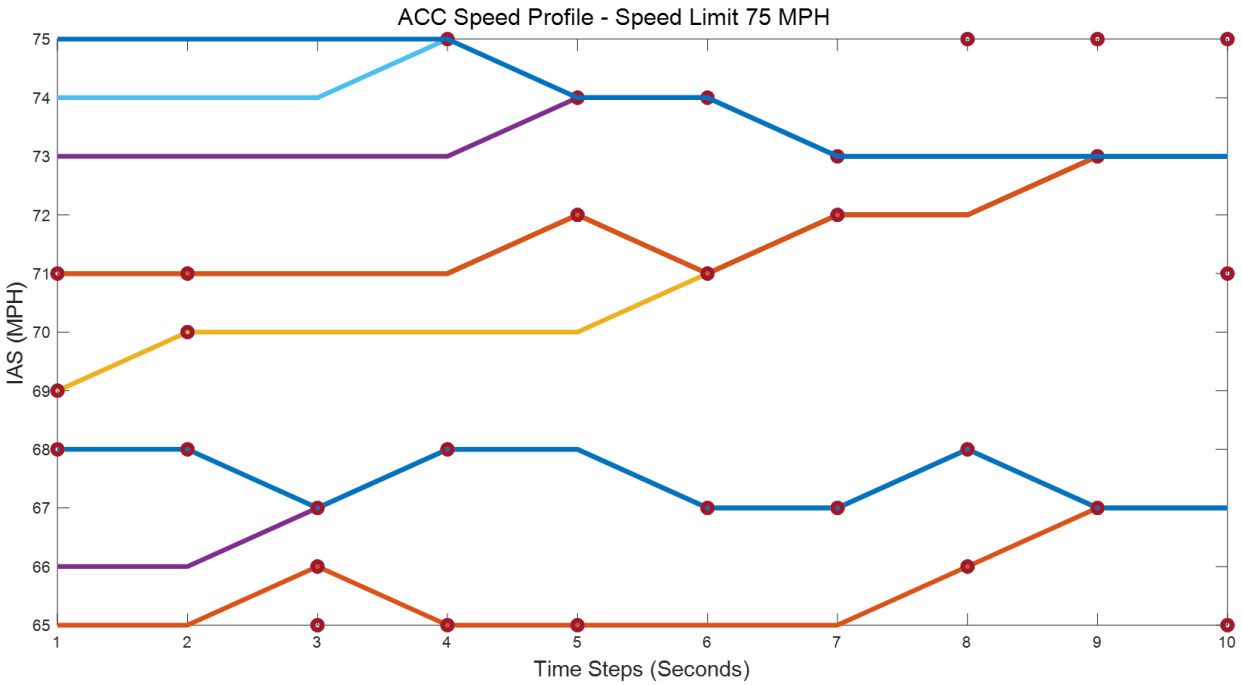

Figure 22: Generated ACCSSP—Speed range = [65 75] MPH.

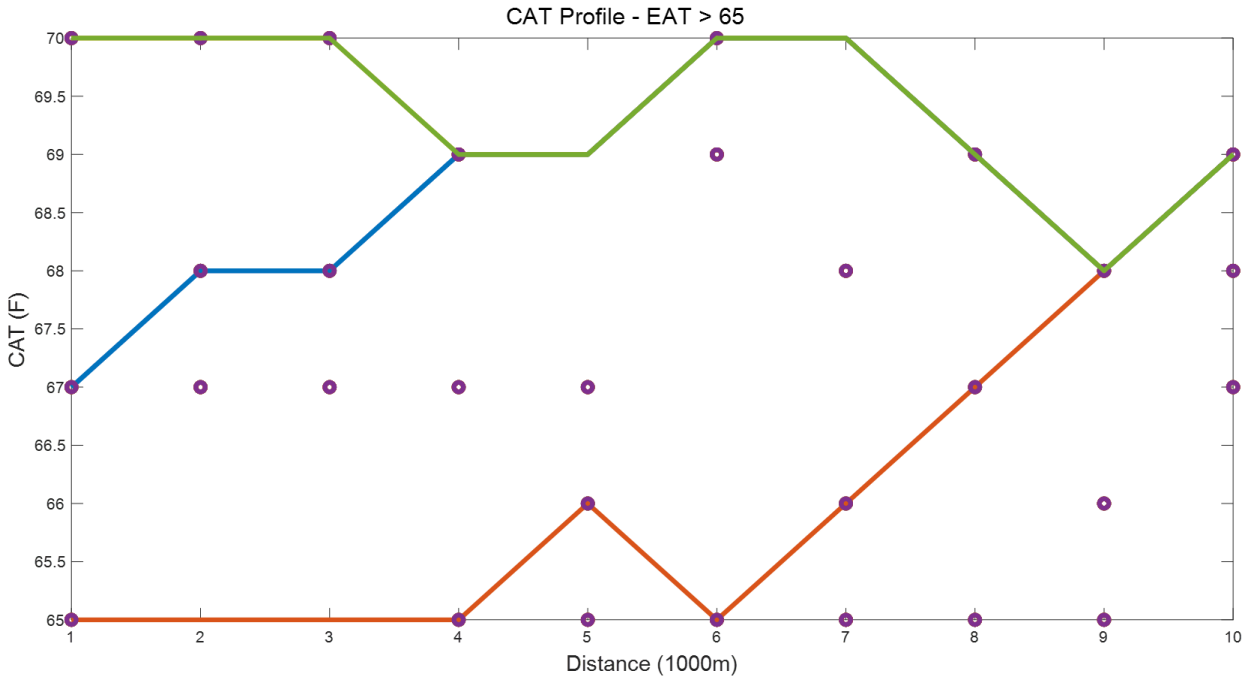

Figure 23: Generated CATSP—CAT range = [65 70] °F.

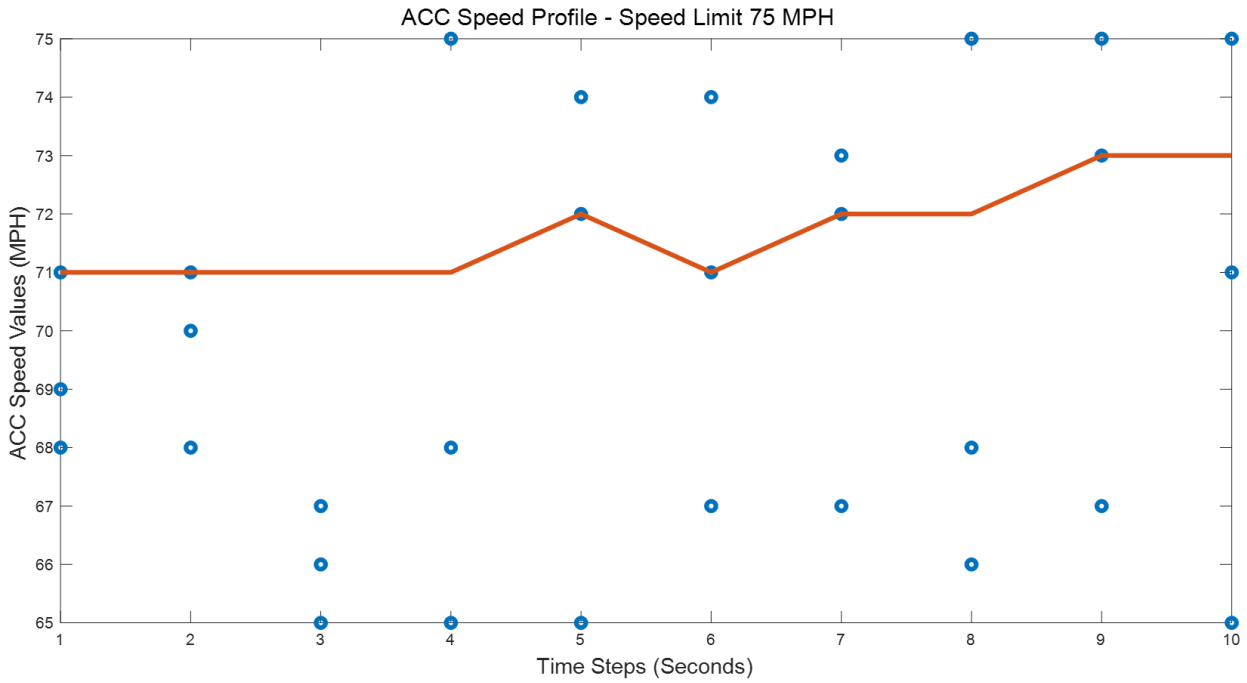

Figure 24: Generated ACCSSP—Initial ACC Speed = 70 MPH

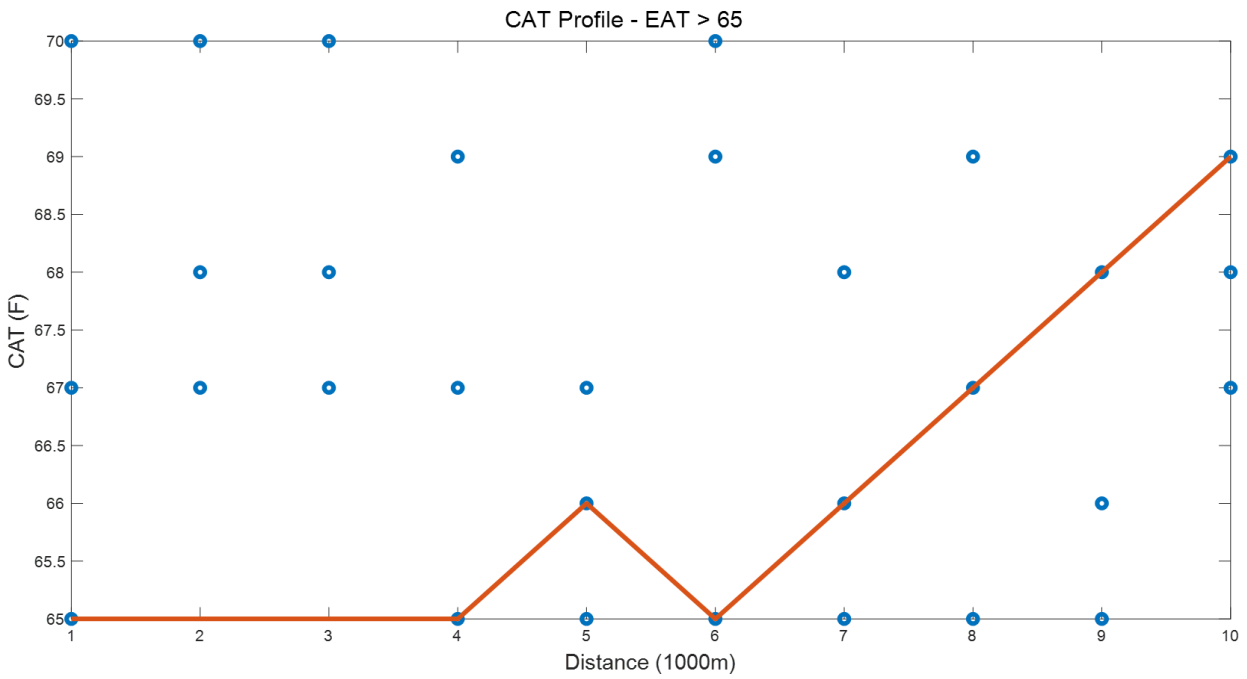

Figure 25: Generated CATSP—Initial CAT = 65 °F

Chapter 8 Results and Validation

The functionality of Intelligent Vehicle Drive Mode (IVDM) was applied to the snippets selected from the 2020 Cadillac CT5 data sets for the ACCSSP = [30 70] MPH. The plots of predicted [ACCSSP, CATSP] resulting from implementing all the steps defined in Chapter 7 for the test cases are depicted in Figures 58–62 and 63–67. The performance of the predicted and constant [ACCSSP, CATSP] was compared using the parameters defined in Section 4: vehicle engine performance (VEP) criteria, whose output is presented in Tables 15 and 16.

The computational methods adopted in this research were quantified using a new precise approach by estimating the instantaneous engine efficiency (IEE) (n_e) and the smoothness measure vector (SMV) of the instantaneous engine map (IEM). The ratio of power output and rate of energy input was calculated to estimate IEE (equation 28) [mean, deviation, variance], assuming the fuel used was gasoline and its properties [calorific Value (C_v), density (ρ_f)] = [45 MJ.Kg^{-1}, 750 Kg.m^{-3}] were unchanged with the effect of temperature and pressure [Ahmed and Bhatti, 2010].

$$n_e = \frac{IET.IES}{C_v.\rho_f.IFCR} \tag{28}$$

The IEM is plotted on a two-dimensional plane using [instantaneous engine torque (IET) and instantaneous engine speed (IES)], and the smoothness measure vector (SMV) was measured using the criteria defined in Chapter 4.4, whose outcome is shown in Figures 68–72.

Parameter	ACC = 30 MPH		ACC = 40 MPH		ACC = 50 MPH		ACC = 60 MPH		ACC = 70 MPH	
Criteria	Constant	Predict	Constant	Predict	Constant	Predict	Constant	Predict	Constant	Predict
Performance Vectors										
Distance	3.00E+4	3.02E+4	4.00E+4	4.10E+4	5.00E+4	5.04E+4	5.99E+4	6.09E+4	6.99E+4	6.94E+4
IET	2.05E+5	2.05E+5	1.60E+5	1.60E+5	2.30E+5	2.30E+5	2.49E+5	2.49E+5	2.45E+5	2.45E+5
IES	2.84E+5	2.84E+5	1.39E+5	1.39E+5	1.66E+5	1.66E+5	1.69E+5	1.69E+5	2.39E+5	2.39E+5
IFCR	5.63E+5	5.62E+5	2.26E+5	2.26E+5	3.53E+5	3.53E+5	4.26E+5	4.27E+5	5.90E+5	5.90E+5
ETC	4.06E+2	4.06E+2	7.13E+2	7.12E+2	6.61E+2	6.62E+2	5.93E+2	5.93E+2	4.09E+2	4.09E+2
ESC	1.44E+3	1.44E+3	8.65E+2	8.67E+2	7.21E+2	7.21E+2	6.85E+2	6.84E+2	1.94E+3	1.90E+3
ED	4.68E+5	4.68E+5	1.27E+5	1.27E+5	2.66E+5	2.66E+5	3.42E+5	3.42E+5	5.08E+5	5.08E+5
Performance Vectors - Conformance (Predicted - Constant)										
Distance	199.000		999.500		400.000		999.000		-499.000	
IET	-223.508		-74.710		-56.149		53.121		-18.207	
IES	-54.606		284.891		2.013		-59.833		20.534	
IFCR	-803.247		171.972		-95.391		33.725		-147.311	
ETC	-0.043		-0.906		0.064		-0.036		0.198	
ESC	3.071		2.158		0.176		-0.396		-33.250	
ED	-792.187		161.953		-107.700		45.969		-222.340	
Smoothness Measure - R^2										
IET	0.997	0.997	0.999	0.999	0.995	0.995	0.999	0.999	0.999	0.999
IES	0.999	0.999	0.999	0.999	0.999	0.999	0.979	0.979	0.999	0.999
IFCR	0.998	0.998	0.972	0.972	0.989	0.989	0.992	0.992	0.998	0.998
ETC	0.996	0.996	0.970	0.971	0.987	0.987	0.979	0.979	0.992	0.992
ESC	0.995	0.995	0.998	0.998	0.999	0.999	0.997	0.997	0.998	0.998
ED	0.998	0.998	0.972	0.972	0.990	0.990	0.993	0.993	0.998	0.998
Smoothness Measure - Adj R^2										
IET	0.993	0.993	0.996	0.996	0.988	0.987	0.998	0.998	0.998	0.998
IES	0.996	0.996	0.998	0.997	0.999	0.999	0.948	0.947	0.998	0.998
IFCR	0.995	0.995	0.929	0.930	0.973	0.973	0.981	0.981	0.995	0.995
ETC	0.991	0.991	0.926	0.927	0.968	0.968	0.947	0.947	0.981	0.981
ESC	0.988	0.989	0.994	0.994	0.998	0.998	0.993	0.993	0.995	0.995
ED	0.995	0.995	0.930	0.931	0.974	0.974	0.984	0.984	0.994	0.994
Smoothness Measure - SSE										
IET	8.26E+3	8.22E+3	74.064	72.920	570.321	572.589	6.47E+2	6.50E+2	3.52E+3	3.51E+3
IES	8.82E+3	8.88E+3	14.117	15.934	91.594	90.776	1.10E+3	1.11E+3	14.170	14.635
IFCR	9.94E+4	9.96E+4	1.60E+4	1.58E+4	2.44E+4	2.46E+4	4.95E+4	4.92E+4	5.75E+4	5.77E+4
ETC	0.074	0.074	0.152	0.150	0.085	0.085	0.089	0.088	0.041	0.041
ESC	1.045	1.019	0.002	0.002	0.004	0.004	0.013	0.013	53.374	46.723
ED	9.90E+4	9.91E+4	1.58E+4	1.56E+4	2.24E+4	2.25E+4	4.62E+4	4.59E+4	5.43E+4	5.45E+4
Smoothness Measure - RMSE										
IET	4.535	4.524	0.429	0.426	1.191	1.194	1.269	1.272	2.960	2.957
IES	4.685	4.701	0.187	0.199	0.477	0.475	1.653	1.662	0.188	0.191
IFCR	15.730	15.741	6.301	6.263	7.795	7.819	11.096	11.061	11.958	11.983
ETC	0.014	0.014	0.019	0.019	0.015	0.015	0.015	0.015	0.010	0.010
ESC	0.051	0.050	0.002	0.002	0.003	0.003	0.006	0.006	0.364	0.341
ED	15.698	15.708	6.270	6.233	7.468	7.492	10.725	10.691	11.621	11.646

Table 15: Prediction of ACCSSP—Performance analysis

Parameter	EAT (°F)	CAT (°F)	Area	Conformance	R^2	Adj R^2	SSE	RMSE
ACCSSP = 30 MPH								
EST (A1+A2)	82.076	69	412.431	-66.097	0.936	0.841	28.869	0.858
		Predicted	346.334		0.803	0.506	223.958	2.391
	37.985	70	695.211	-0.457	0.989	0.971	13.008	0.576
		Predicted	694.754		0.989	0.972	13.015	0.576
ACRFP (B)	82.076	69	4796.364	-271.024	0.991	0.978	596.296	3.901
		Predicted	4525.340		0.988	0.969	703.936	4.239
	37.985	70	28447.657	-12.325	0.992	0.980	8.751	0.473
		Predicted	28435.331		0.992	0.980	8.755	0.473
ACCSSP = 40 MPH								
EST (A1+A2)	85.289	68	269.142	0.051	0.951	0.878	16.910	0.657
		Predicted	269.193		0.963	0.907	12.982	0.576
	37.634	71	429.335	-37.710	0.991	0.977	7.832	0.447
		Predicted	391.625		0.990	0.975	9.661	0.497
ACRFP (B)	85.289	68	5992.344	-550.425	0.968	0.919	447.093	3.378
		Predicted	5441.919		0.974	0.935	367.982	3.065
	37.634	71	28028.615	-6.797	0.988	0.970	18.523	0.688
		Predicted	28021.818		0.988	0.970	18.590	0.689
ACCSSP = 50 MPH								
EST (A1+A2)	80.726	67	561.773	2.441	0.962	0.905	7.244	0.430
		Predicted	564.214		0.959	0.898	7.967	0.451
	40.1	72	876.469	-1.070	0.885	0.713	1.246	0.178
		Predicted	875.399		0.884	0.709	1.252	0.179
ACRFP (B)	80.726	67	1904.872	59.813	0.981	0.952	382.367	3.124
		Predicted	1964.686		0.983	0.957	351.031	2.993
	40.1	72	28276.442	0.118	0.980	0.951	0.613	0.125
		Predicted	28276.559		0.980	0.951	0.613	0.125
ACCSSP = 60 MPH								
EST (A1+A2)	79.44	66	738.825	-192.196	0.961	0.902	13.422	0.585
		Predicted	546.629		0.957	0.893	17.459	0.668
	38.858	73	783.449	-3.056	0.981	0.953	4.052	0.322
		Predicted	780.393		0.982	0.954	4.099	0.323
ACRFP (B)	79.44	66	8978.425	-2153.683	0.909	0.772	13.125	0.579
		Predicted	6824.742		0.993	0.982	669.514	4.134
	38.858	73	28658.279	1.219	0.988	0.970	0.004	0.010
		Predicted	28659.498		0.991	0.977	0.004	0.010
ACCSSP = 70 MPH								
EST (A1+A2)	76.1	65	1427.487	-904.718	0.990	0.976	1.027	0.162
		Predicted	522.768		0.997	0.993	5.569	0.377
	36.518	74	118.232	-10.842	0.934	0.835	2.274	0.241
		Predicted	107.390		0.944	0.861	2.069	0.230
ACRFP (B)	76.1	65	1433.399	253.377	0.862	0.655	6501.550	12.882
		Predicted	1686.776		0.873	0.681	6049.353	12.426
	36.518	74	28851.815	2.671	0.806	0.514	0.000	0.003
		Predicted	28854.486		0.980	0.950	0.000	0.002

Table 16: Prediction of CATSP — Performance analysis

Additionally, the parameters [IFCR, Distance] for constant and predicted [ACCSSP, CATSP], were estimated and the results are presented in the following Table 17.

Speed (MPH)	Speed Profile	IEE			IEM			Performance	
		Mean	Deviation	Variance (1E-3)	R^2	Adj R^2	RMSE	IFCR (1E-3 m^3)	Distance (1E+5 m)
30	Constant	0.3210	0.0424	0.0018	0.9968	0.7878	12.4481	4.7716	0.1338
	Predicted	0.3180	0.0415	0.0017	0.9983	0.8956	8.6682	4.7857	0.1401
40	Constant	0.3256	0.0281	0.7898	0.9998	0.9966	1.3902	3.4894	0.1785
	Predicted	0.3254	0.0281	0.7870	0.9999	0.9982	1.0034	3.4882	0.1811
50	Constant	0.3320	0.0313	0.001	0.9981	0.9560	5.1152	3.7634	0.2231
	Predicted	0.3339	0.0317	0.001	0.9961	0.9425	5.8793	3.7477	0.2146
60	Constant	0.3295	0.0286	0.8164	0.9964	0.7411	10.3102	3.8386	0.2677
	Predicted	0.3298	0.0286	0.8204	0.9933	0.8836	6.9115	3.8330	0.2628
70	Constant	0.3154	0.0221	0.4889	0.9991	0.9900	0.6721	3.6281	0.3123
	Predicted	0.3138	0.0219	0.4817	0.9998	0.9964	0.4067	3.6415	0.3181

Table 17: Quantification of IVDM — IEE and IEM

Chapter 9 Discussion

In this research, multiple engineering concepts were utilized to develop the concept of Intelligent Vehicle Drive Mode (IVDM). The steps included real-time testing, data acquisition through CAN, developing the deep learning (DL) predictive models, feature functionality of vehicle engine performance (VEP), empirical methods to estimate vehicle-level vectors (VLV) for future time steps, and iterative analysis to predict the driver behavior vector (DBV).

The constant and predicted [adaptive cruise control set speed profile (ACCSSP), cabin air temperature set profile (CATSP)] were generated based on the developed concepts, as shown in Figures 58–67. The selected snippets of Speeds and CATs ranging [30 70] MPH and [65 75] °F were selected, to generate a unique [ACCSSP, CATSP] based on the [initial ACC speed (IAS), initial cabin air temperature (ICAT)]. The results of the performance analysis corresponding to the VEP criteria were shown in Tables 11 and 12. The smoothness measure vector (SMV)s for constant and predicted [ACCSSP, CATSP] were interpreted, and it was observed that in most cases, the predicted profile outperformed the constant values. The criteria for SMV were defined in Table 28, and in 70% of the cases, the predicted [ACCSSP, CATSP] has higher [R^2 Adjusted R^2] and lower [Sum of squares error (SSE) root mean square error (RMSE)], whereas 30% of the scenarios scored the same (Table 17).

Among all the parameters (Chapter 4), the most critical elements of interest for VEP are [IFCR, Distance], and the conformance of predicted and constant ACCSSP test cases was shown in Table 17. The predicted ACCSSP with the snippet speed = [30 50] MPH resulted in lower IFCR by

[803.247 95.391], with an additional distance traversed of [199 400] m. The constant ACCSSP with speed = [70] MPH resulted in higher IFCR [147.311], ED [222.34], and distance [499] m and lower [ESC ETC] = [20.54, 0.198], which depicts vehicle movement on higher-gradient terrain. The algorithm developed for this work also allots priority to lowering the trip time, and hence the predicted ACCSSP with speed snippet = [40 60] MPH resulted in higher Distance = [999.5 999] m and IFCR = [171.972, 33.725].

Similarly, the performance of the predicted and constant [CATSP] was analyzed by the conformance vectors [EST, ACRFP] = [A1+A2, B], as shown in Table 16. The two test scenarios with EAT $\geq$ 65 °F and EAT < 45 °F were investigated, and lower values of the area [A1+A2] (EST) and B (ACRFP) are desired for enhanced HVAC performance. In the test case scenario with ACCSSP = 70 MPH, the predicted CATSP with EAT = [76.1 36.5] °F resulted in lower EST by [904.718, 10.842]. However, the ACRFP had higher magnitudes for the predicted CATSP, which was compensated for by the better smoothness measure vector (SMV), similar to the snippet with ACCSSP = 50 MPH. The [EST, ACRFP] for predicted CATSP were higher by 2.441 and 59.813 for EAT = 80.72 °F, which is not desirable, but the smoothness measure vector (SMV) of ACRFP for the predicted CATSP had higher [R^2, Adjusted R^2] = [0.983 0.957] and lower [SSE RMSE] = [351.03 2.993]. Similarly, for EAT = 40.1 °F, the EST for the constant CATSP was higher by 1.07, and the rest of the criteria had comparable values. Thus, enhanced performance was concluded by analyzing the VEP parameters for the test cases with ACCSSP = [30, 40, 60] MPH.

Additionally, the efficacy of Intelligent Vehicle Drive Mode (IVDM) was quantified by estimating the [IEE, SMV IEM] and [IFCR, Distance] for another set of snippets selected in a similar speed range [30 70] MPH. The plots and analytical results are depicted in Figures 68–72 and Table 17. The smoothness measure vector (SMV) criteria defined in Chapter 4.4 were adopted for

instantaneous engine map (IEM), whereas higher IEE [mean] and lower IEE [deviation, variance] was desired for optimal VEP. It was observed that the IEM RMSE of the predicted ACCSSP had lower values than the constant ACCSSP for all the test cases except for ACCSSP = 50 MPH, where the RMSE = [5.115 5.879] shared similar magnitudes. The test case with constant ACCSSP = 30 MPH had a lower IFCR = 4.77, but the vehicle traversed an additional 630 m with predicted ACCSSP. The IEE [mean, variance] for constant ACCSSP = 40 MPH were [0.3256, 0.7898E-3], and the predicted ACCSSP scored [0.3254, 0.787E-3]. Thus IEE [variance] of the predicted ACCSSP was lower, and the IEE [mean, deviation] shared similar values. This approach of analyzing the [IEE, IEM] was not discussed in the existing literature, and the computational results were assumed to be satisfactory. Therefore, the overall observation was that the predicted ACCSSP satisfied the desired criteria in most scenarios and the results best confirmed the validation of the proposed Intelligent Vehicle Drive Mode (IVDM).

The analytic results depicted that IVDM ameliorated vehicle engine performance (VEP) by predicting [ACCSSP, CATSP], optimizing [EOP, CATOP]. The IVDM could emerge as a significant feature in automotive systems answering the following two main questions.

What's in it for the customer? The IVDM would optimize the two parameters [IFCR, distance] for every trip traversed.

What's in it for the engineer? The SMV for the predicted IEM showed better performance in every case depicted in Table 17, which minimized the vibrations transmitted by the engine along with achieving optimal efficiency.

Chapter 10 Conclusion

This research proposes a novel drive mode named “Intelligent Vehicle Drive Mode” (IVDM), which augments the vehicle engine performance (VEP) in real time without increasing the trip time under normal driving conditions. The IVDM is not currently integrated into any vehicle segment and predicts the DBV [speed, longitudinal acceleration (LOT), lateral acceleration (LAT), yaw rate (YAR), cabin air temperature (CAT)] by optimizing the vectors [engine operating point (EOP), cabin air temperature operating point (CATOP)], obliging the driver’s commands in real time. The IVDM activates the adaptive cruise control (ACC) feature when triggered; thus, longitudinal acceleration (LOT) is automatically determined by the ACC controller, and the parameters [lateral acceleration (LAT), yaw rate (YAR)] are estimated by the defined mathematical models assuming ideal steering behavior (ISB). The prediction of [adaptive cruise control set speed profile (ACCSSP), cabin air temperature set profile (CATSP)] was done by applying the optimal engine operating conditions (EOC) criteria on the predicted parameters [EOP, CATOP]. Nonlinear autoregressive network with exogenous inputs (NARX) DL models were developed to map the vehicle-level vectors (VLV) and [EOP, CATOP], whose performance was validated using a traditional statistical measures vector (STMV). The quantification of the computational model was performed by comparing the engine operating conditions (EOC) parameters for constant and predicted [ACCSSP, CATSP] and analyzing the [instantaneous engine efficiency (IEE), instantaneous engine map (IEM)] using the single test vehicle 2020 Cadillac CT5. The results were satisfactory, and this concept could develop into a new feature in the vehicle.

Chapter 11 Future Work

This research was performed with real-time datasets and valid assumptions were taken to develop the concept of the new drive mode. The validation was conducted with specific limitations which produced best results as described in the Chapter 9. Hence in this chapter, the following ideas were proposed which could augment the deployment of the Intelligent Vehicle Drive Mode (IVDM).

11.1 Extended Validation — Multiple Vehicle Lines

The computational model of IVDM validated the vehicle engine performance (VEP) criteria using the elements [engine operating point (EOP), cabin air temperature operating point (CATOP)] for the internal combustion engine (ICE)-driven segment with a single test vehicle, a 2020 Cadillac CT5, under normal driving conditions. As future work, the validation could be enhanced, including multiple vehicle lines, conducting tests for critical scenarios of mountain regions (> 14% slope), and considering slip and extreme weather conditions (EAT > 85 °F or < 25 °F). Also, the concept of Intelligent Vehicle Drive Mode (IVDM) could be extended with new criteria for road segments of either parking lots or arterial roads (vehicles speed < 25 miles per hour (MPH)), whose effect on engine operating conditions (EOC) is insignificant. Also, the quantification was done with 10-second snippets, for the test cases that showed lower conformance of results for the parameters [IFCR, distance]. Extended time period (1 hour) or distance (50 miles) segments can be selected to evaluate the efficacy of the proposed model.

11.2 Enhancing the Deep Learning Model — Additional Parameters

In this research, the environmental factors [humidity (HUM - %rh), absolute wind velocity vector (WIND - [$\underline{W_x}$+ $\underline{W_y}$] m.s^{-1}, atmospheric pressure (ATP - N.m^{-2})], HVAC elements [engine fan speed, power, Nusselt number] were not included in the DL model. The valid assumptions that include insensitivity of gasoline fuel [calorific Value (C_v), density (ρ_f)] due to pressure and temperature changes and invariant CATSP to predict ACCSSP were undertaken to simplify the analytical approach. Also, built-in MATLAB functions with default properties were utilized to develop deep learning (DL) models. Therefore, the analysis can be extended by considering all the affecting parameters on VEP, and customized deep learning (DL) models could be developed for each vehicle model's data to enhance prediction precision.

11.3 Optimization Criteria — Priority Index

The optimal performance criteria were defined with basic relations between the vector elements [EOP, CATOP] to simplify the analysis. Therefore, enhanced vehicle engine performance (VEP) criteria could be defined with categorical allocation of the priority index depending on the dynamic state of the vehicle, e.g., HVAC elements [EST (°F), ACRFP (PSI)] have more priority in extreme climatic conditions when EAT > 80 °F or EAT < 25 °F, higher IET is required for the terrains with larger elevation coefficients (e), and smoothness measure of the EOP vector is necessary for uneven terrain. Additionally, along with the performance elements, the optimization criteria could be enhanced by including the engine and powertrain parameters reflecting vehicle health, i.e., durability, reliability, and rate of wear and tear of the engine components can be defined for the vehicles with the odometer reading > 80,000 miles.

11.4 Generating Smooth Profiles — [ACCSSP, CATSP]

The failure soft action was implemented to generate unique [adaptive cruise control set speed profile (ACCSSP), cabin air temperature set profile (CATSP)], which produced satisfactory results of augmented engine operating conditions (EOC). However, the generated profile might not be the only optimal solution, and basic iterative analysis was adopted to estimate [eligible vehicle speeds (EVS), eligible vehicle cabin air temperatures (EVC)]; further research could ameliorate the results by developing an enhanced algorithm (e.g., reinforcement model adapting the driver behavior).

11.5 Feature Development — Further Steps

Feature development is a multi-stage process, and as the next step of this work, the plant simulation model controls algorithm, and software integration followed by validation could be deployed as shown in the Figure 26. Also, an interface could be developed between this drive mode (IVDM) and integrated path planning algorithms of autonomous systems to enhance driving behavior.

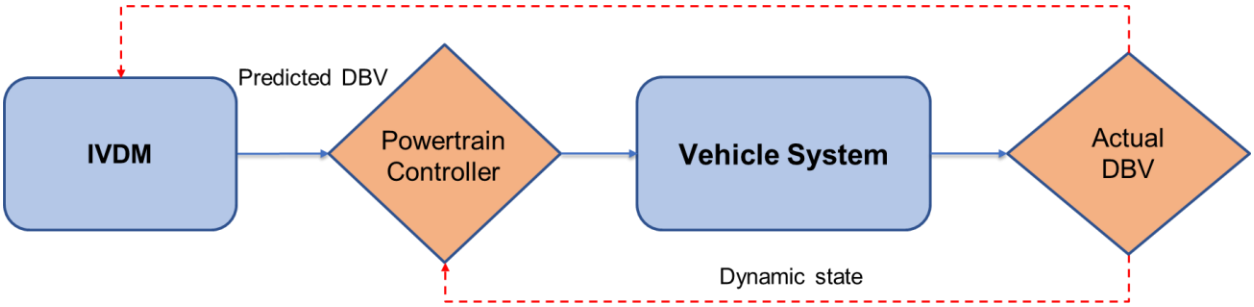

Figure 26: Future work: Electric Vehicle — IVDM Proposed powertrain controls

11.6 Electric Vehicle Implementation

The emergence of electric and autonomous vehicles has triggered a new research path for the automotive sector in recent years. Hence, IVDM could be extended for the components of electric vehicles by defining new performance criteria for [battery operating point (BOP), motor operating point (MOP), inverter operating point (IOP), HVAC], that enhance the operating conditions of [battery, motor]. The deep learning (DL) model applicable to electrical vehicles is shown in Figure

27, and a brief description is presented in the following sections. Similar to the internal combustion engine (ICE) vehicles, substantial validation can be performed with multiple electric vehicle test vehicle segments (e.g., 2023 Cadillac Lyriq, Chevrolet Bolt/Volt, 2024 Chevrolet Silverado pickup truck, 2024 Chevrolet Equinox/Blazer) to enhance the efficacy of the proposed concept.

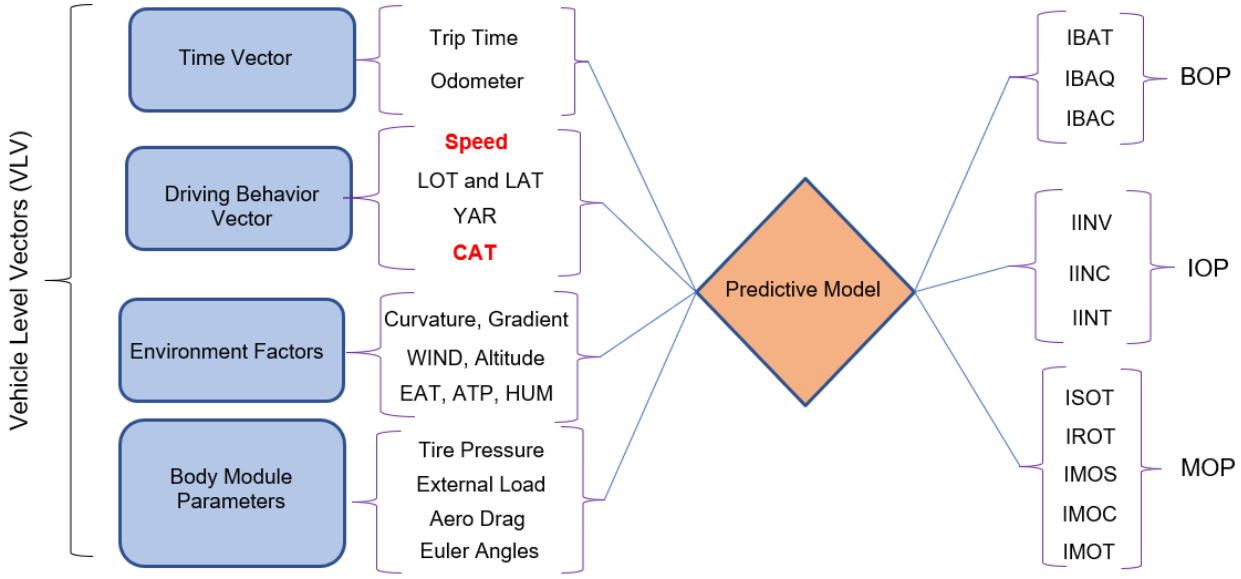

Figure 27: Future work: Electric Vehicle — IVDM Proposed predictive model

11.7 Electric Vehicle — Analysis

Electric vehicles are zero-emission systems propelled by the battery pack module and driven by electric motors (single or multiple). The internal combustion engine (ICE) driven vehicle has more than three thousand (3000) moving components in the powertrain, whereas electric vehicles are less complex, consisting of less than three hundred (300) parts which reflect a simpler design. The analogous elements of the electric vehicle operating point include three vectors [motor operating point (MOP), inverter operating point (IOP), battery operating point (BOP)], similar to EOP [IET, IES, IFCR] [108]. The MOP consists of the parameters [instantaneous motor torque (IMOT), instantaneous motor speed (IMOS), instantaneous rotor temperature (IROT), instantaneous stator temperature (ISOT)], which needs to be calibrated for every vehicle line. In the recent

developments of electrical machines, direct current motors are obsolete due to the requirements of additional maintenance (e.g., replacing brushes at regular intervals). Therefore, alternating current motors have gained more importance in practical applications (e.g., Tesla Model S: three-phase induction motor; 1300 Nm of torque; 615 kW of power) and the torque transmission model was shown in Figure 28.

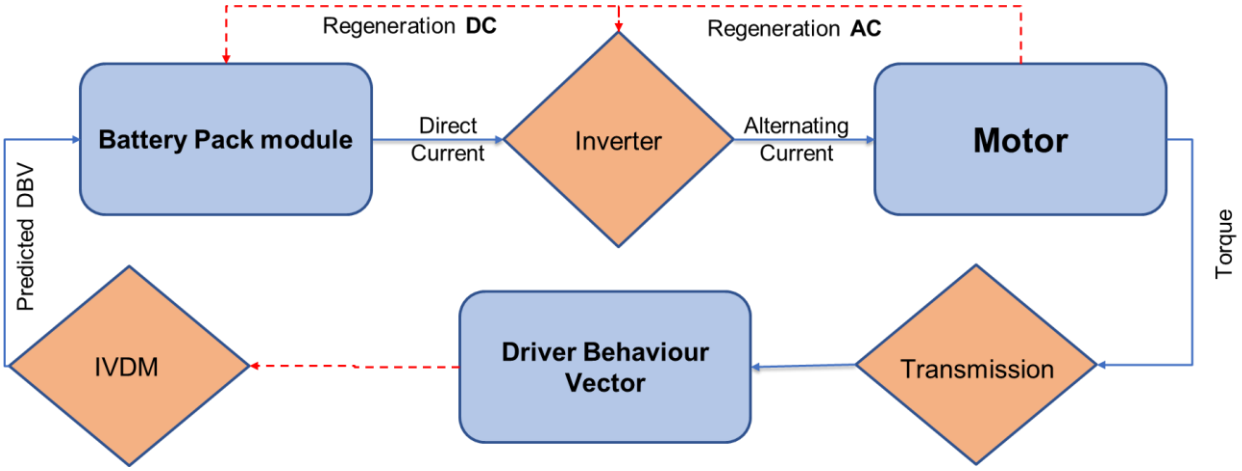

Figure 28: Future work: Electric Vehicle — IVDM Torque transmission

In an electric vehicle system, the direct current is discharged by the battery, and is fed into the motor as alternating current converted by the inverter [108]. Thus, BOP is an additional operating parameter intrinsic to the electric vehicle and defined with the elements [instantaneous battery charge (IBAQ), instantaneous battery current (IBAC), instantaneous battery temperature (IBAT)]. The inverter converts the direct current to alternating current under normal driving conditions, and during the braking process, a regenerative methodology is triggered, and alternating current generated by the motor is fed into the inverter, which recharges the battery. Thus, inverter operating point (IOP) was defined with [instantaneous inverter voltage (IINV), instantaneous inverter current (IINC), instantaneous inverter temperature (IINT)]. Therefore, minimal loss of energy is desired during the torque transmission phenomena, and hence the applicable optimization criteria for all the parameters are defined in the following sub-chapters.

11.8 Electric Vehicle — Optimization Criteria

11.8.1 Battery Thermal Management

In real-time, the dynamics of the Lithium-ion battery encounters a generic scenario where the anode can discharge into the electrolyte, which could cause a short circuit and potentially reduce the capacity of the battery. Hence, to enhance the performance, the battery pack module must be maintained in the range of allowable temperatures (Ideal IBAT range = [71 77] °F), which is achieved by the thermal management system. In electric vehicles CAT is maintained by the heating element - instantaneous heating element temperature (IHEAT), which extracts direct current from the battery and discharges heat to the vehicle cabin. The flow model of the thermal energy exchange for the electric vehicle was shown in Figure 29. Similar to Figure 7, the heat exchange between the components is shown by the red colored connecting elements, whereas blue color corelates to cooling.

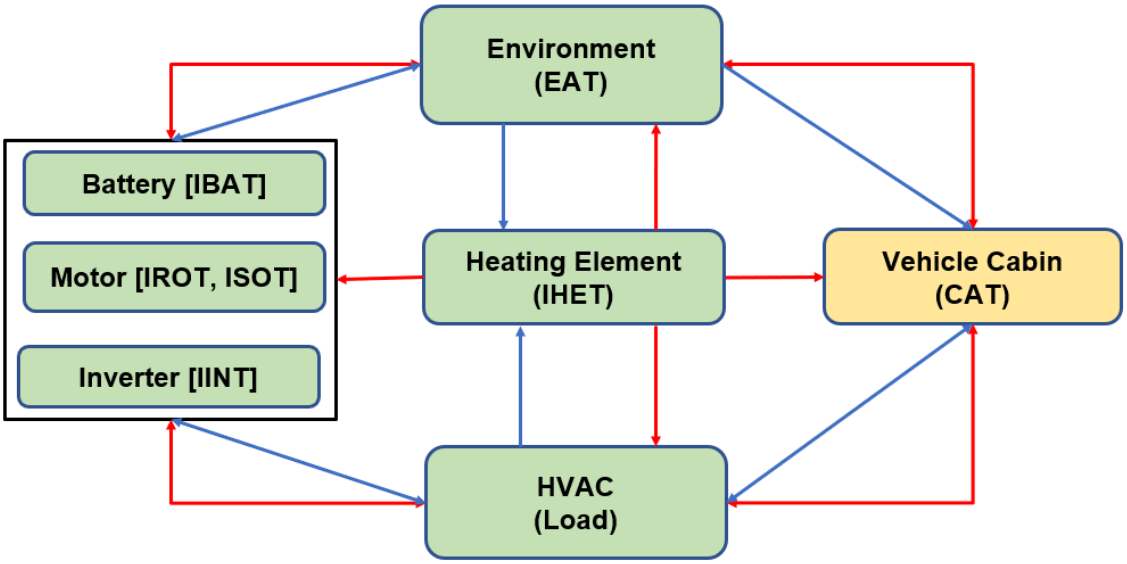

Figure 29: Future work: Electric Vehicle — Heat exchange

11.8.2 Motor Thermal Management

The electric motor generates the required torque with alternating current as input, which is affected by the earth's magnetic field and thus the altitude of operation. The firm Berman Motors developed

an empirical relation to estimate the optimal threshold for instantaneous stator temperature (ISOT) based on the altitude (Km) of operation (ALT > 1 Km), as shown in equations (29)–(30) (Figure 30). The parameter IROT > ISOT in every generic scenario and empirical relationship for optimal IROT is still under investigation by the researchers.

$$\text{ISOT} = \frac{3ALT^3}{5} - \frac{9ALT^2}{2} - \frac{216ALT}{25} + \frac{583}{5} \ ^\circ\text{F} \quad (4 \text{ Km} \geq \text{ALT} \geq 1 \text{ Km}) \qquad (29)$$

$$\text{ISOT} = 104 \ ^\circ\text{F} \ (\text{ALT} \leq 1 \text{ Km}) \qquad (30)$$

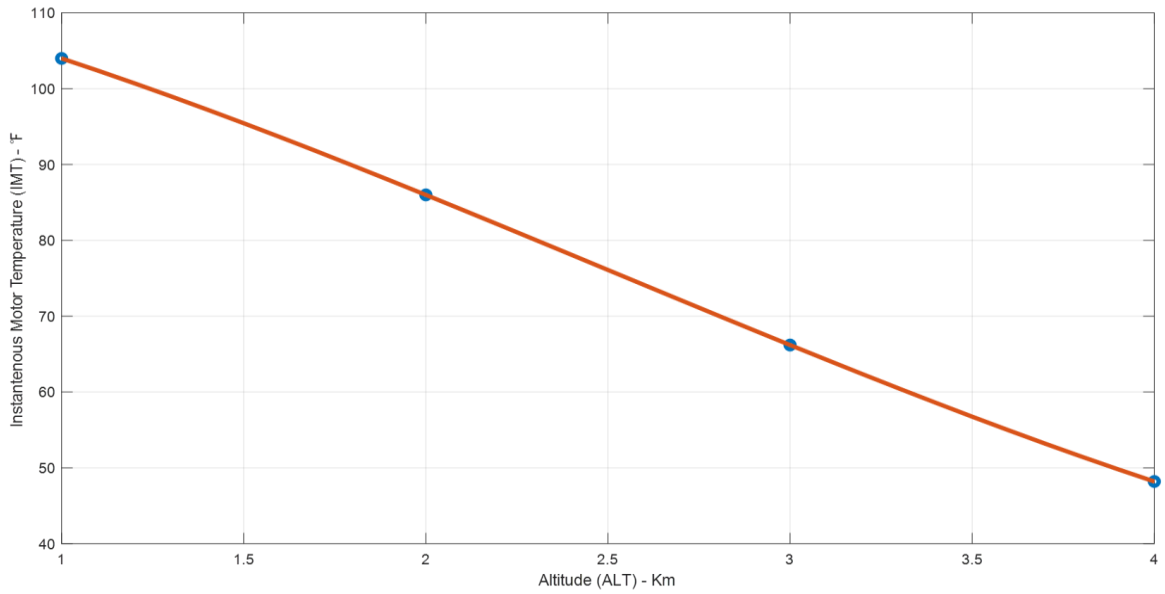

Figure 30: Future work: Electric Vehicle — Relationship [ISOT, ALT]

11.8.3 State of Battery Charge (Q)

The battery analytics and its performance measure directly affect the instantaneous battery charge (IBAQ). To maintain optimal battery health, the following are desired conditions. The battery charge rate is not a measurable parameter because of the pre-existing conditions of the battery and well-defined charging equipment. In contrast, the battery charge rate depends substantially on the dynamic state of the vehicle (e.g., feature usage, driver behavior, vehicle dynamics, environmental

factors). The battery charge rate is a differential function (equation 32); thus, lower values and smooth curve behavior in real-time are desired for augmented battery performance.

$$\text{Ideal IBAQ} = [\ Q_{min},\ Q_{max}] = [10\ 90]\ \% \tag{31}$$

$$\text{Ideal rate of IBAQ} = \frac{dQ}{dt}\ ;\ \text{If}\quad Q = [10\ 90]\ \%, \text{ then } \frac{dQ}{dt} < 0$$

$$\text{If}\quad Q \leq\ 10\ \%, \text{ then } \frac{dQ}{dt} < 0\ ;\ \text{If}\quad Q \geq 90\ \%, \text{ then } \frac{dQ}{dt} > 0 \tag{32}$$

11.8.4 Electric Motor

In the current scenario of electric vehicle segment of General Motors Inc., the following models had entered the phase of production [single motor (Chevrolet Volt), dual motor (Cadillac ESV), trio motor (Hummer Electric Vehicle)]. All the electrical motors produced are pre-defined with nominal operating conditions (e.g., 2022 Hummer Electric Vehicle: 255kW, 15400 Nm), and real-time actual operating points of the motor are affected by the dynamic state of the vehicle. Hence, the optimal functionality of the electric motor is achieved when the [instantaneous motor torque (IMOT), instantaneous motor power (IMOP), instantaneous motor frequency (IMOF)] are maintained in the vicinity of the nominal operating conditions as defined by the following three empirical parameters [M_T, M_P, M_F].

$$M_T\ =\ [abs(Nominal\ IMOT\ -\ Actual\ IMOT)\ ]\ ; \tag{33}$$

$$M_P\ =\ [abs(Nominal\ IMOP\ -\ Actual\ IMOP)\ ]\ ; \tag{34}$$

$$M_F\ =\ [abs(Nominal\ IMOF\ -\ Actual\ IMOF)\ ]\ ; \tag{35}$$

$$\text{Ideal MOP} = min\ [M_T, M_P, M_F]\ ; \tag{36}$$

11.8.5 Inverter

The inverter is the prominent component in the entire system, controlled by the built-in power electronics module. This component converts the direct current into alternating current based on

the demand; similarly, the alternating current is converted into the direct current during regenerative braking and charges the battery. During this exchange process, the module consumes a fraction of power for its functionality, and some part of the power is lost due to resistance (thermal loss) and the environment. The parameters $[P_{dc},\ P_{ac}]$ represent the power of the currents (direct and alternating); thus, minimal loss of power is an obvious criterion for inverter functionality. The relations $[n_{inC}, n_{inD}]$ reflect the efficiency of the inverter while battery charging (regeneration) and discharging.

$$\text{Regeneration: } n_{inC} = \frac{P_{dc}}{P_{ac}} \tag{37}$$

$$\text{Discharging: } n_{inD} = \frac{P_{ac}}{P_{dc}} \tag{38}$$

$$\text{Ideal Inverter functionality} = \text{Higher } [n_{inC}, n_{inD}] \tag{39}$$

11.8.6 Smoothness Measure Vector

The final criteria of all the measured battery and motor parameters include the desired smoothness behavior of the curves plotted in real-time. Hence, the smoothness measure vector (SMV) = [R^2, Adjusted R^2, Sum of squares error (SSE), root mean square error (RMSE)] defined in Chapter 4 needs to be estimated for the proposed electric vehicle operating point EVOP = [MOP, IOP, BOP].

Appendices

Appendix A

Tables: Datasets—Cadillac Test Vehicle Segment (ICE)

Parameters	Data Set 1			Data Set 2		
Inputs	**Mean**	**Deviation**	**Variance**	**Mean**	**Deviation**	**Variance**
Odometer (km)	12723	7.000	0.00055	12750.47	7.321	0.0006
Speed (MPH)	70.092	1.184	0.0169	69.8071	2.529	0.0362
Longitudinal acceleration (m.s^{-2})	-0.0092	0.144	-15.755	0.0433	0.253	5.8505
Lateral acceleration (m.s^{-2})	0.0174	0.288	16.5578	-0.0313	0.300	-9.6047
Yaw rate (deg.s^{-1})	0.217	0.831	3.81748	0.0001	0.763	6157.353
Cabin air temperature (°F)	68.786	0.329	0.0048	68.899	0.149	0.0022
External air temperature (°F)	39.225	0.301	0.0077	40.819	0.653	0.0160
Tire Pressure Left Front (kPa)	241.263	2.444	0.01013	240.850	1.636	0.0068
Tire Pressure Left Rear (kPa)	235.894	0.642	0.00272	235.683	1.080	0.0046
Tire Pressure Right Front (kPa)	243.69	1.070	0.00439	243.440	1.387	0.0057
Tire Pressure Right Rear (kPa)	235.25	1.560	0.00664	234.195	1.990	0.0085
Outputs	**Mean**	**Deviation**	**Variance**	**Mean**	**Deviation**	**Variance**
IET (Nm)	149.93	60.210	0.40159	158.333	87.714	0.554
IES (rad.s^{-1})	183.151	7.129	0.03893	195.442	31.653	0.162
IFCR (1E-8 m^3s^{-1})	265.289	90.471	0.34103	311.094	177.058	0.569
EST (°F)	204.996	0.869	0.00424	204.797	0.701	0.003
ACRFP (PSI)	39.517	1.038	0.02627	41.442	1.042	0.025

Table 18: 2019 Cadillac XT6— (Date: March 11, 2020)

Parameters	Data Set 1			Data Set 2		
Inputs	**Mean**	**Deviation**	**Variance**	**Mean**	**Deviation**	**Variance**
Odometer (km)	30343.02	0.426	0.000	30308.69	0.700	0.000
Speed (MPH)	74.541	6.427	0.086	72.194	2.719	0.038
Longitudinal acceleration (m.s^{-2})	0.254	0.268	1.053	-0.109	0.151	-1.388
Lateral acceleration (m.s^{-2})	0.049	0.245	4.960	0.109	0.215	1.968
Yaw rate (deg.s^{-1})	0.121	0.573	4.749	-0.247	0.398	-1.615
Cabin air temperature (°F)	69.000	0.000	0.000	70.000	0.000	0.000
External air temperature (°F)	83.355	0.215	0.003	85.612	0.782	0.009
Tire Pressure Left Front (kPa)	227.310	0.000	0.000	227.310	0.000	0.000
Tire Pressure Left Rear (kPa)	248.000	0.000	0.000	248.000	0.000	0.000
Tire Pressure Right Front (kPa)	227.310	0.000	0.000	227.310	0.000	0.000
Tire Pressure Right Rear (kPa)	248.000	0.000	0.000	248.000	0.000	0.000
Outputs	**Mean**	**Deviation**	**Variance**	**Mean**	**Deviation**	**Variance**
IET (Nm)	105.647	71.676	0.678	130.339	62.899	0.483
IES (rad.s^{-1})	196.371	15.530	0.079	186.821	7.514	0.040
IFCR (1E-8 m^3s^{-1})	234.445	142.880	0.609	231.247	99.410	0.430
EST (°F)	200.499	1.979	0.010	198.760	3.202	0.016
ACRFP (PSI)	108.982	2.256	0.021	106.842	2.062	0.019

Table 19: 2021 Cadillac CT4— (Date: August 07, 2020)

Parameters	Data Set 1 (AWD)			Data Set 2		
Inputs	**Mean**	**Deviation**	**Variance**	**Mean**	**Deviation**	**Variance**
Odometer (km)	34394.04	0.662	0.000	13001.92	0.889	0.000
Speed (MPH)	75.985	1.039	0.014	72.764	1.979	0.027
Longitudinal acceleration (m.s^{-2})	-0.001	0.102	-69.281	0.080	0.256	3.206
Lateral acceleration (m.s^{-2})	-0.047	0.237	-5.035	0.036	0.125	3.440
Yaw rate (deg.s^{-1})	-0.346	0.528	-1.525	-0.210	0.496	-2.359
Cabin air temperature (°F)	71.000	0.000	0.000	70.000	0.000	0.000
External air temperature (°F)	76.993	0.564	0.007	90.921	0.768	0.008
Pitch (rad)	-0.001	0.001	-0.975	0.006	0.002	0.380
Roll (rad)	0.003	0.000	0.000	0.008	0.000	0.000
Tire Pressure Left Front (kPa)	248.000	0.000	0.000	248.000	0.000	0.000
Tire Pressure Left Rear (kPa)	248.000	0.000	0.000	248.000	0.000	0.000
Tire Pressure Right Front (kPa)	248.000	0.000	0.000	248.000	0.000	0.000
Tire Pressure Right Rear (kPa)	248.000	0.000	0.000	248.000	0.000	0.000
Outputs	**Mean**	**Deviation**	**Variance**	**Mean**	**Deviation**	**Variance**
IET (Nm)	268.991	41.284	0.153	237.077	63.279	0.267
IES (rad.s^{-1})	173.451	4.363	0.025	165.538	4.279	0.026
IFCR (1E-8 m^3s^{-1})	454.373	68.957	0.152	398.614	93.198	0.234
EST (°F)	200.444	2.289	0.011	204.594	4.690	0.023
ACRFP (PSI)	119.427	2.489	0.021	196.758	3.172	0.016

Table 20: 2021 Cadillac Escalade ESV — (Date: August 11, 2020)

Parameters	ACC Speed [25 40] MPH			ACC Speed [40 55] MPH		
Inputs	**Mean**	**Deviation**	**Variance**	**Mean**	**Deviation**	**Variance**
Absolute time (s)	3807.133	1922.575	0.505	4182.933	1968.170	0.471
Odometer (km)	15230.66	44.699	0.003	15239.96	45.639	0.003
Speed (MPH)	34.433	4.231	0.123	47.734	4.659	0.098
Longitudinal acceleration (m.s^{-2})	0.411	0.582	1.415	0.260	0.441	1.698
Lateral acceleration (m.s^{-2})	0.352	0.303	0.861	0.348	0.353	1.016
Yaw rate (rad.s^{-1})	0.009	0.024	2.646	0.008	0.021	2.495
Cabin air temperature (°F)	66.000	0.000	0.000	66.000	0.000	0.000
External air temperature (°F)	85.501	3.770	0.044	86.337	3.434	0.040
Tire Pressure Left Front (kPa)	270.424	2.822	0.010	269.869	3.170	0.012
Tire Pressure Left Rear (kPa)	270.886	2.307	0.009	270.885	2.570	0.009
Tire Pressure Right Front (kPa)	267.259	2.961	0.011	266.713	3.259	0.012
Tire Pressure Right Rear (kPa)	270.081	3.164	0.012	270.792	3.007	0.011
Outputs	**Mean**	**Deviation**	**Variance**	**Mean**	**Deviation**	**Variance**
IET (Nm)	119.135	69.890	0.587	142.408	78.788	0.553
IES (rad.s^{-1})	199.642	66.334	0.332	210.297	53.398	0.254
IFCR (1E-8 m^3s^{-1})	277.618	199.441	0.718	324.459	190.869	0.588
EST (°F)	199.262	2.478	0.012	199.546	2.112	0.011
ACRFP (PSI)	156.398	18.163	0.116	164.076	15.808	0.096

Table 21: 2020 Cadillac CT5 — Dataset 1 (Date: June 16, 2020)

Parameters	ACC Speed [55 65] MPH			ACC Speed [65 75] MPH		
Inputs	**Mean**	**Deviation**	**Variance**	**Mean**	**Deviation**	**Variance**
Absolute time (s)	4773.918	2424.428	0.508	4620.057	2330.081	0.504
Odometer (km)	16042.450	33.226	0.002	16042.910	29.183	0.002
Speed (MPH)	60.451	2.774	0.046	68.834	2.536	0.037
Longitudinal acceleration (m.s^{-2})	0.114	0.330	2.902	0.021	0.269	13.035
Lateral acceleration (m.s^{-2})	0.388	0.414	1.065	0.387	0.442	1.143
Yaw rate (rad.s^{-1})	0.015	0.021	1.353	0.014	0.019	1.355
Cabin air temperature (°F)	84.250	3.709	0.044	85.353	2.194	0.026
External air temperature (°F)	72.850	0.989	0.014	72.992	1.000	0.014
Tire Pressure Left Front (kPa)	264.708	6.304	0.024	264.692	5.024	0.019
Tire Pressure Left Rear (kPa)	264.608	3.973	0.015	264.662	3.418	0.013
Tire Pressure Right Front (kPa)	262.423	7.459	0.028	263.400	6.077	0.023
Tire Pressure Right Rear (kPa)	262.869	7.223	0.027	264.923	4.024	0.015
Outputs	**Mean**	**Deviation**	**Variance**	**Mean**	**Deviation**	**Variance**
IET (Nm)	172.568	75.253	0.436	172.744	76.107	0.441
IES (rad.s^{-1})	198.841	45.060	0.227	209.786	38.033	0.181
IFCR (1E-8 m^3s^{-1})	347.000	176.180	0.508	360.484	160.091	0.444
EST (°F)	200.148	3.164	0.016	200.331	2.599	0.013
ACRFP (PSI)	175.395	14.489	0.083	173.653	19.962	0.115

Table 22: 2020 Cadillac CT5 — Dataset 2 (Date: June 16, 2020)

Parameters	ACC Speed [25 40] MPH			ACC Speed [40 55] MPH		
Inputs	**Mean**	**Deviation**	**Variance**	**Mean**	**Deviation**	**Variance**
Absolute time (s)	1580.287	783.077	0.496	1588.548	206.355	0.130
Odometer (km)	24875.92	12.858	0.001	24875.52	2.893	0.000
Speed (MPH)	34.747	4.831	0.139	46.602	3.800	0.082
Longitudinal acceleration (m.s^{-2})	0.111	0.487	4.388	-0.129	0.160	-1.239
Lateral acceleration (m.s^{-2})	0.269	0.201	0.748	0.198	0.210	1.062
Yaw rate (rad.s^{-1})	0.234	0.244	1.042	0.274	0.287	1.049
Cabin air temperature (°F)	74.746	4.628	0.062	74.375	7.544	0.101
External air temperature (°F)	39.664	1.039	0.026	39.954	1.225	0.031
Tire Pressure Left Front (kPa)	226.523	1.930	0.009	227.253	1.984	0.009
Tire Pressure Left Rear (kPa)	229.404	2.787	0.012	228.670	1.680	0.007
Tire Pressure Right Front (kPa)	248.317	3.511	0.014	250.345	2.399	0.010
Tire Pressure Right Rear (kPa)	227.405	2.628	0.012	227.787	1.980	0.009
Outputs	**Mean**	**Deviation**	**Variance**	**Mean**	**Deviation**	**Variance**
IET (Nm)	79.217	51.955	0.656	85.042	35.108	0.413
IES (rad.s^{-1})	185.691	60.608	0.326	144.195	7.987	0.055
IFCR (1E-8 m^3s^{-1})	174.504	150.452	0.862	125.877	49.408	0.393
EST (°F)	202.714	4.250	0.021	203.877	2.251	0.011
ACRFP (PSI)	49.462	4.939	0.100	47.960	1.814	0.038

Table 23: 2020 Cadillac CT5 — Dataset 3 (Date: February 25, 2021)

Parameters	ACC Speed [55 65] MPH			ACC Speed [65 75] MPH		
Inputs	**Mean**	**Deviation**	**Variance**	**Mean**	**Deviation**	**Variance**
Absolute time (s)	3018.585	1042.301	0.345	2648.426	202.247	0.076
Odometer (km)	24822.230	26.519	0.001	24813.59	6.433	0.000
Speed (MPH)	60.789	3.287	0.054	69.476	2.617	0.038
Longitudinal acceleration (m.s^{-2})	-0.135	0.209	-1.544	-0.170	0.150	-0.886
Lateral acceleration (m.s^{-2})	0.413	0.333	0.807	0.307	0.156	0.510
Yaw rate (rad.s^{-1})	1.049	1.112	1.060	0.779	0.312	0.400
Cabin air temperature (°F)	79.397	6.916	0.087	75.831	5.311	0.070
External air temperature (°F)	37.816	1.672	0.044	37.931	0.487	0.013
Tire Pressure Left Front (kPa)	248.338	3.060	0.012	247.232	1.939	0.008
Tire Pressure Left Rear (kPa)	226.759	3.717	0.016	226.654	3.352	0.015
Tire Pressure Right Front (kPa)	225.709	2.882	0.013	224.917	1.834	0.008
Tire Pressure Right Rear (kPa)	227.795	3.674	0.016	227.426	2.707	0.012
Outputs	**Mean**	**Deviation**	**Variance**	**Mean**	**Deviation**	**Variance**
IET (Nm)	121.307	49.420	0.407	128.956	43.276	0.336
IES (rad.s^{-1})	158.194	27.338	0.173	172.430	6.571	0.038
IFCR (1E-8 m^3s^{-1})	189.586	90.905	0.479	216.109	72.691	0.336
EST (°F)	200.331	3.881	0.019	198.797	4.055	0.020
ACRFP (PSI)	41.700	1.535	0.037	40.571	0.241	0.006

Table 24: 2020 Cadillac CT5 — Dataset 4 (Date: February 25, 2021)

Appendix B

Tables: Data Retrieval and VEP—Optimization Criteria

Road types	Speed Limits - MPH	Properties
Parking lot, critical points	[0 15]	No significant effect on EOP
Arterial local segments	[15 25]	No significant effect on EOP
Low curvatures	[15 25]	RRC = [8.34 42.57] m
Arterial connecting segments	[25 45]	Ideal zone: Higher IET
State ways	[45 65]	Green zone: Lower IFCR
Freeways	[65 85]	High-speed zone: Higher IES

Table 25: Categorization of road segments.

Body module	Driver behavior	Environmental factors	EOP	CATOP
Odometer	Speed and set CAT	EAT, ATP	IET	EST
Tire pressure and Load	LOT and LAT	HUM, WIND	IES	ACRFP
Vehicle type, Euler Angles	Yaw rate	Gradient, RRC	IFCR	CAT

Table 26: CAN data retrieved—Cadillac vehicle segment.

EAT (°F)	Higher limit (PSI)	EAT (°F)	Higher limit (PSI)
65	135	90	250
70	140	95	275
75	150	100	300
80	175	105	325
85	220	110	335

Table 27: ACS R134a refrigerant—ACRFP referral range.

Generic		Engine specific		Smoothness Measure - Spline fit	
Parameter	Condition	Parameter	Condition	Parameter	Condition
IET	Higher	ED	Lower	R^2/Adj R^2	Higher
IES	Higher	ESC	Higher	SSE	Lower
IFCR	Lower	ETC	Higher	RMSE	Lower

Table 28: Vehicle engine performance — Criteria.

Appendix C

Tables: Deep Learning [EOP, CATOP] — Performance of [NARX, LSTM]

NARX		LSTM	
Model Parameter	**Value**	**Model Parameter**	**Value**
Training Function	Levenberg-Marquardt backpropagation	Training Function	Stochastic Gradient Descent with Momentum Optimizer
Input Delays	1:2	Output Layer	Connected and Regression
Feedback Delays	1:2	Network Layer	LSTM
Hidden Layer Size	10	Input Layer	Sequence Input
Network	Open	Gradient Threshold	1
Dataset analysis	[70 % training, 30 % testing]	Dataset analysis	[70 % training, 30 % testing]
Performance	RMSE	Hidden Units	200

Table 29: Cadillac datasets — NARX and LSTM modelling parameters (MATLAB)

	NARX—DL Model Validation								
EOP	**IET**			**IES**			**IFCR**		
Data	RMSE	FOD	SNR	RMSE	FOD	SNR	RMSE	FOD	SNR
XT6 - Set 1	1.504	0.515	20.644	0.337	0.158	1.893	4.354	3.045	11.628
XT6 - Set 2	1.84	0.802	9.807	0.248	0.177	41.559	6.503	4.561	78.539
CT4 - Set 1	2.465	1.744	49.421	1.607	1.129	31.356	21.577	21.098	27.328
CT4 - Set 2	0.967	0.666	160.83	0.122	0.072	27.012	8.175	6.539	27.012
ESV - Set 1	2.415	1.723	53.748	0.26	0.179	39.937	15.072	13.034	26.963
ESV - Set 2	1.791	1.235	30.921	0.063	0.036	10.636	14.259	10.049	16.201
	LSTM—DL Model Validation								
EOP	**IET**			**IES**			**IFCR**		
Data	RMSE	FOD	SNR	RMSE	FOD	SNR	RMSE	FOD	SNR
XT6 - Set 1	24.059	10.096	47.943	1.301	0.225	36.399	31.402	13.458	40.790
XT6 - Set 2	18.515	6.0731	24.716	1.913	0.694	19.515	33.491	10.103	186.338
CT4 - Set 1	53.504	4.399	128.137	7.738	1.420	32.036	122.147	12.143	209.046
CT4 - Set 2	21.945	9.555	112.411	1.392	0.092	72.916	31.232	13.254	78.809
ESV - Set 1	49.151	9.599	415.063	6.240	0.825	69.872	69.086	20.667	72.669
ESV - Set 2	46.721	21.417	59.115	2.803	0.359	51.746	62.047	31.235	66.147

Table 30: Prediction of EOP—NARX and LSTM performance.

NARX—DL Model Validation									
CATOP				EST			ACRFP		
Data	ACCSSP	CAT (°F)	EAT (°F)	RMSE	FOD	SNR	RMSE	FOD	SNR
XT6 - Set 1	71	67	39.2	0.001	0.001	126.79	0.262	0.184	45.765
XT6 - Set 2	74	68	40.96	0.000	0.000	0.239	0.09	0.063	71.956
CT4 - Set 1	76	69	83.3	0.117	0.082	27.151	0.361	0.255	59.722
CT4 - Set 2	70	70	86	0.098	0.069	70.436	0.1	0.063	2.139
ESV - Set 1	75	71	77	0.058	0.041	13.827	0.22	0.155	37.714
ESV - Set 2	73	70	90.5	0.057	0.04	19.125	0.156	0.109	15.93
LSTM—DL Model Validation									
CATOP				EST			ACRFP		
Data	ACCSSP	CAT (°F)	EAT (°F)	RMSE	FOD	SNR	RMSE	FOD	SNR
XT6 - Set 1	71	67	39.2	0.000	0.000	0.000	1.266	0.235	639.558
XT6 - Set 2	74	68	40.96	0.000	0.000	0.000	0.313	0.080	50.129
CT4 - Set 1	76	69	83.3	0.690	0.096	162.252	3.030	0.329	831.615
CT4 - Set 2	70	70	86	0.587	0.075	102.061	0.216	0.070	217.073
ESV - Set 1	75	71	77	0.837	0.084	445.166	1.297	0.212	228.327
ESV - Set 2	73	70	90.5	0.557	0.106	162.946	0.422	0.113	78.275

Table 31: Prediction of CATOP—NARX and LSTM performance.

Appendix D

Tables: Deep Learning [EOP, CATOP]—Performance of [NARX]

NARX—DL Model				
EOP		ACCSSP (MPH)	CATOP- Set 1	CATOP- Set 2
ACCSSP (MPH)	Training		Training	Training
30	1–11082	35	1–1578	1–4842
40	1–24439	45	1–1913	1–4842
50	1–39191	55	1–5097	1–4842
60	1–54200	65	1–5563	1–4382
70	1–145925	75	1–2242	1–4382

Table 32: 2020 Cadillac CT5: Prediction of [EOP, CATOP] — Training sets

Data	NARX—DL Model Validation								
EOP	IET			IES			IFCR		
ACCSSP (MPH)	RMSE	FOD	SNR	RMSE	FOD	SNR	RMSE	FOD	SNR
30	1.654	1.080	39.247	0.485	0.269	2.984	11.881	9.122	164.660
40	1.100	0.734	33.074	0.116	0.053	119.413	8.645	6.361	44.122
50	0.993	0.708	5.980	0.044	0.017	2.714	10.426	7.472	193.144
60	1.337	0.883	8.191	0.136	0.038	0.957	9.130	6.444	985.731
70	0.948	0.660	90.595	0.033	0.016	15.063	5.341	4.122	6.365

Table 33: 2020 Cadillac CT5: Prediction of EOP—NARX performance.

EAT ≥ 65 °F			Data Set 1: NARX—DL Model Validation					
			EST			ACRFP		
ACCSSP (MPH)	CAT (°F)	EAT (°F)	RMSE	FOD	SNR	RMSE	FOD	SNR
35	67	83.30	2.206	1.587	5.107	14.002	10.561	16.135
45	65	80.375	1.817	1.429	7.118	10.815	7.439	12.112
55	66	70.205	1.131	0.835	11.140	4.668	2.931	4.442
65	68	80.942	1.082	0.7507	6.152	3.900	2.764	8.754
75	69	84.623	1.278	0.788	37.280	8.419	5.000	2.286

Table 34: 2020 Cadillac CT5: Prediction of CATOP—NARX performance (EAT > 65 °F).

EAT < 45 °F			Data Set 2: NARX—DL Model Validation					
			EST			ACRFP		
ACCSSP (MPH)	CAT (°F)	EAT (°F)	RMSE	FOD	SNR	RMSE	FOD	SNR
35	76	36.37	0.872	0.622	19.872	0.423	0.281	3.210
45	71	39.05	0.570	0.408	26.249	0.039	0.015	2.032
55	85	34.7	0.194	0.131	22.742	0.034	0.017	1.277
65	80	38.89	0.444	0.312	32.048	0.006	0.004	2.501
75	75	37.4	0.314	0.265	3.284	0.000	0.000	1.717

Table 35: 2020 Cadillac CT5: Prediction of CATOP—NARX performance (EAT < 45 °F).

Appendix E

Figures: Prediction of [EOP, CATOP] — [NARX, LSTM]

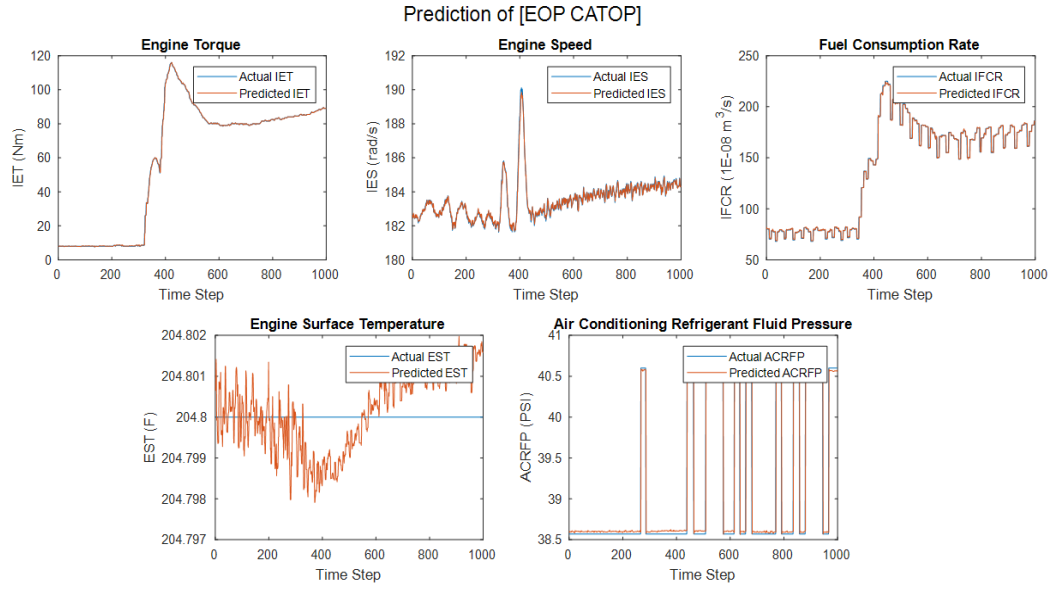

Figure 31: NARX Prediction of [EOP, CATOP] — 2019 Cadillac XT6, Dataset 1

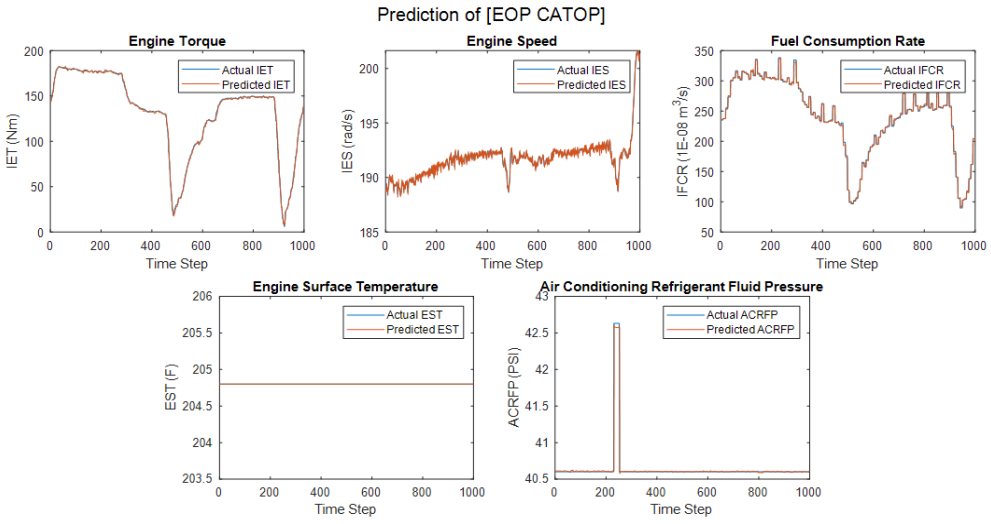

Figure 32: NARX Prediction of [EOP, CATOP] — 2019 Cadillac XT6, Dataset 2

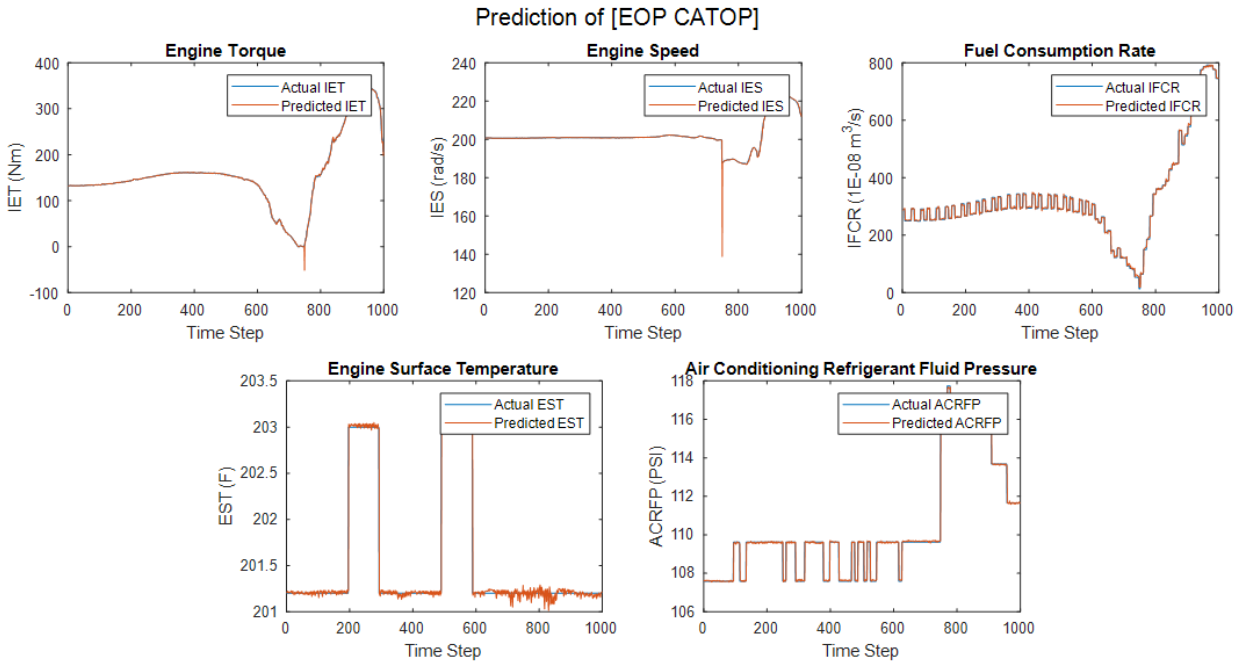

Figure 33: NARX Prediction of [EOP, CATOP] — 2021 Cadillac CT4, Dataset 1

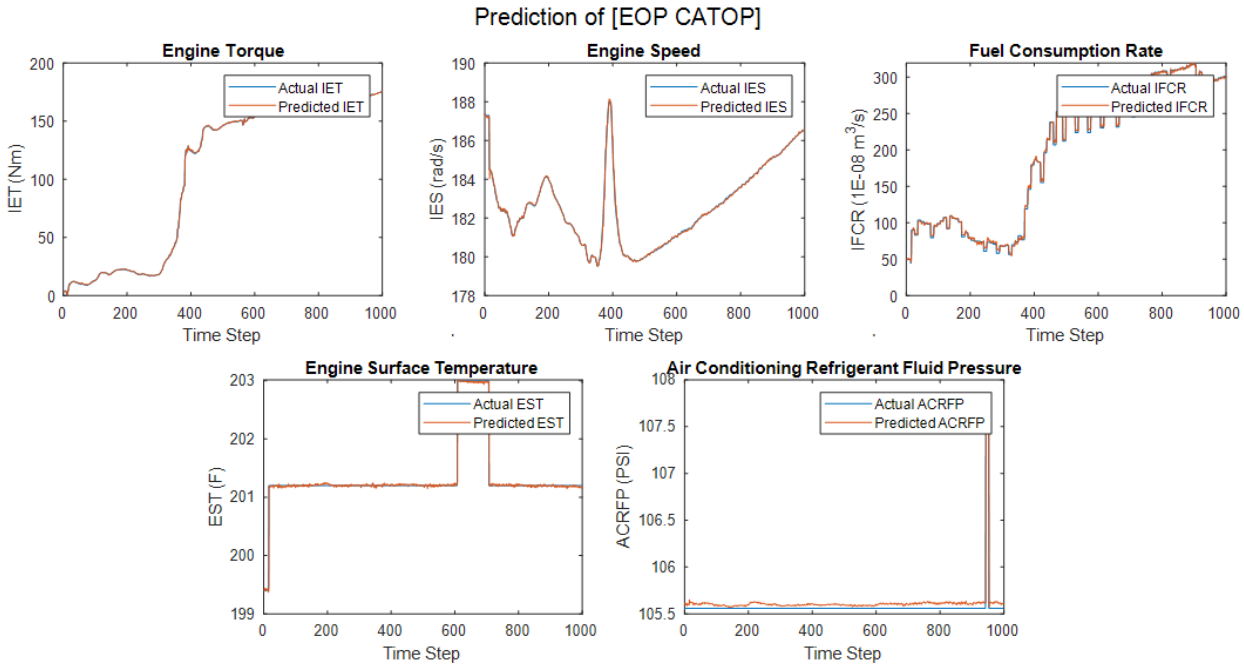

Figure 34: NARX Prediction of [EOP, CATOP] — 2021 Cadillac CT4, Dataset 2

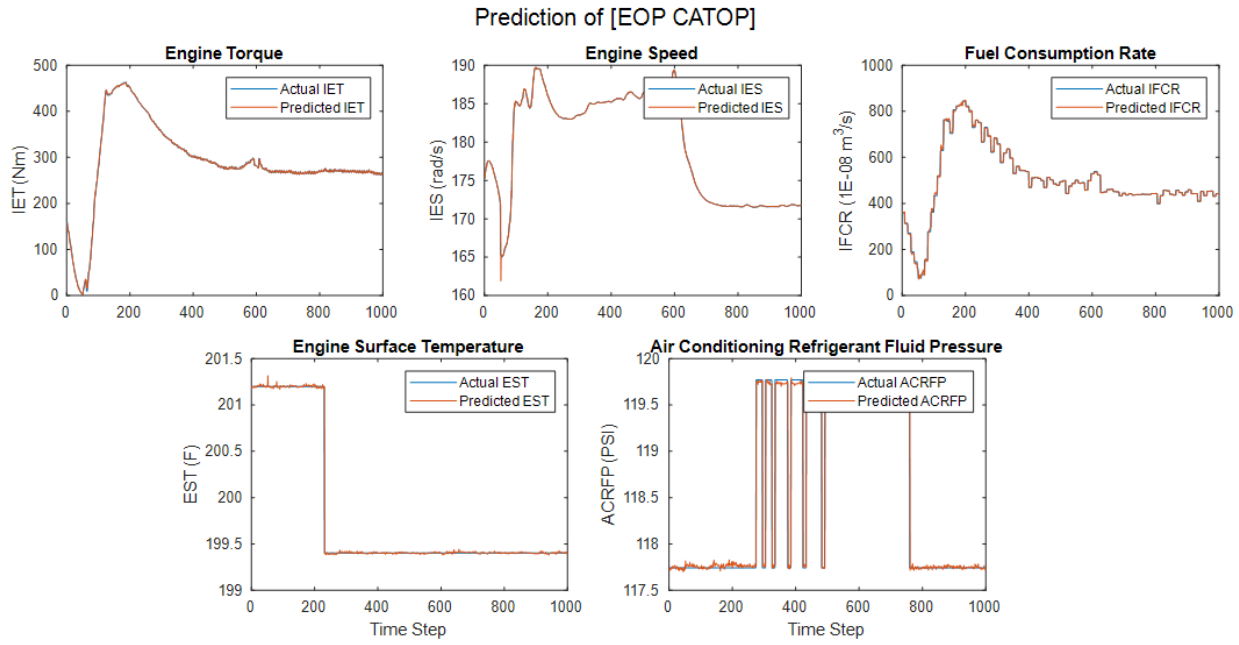

Figure 35: NARX Prediction of [EOP, CATOP] — 2021 Cadillac Escalade ESV, Dataset 1

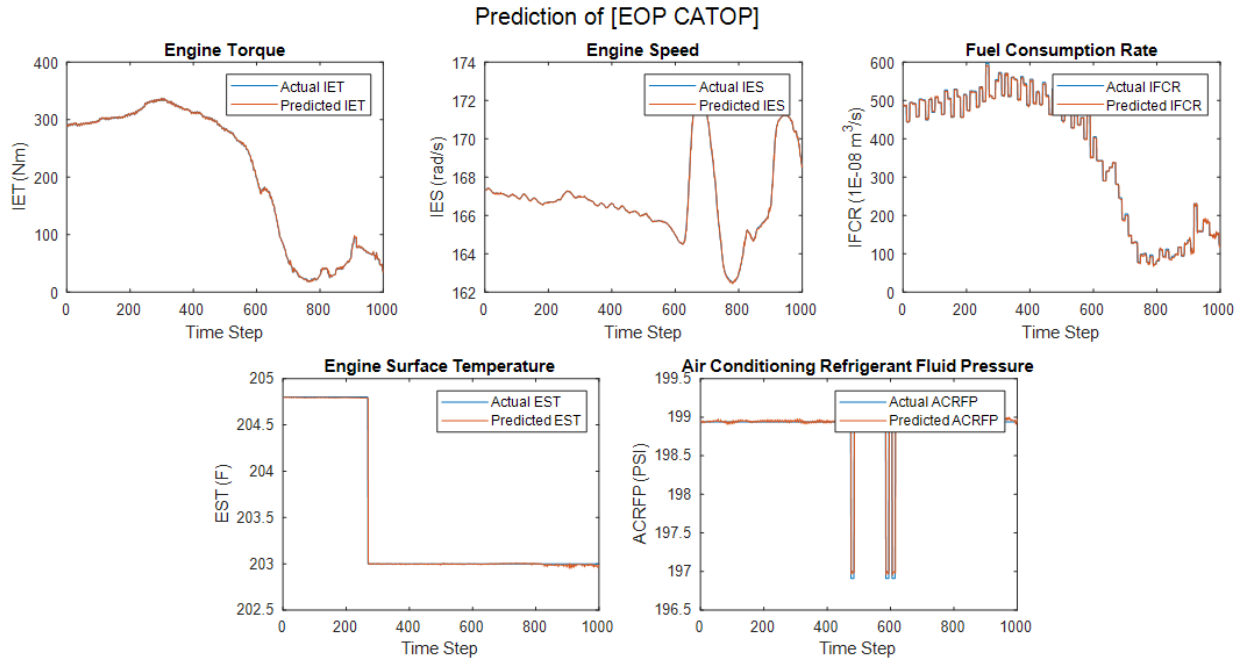

Figure 36: NARX Prediction of [EOP, CATOP] — 2021 Cadillac Escalade AWD, Dataset 2

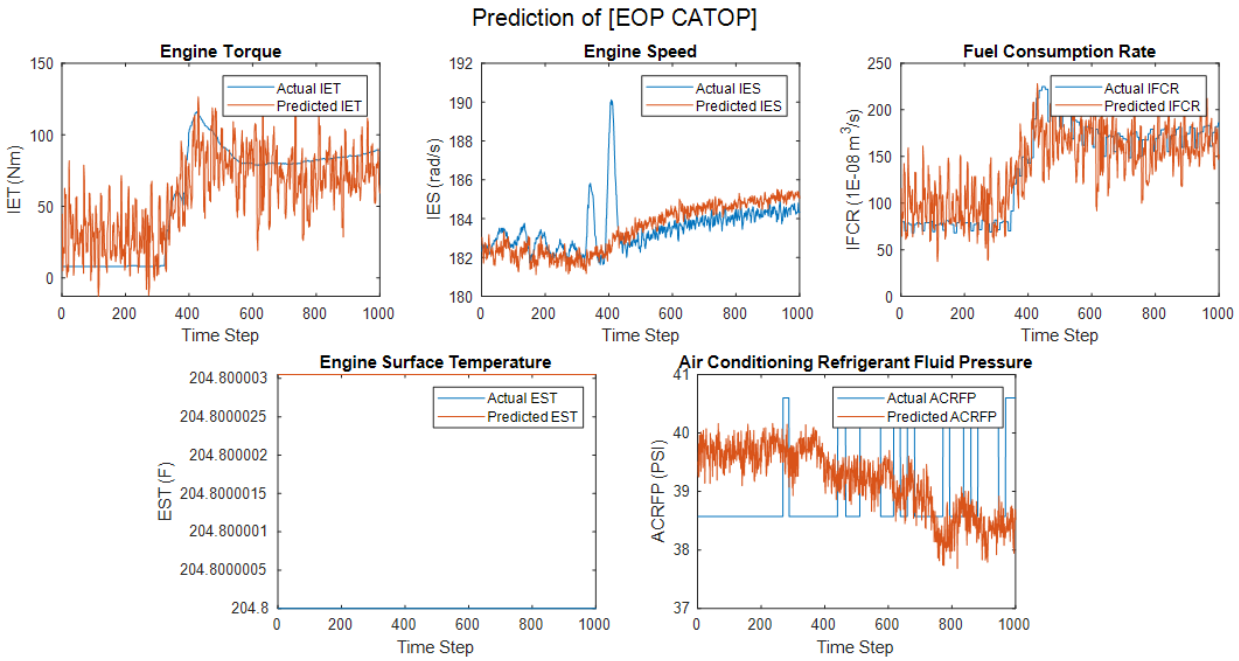

Figure 37: LSTM Prediction of [EOP, CATOP] — 2019 Cadillac XT6, Dataset 1

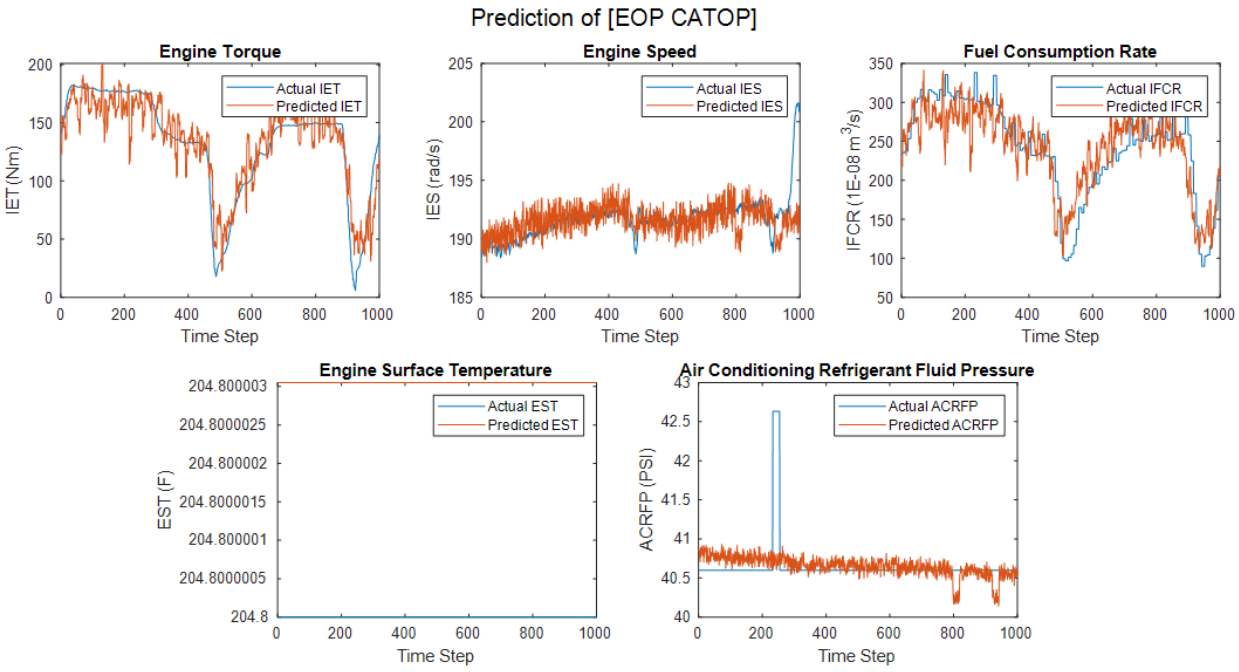

Figure 38: LSTM Prediction of [EOP, CATOP] — 2019 Cadillac XT6, Dataset 2

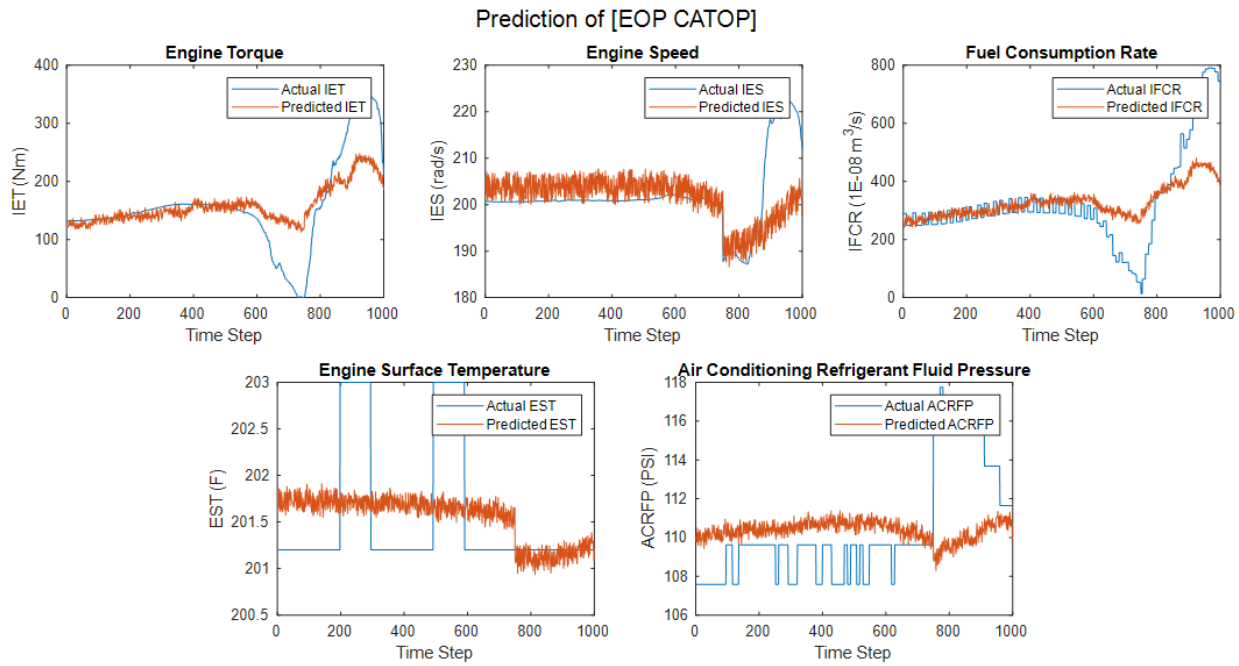

Figure 39: LSTM Prediction of [EOP, CATOP] — 2021 Cadillac CT4, Dataset 1

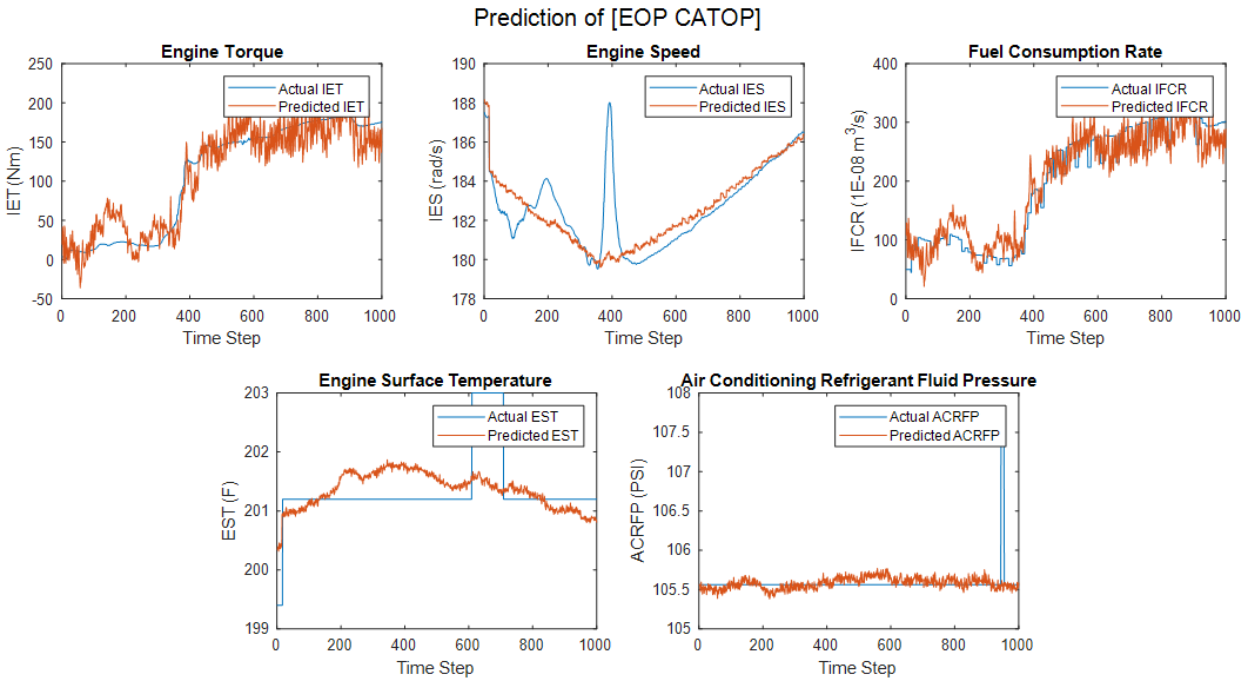

Figure 40: LSTM Prediction of [EOP, CATOP] — 2021 Cadillac CT4, Dataset 2

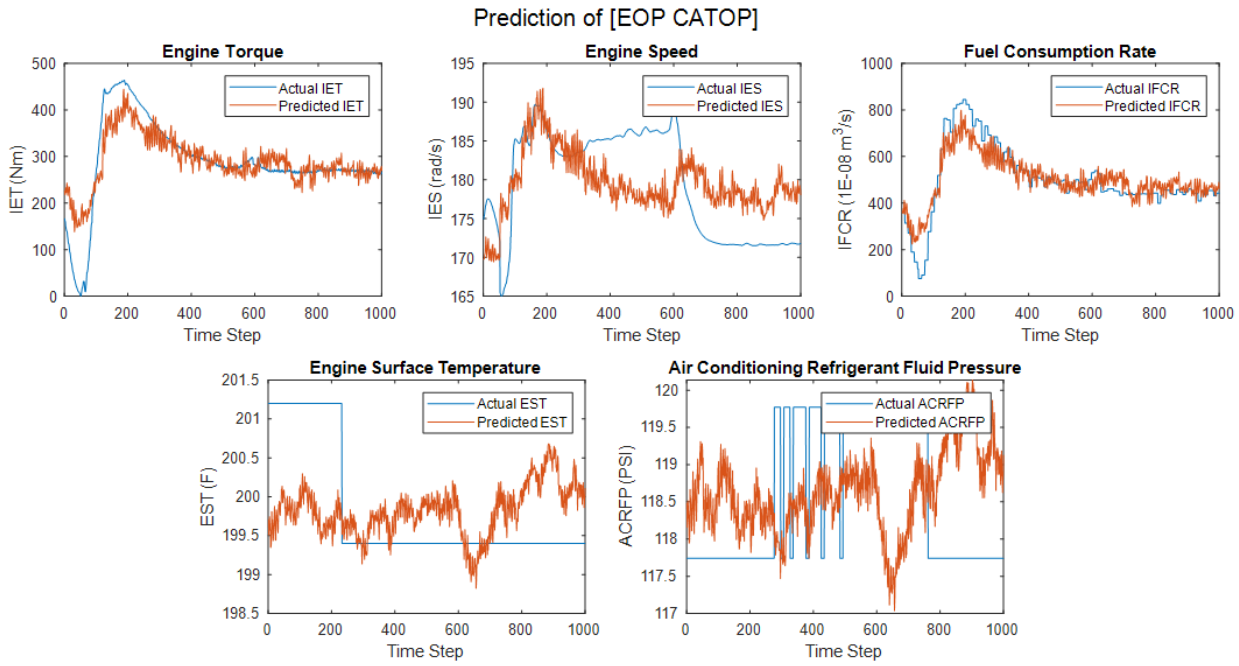

Figure 41: LSTM Prediction of [EOP, CATOP] — 2021 Cadillac Escalade ESV, Dataset 1

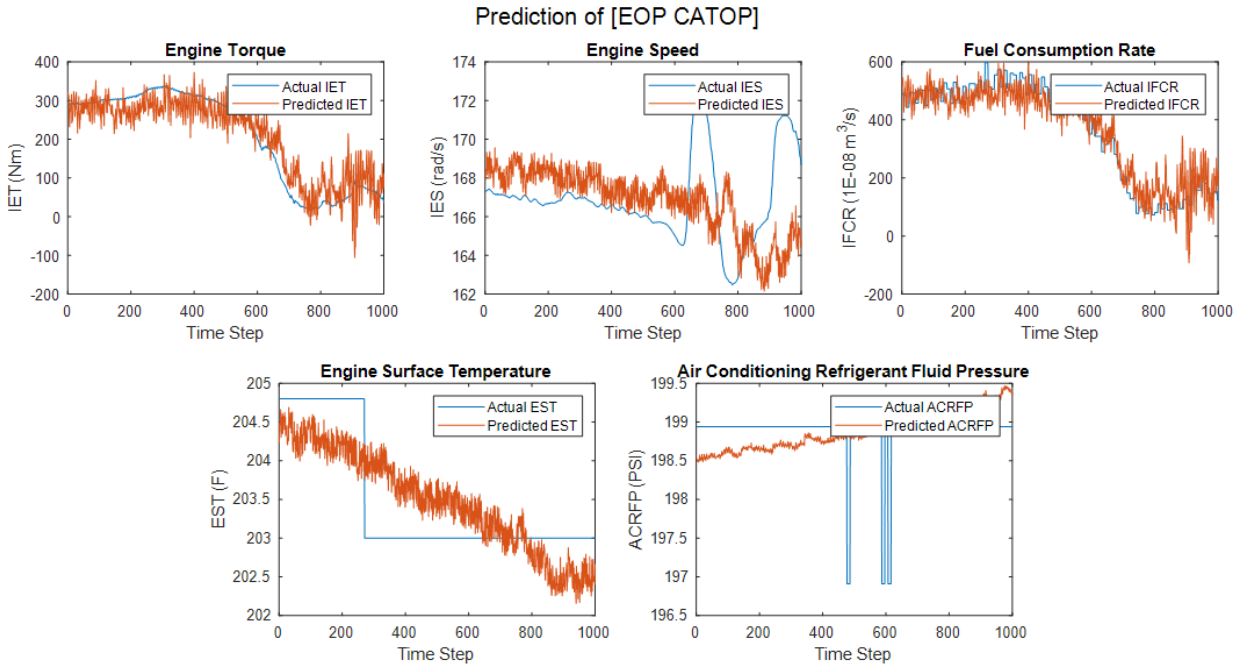

Figure 42: LSTM Prediction of [EOP, CATOP] — 2021 Cadillac Escalade AWD, Dataset 2

Appendix F

Figures: Prediction of [EOP]—2020 Cadillac CT5

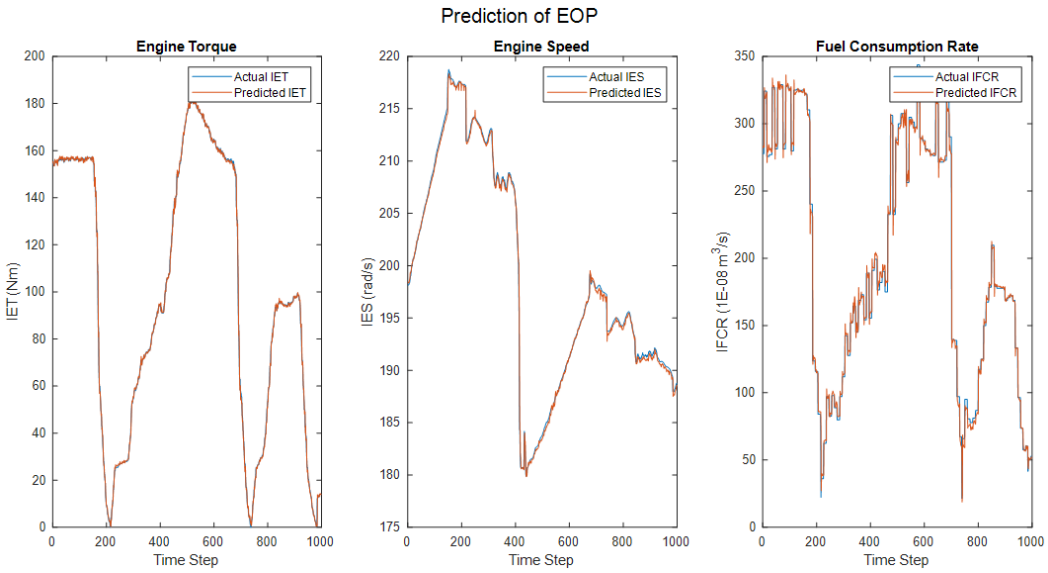

Figure 43: EOP — ACCSSP = 30 MPH

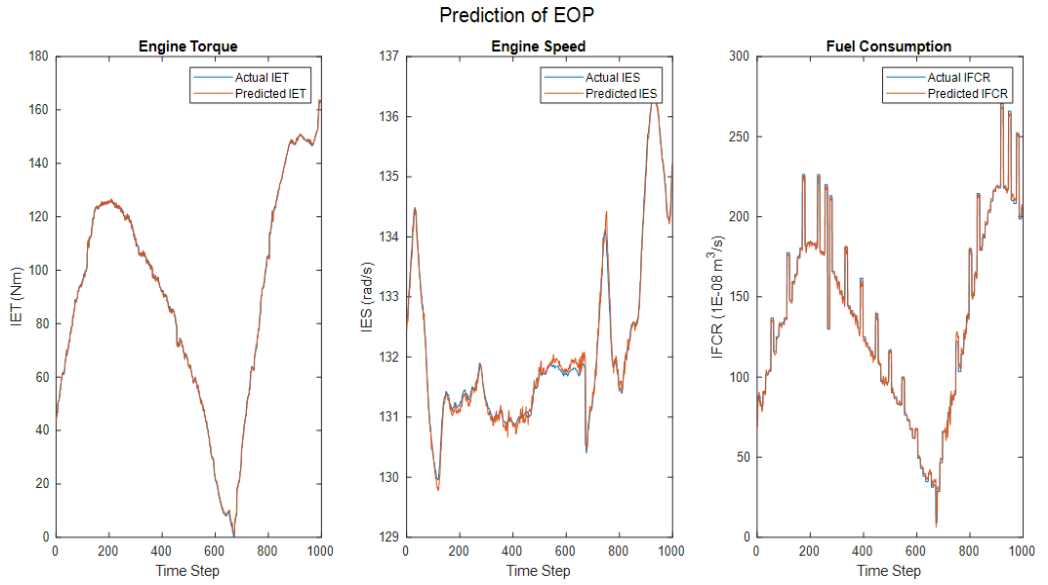

Figure 44: EOP — ACCSSP = 40 MPH

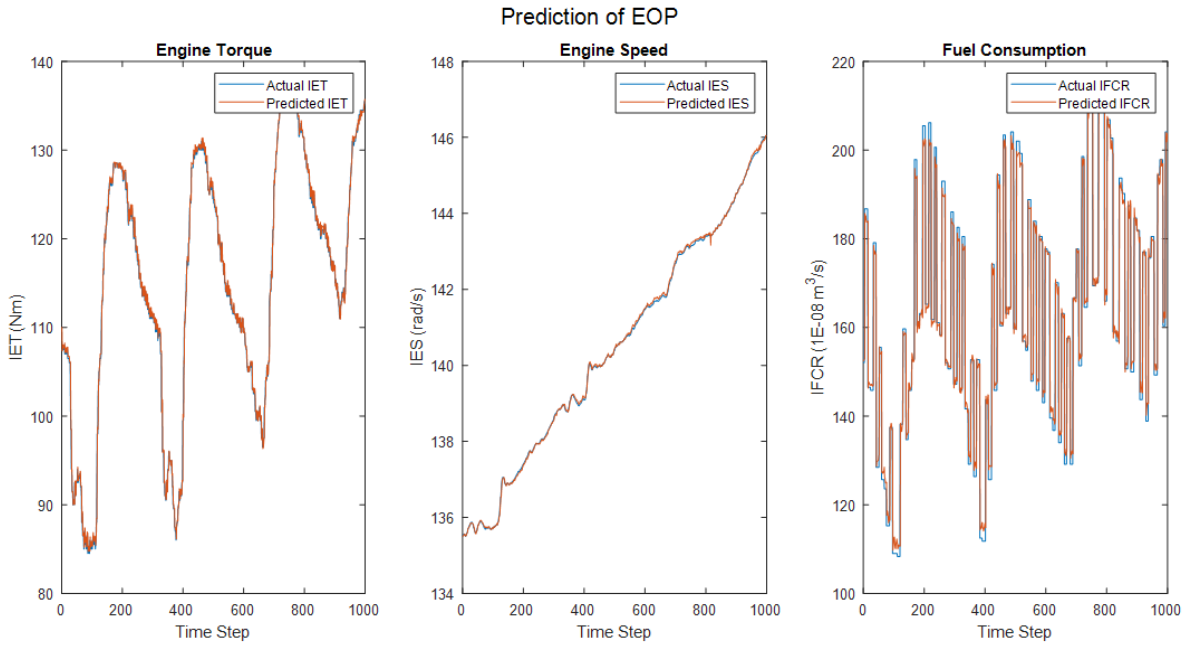

Figure 45: EOP — ACCSSP = 50 MPH

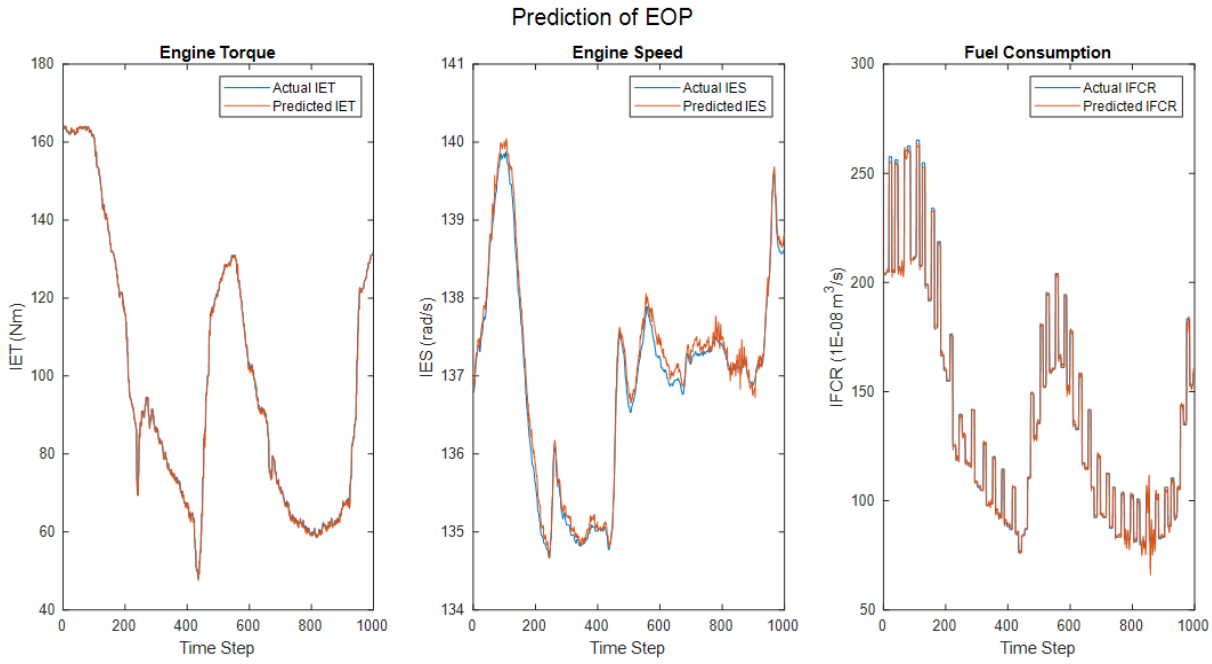

Figure 46: EOP — ACCSSP = 60 MPH

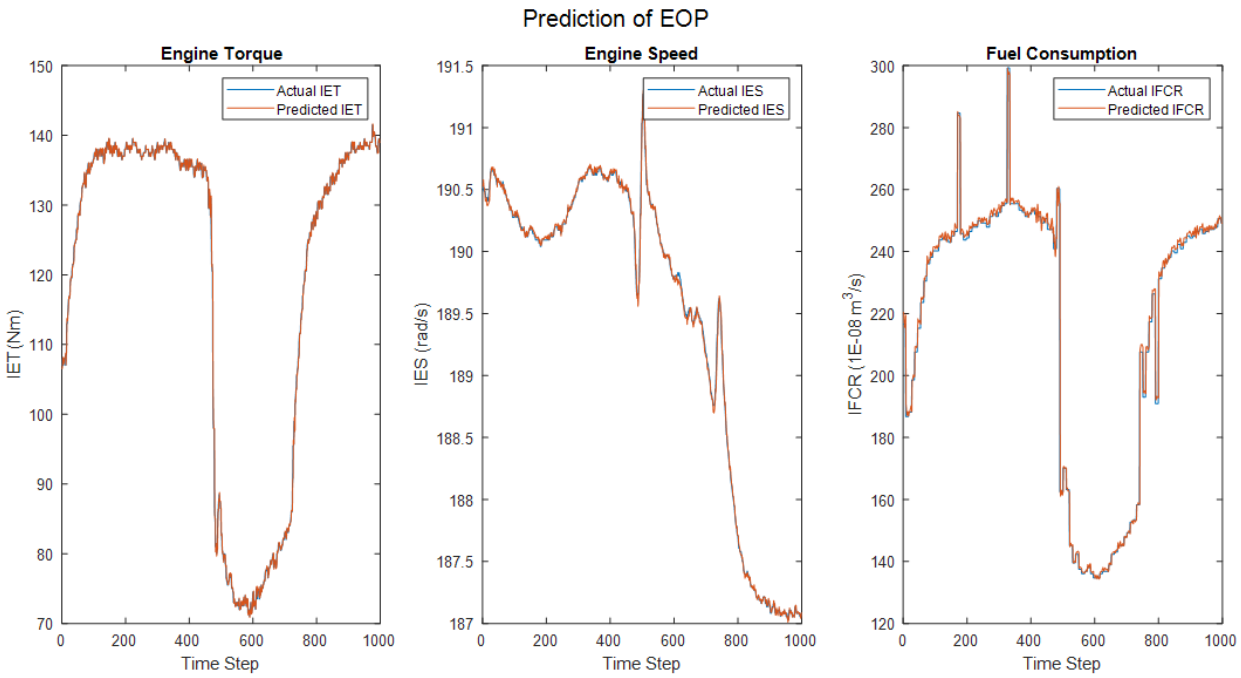

Figure 47: EOP — ACCSSP = 70 MPH

Appendix G

Figures: Prediction of [CATOP]—2020 Cadillac CT5 (EAT > 65 °F)

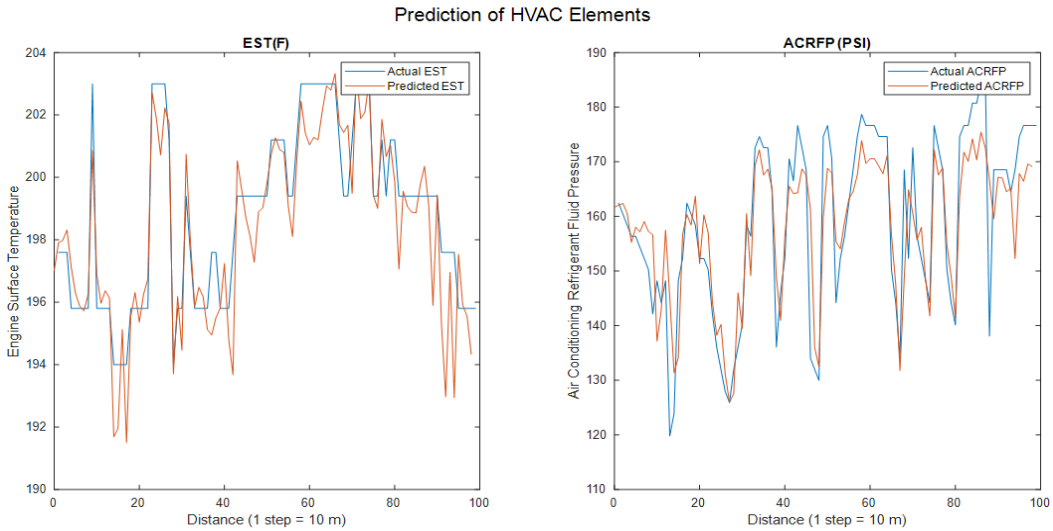

Figure 48: ACCSSP = 35 MPH, CAT = 67 °F, EAT = 83.3°F

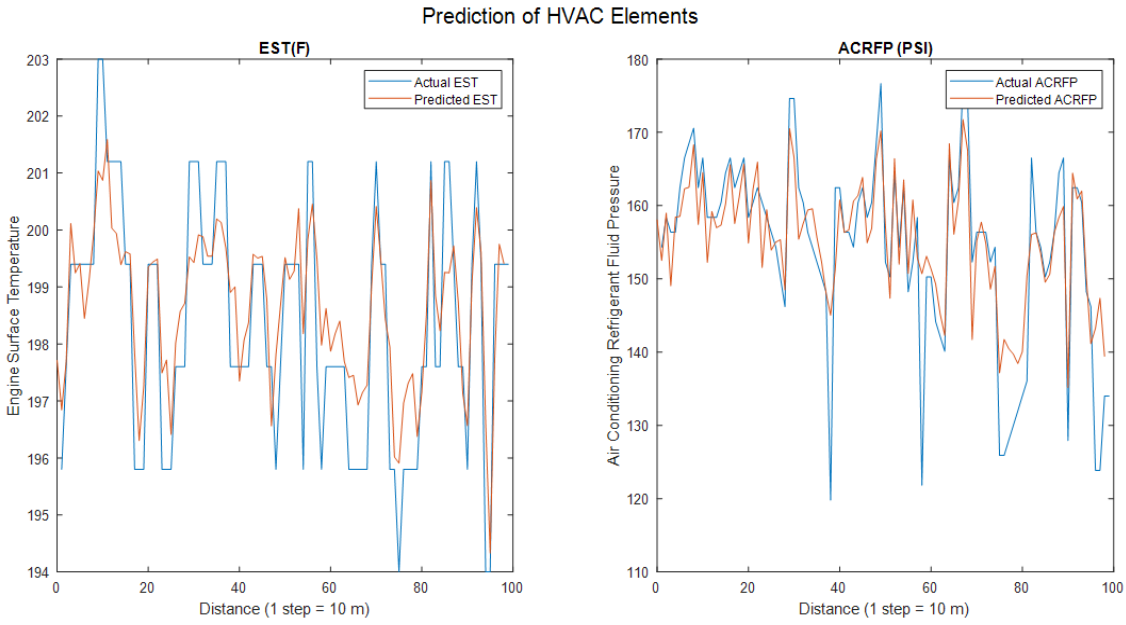

Figure 49: ACCSSP = 45 MPH, CAT = 65 °F, EAT = 80.3°F

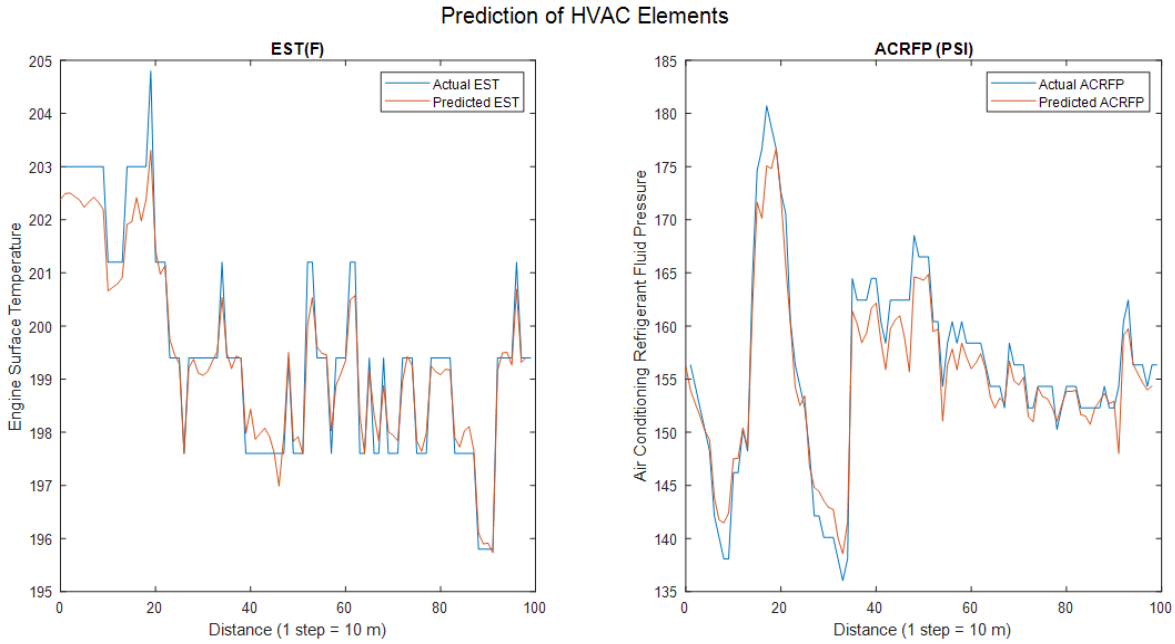

Figure 50: ACCSSP = 55 MPH, CAT = 66 °F, EAT = 70.2°F

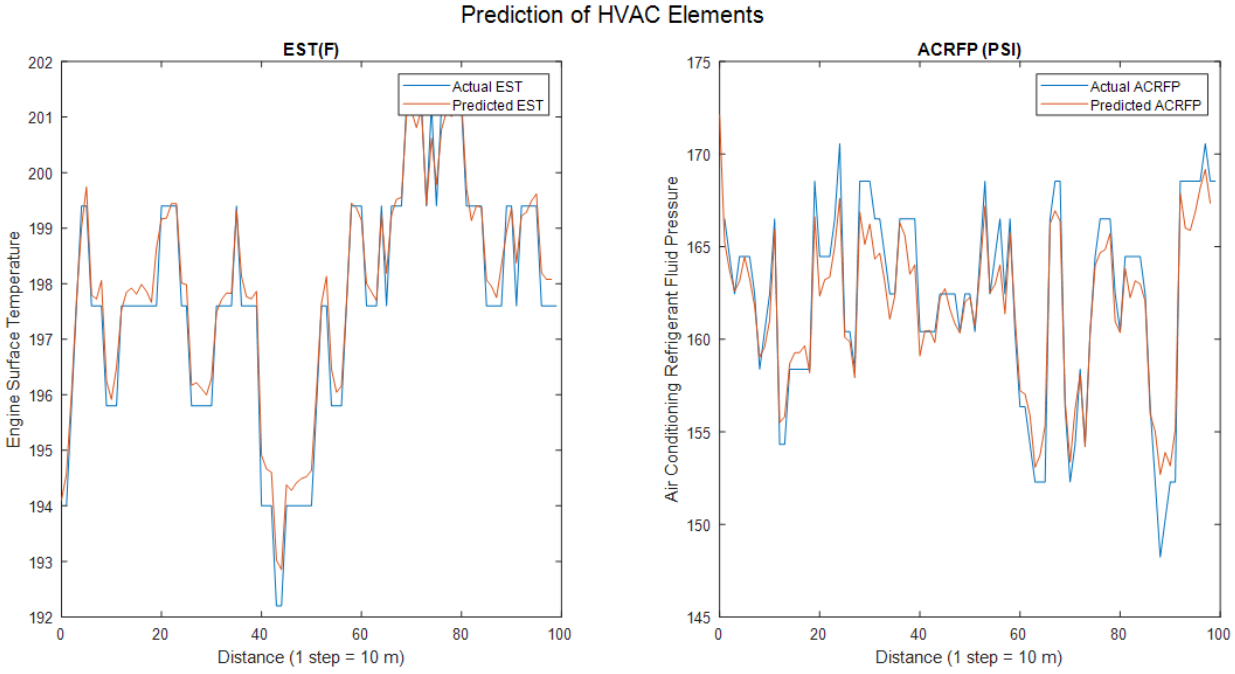

Figure 51: ACCSSP = 65 MPH, CAT = 68 °F, EAT = 80.9°F

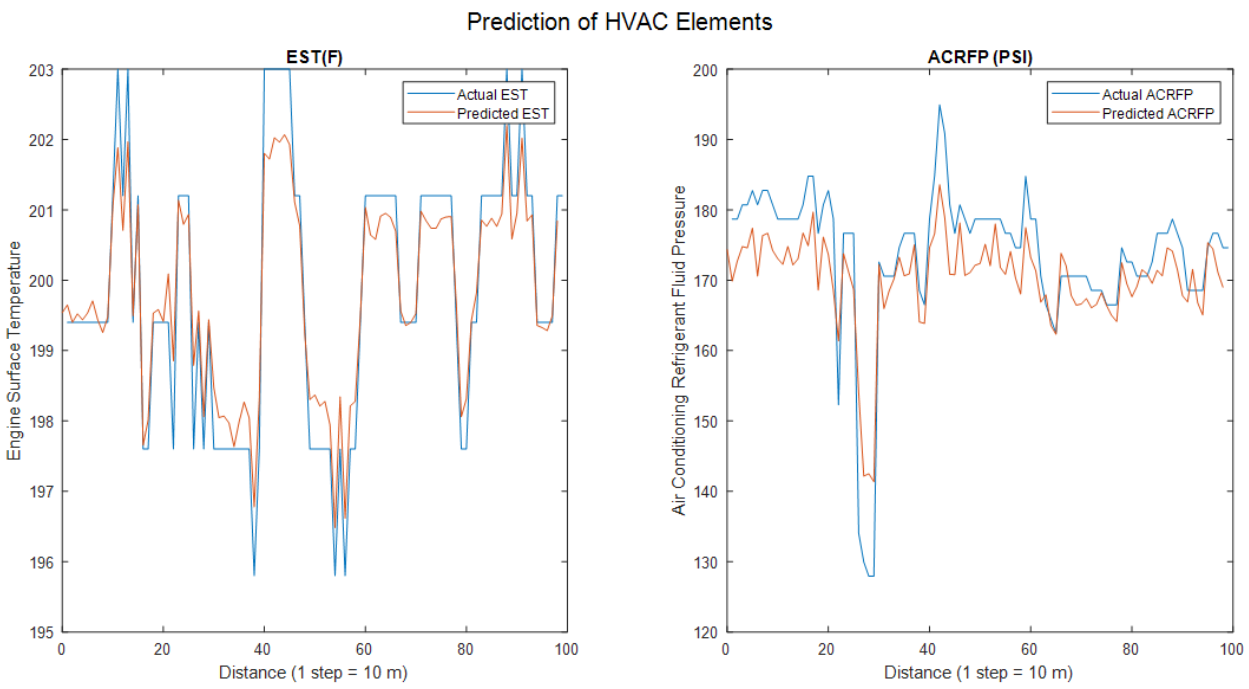

Figure 52: ACCSSP = 75 MPH, CAT = 69 °F, EAT = 84.62 °F

Appendix H

Figures: Prediction of [CATOP]—2020 Cadillac CT5 (EAT < 45 °F)

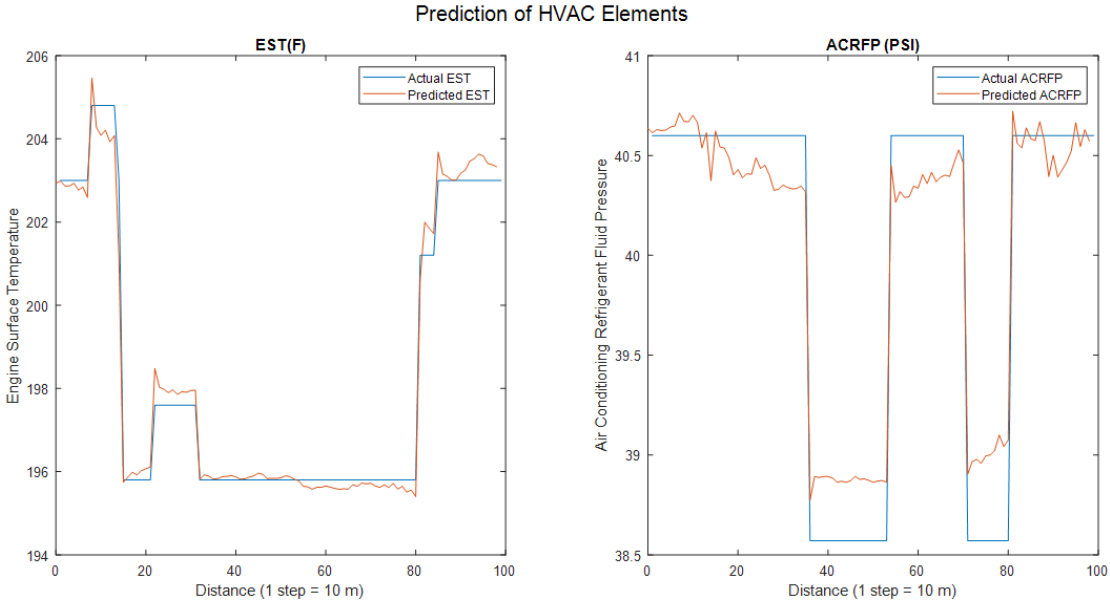

Figure 53: ACCSSP = 35 MPH, CAT = 76 °F, EAT = 36.4 °F

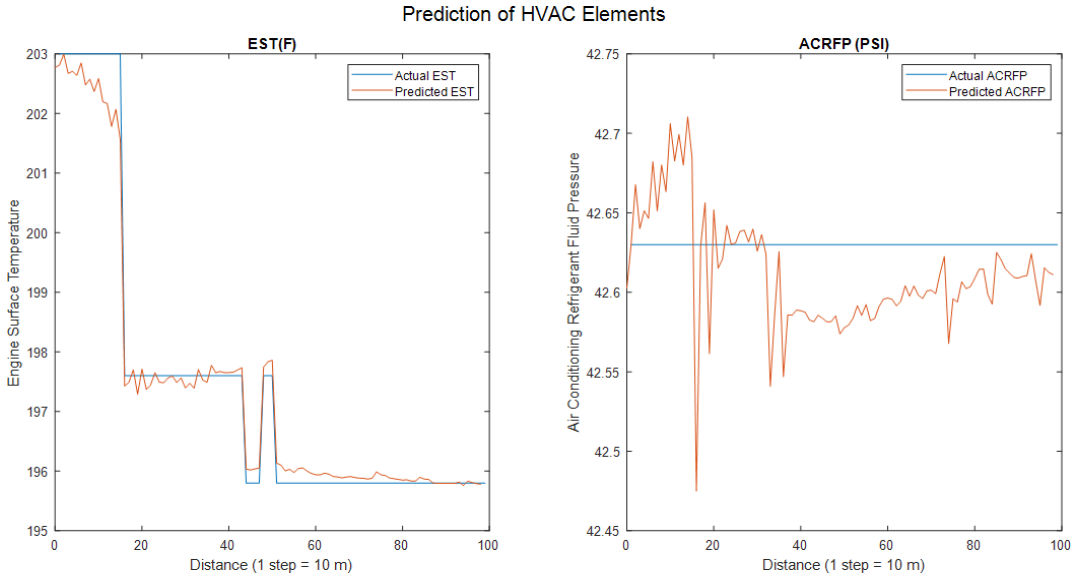

Figure 54: ACCSSP = 45 MPH, CAT = 71 °F, EAT = 39.1 °F

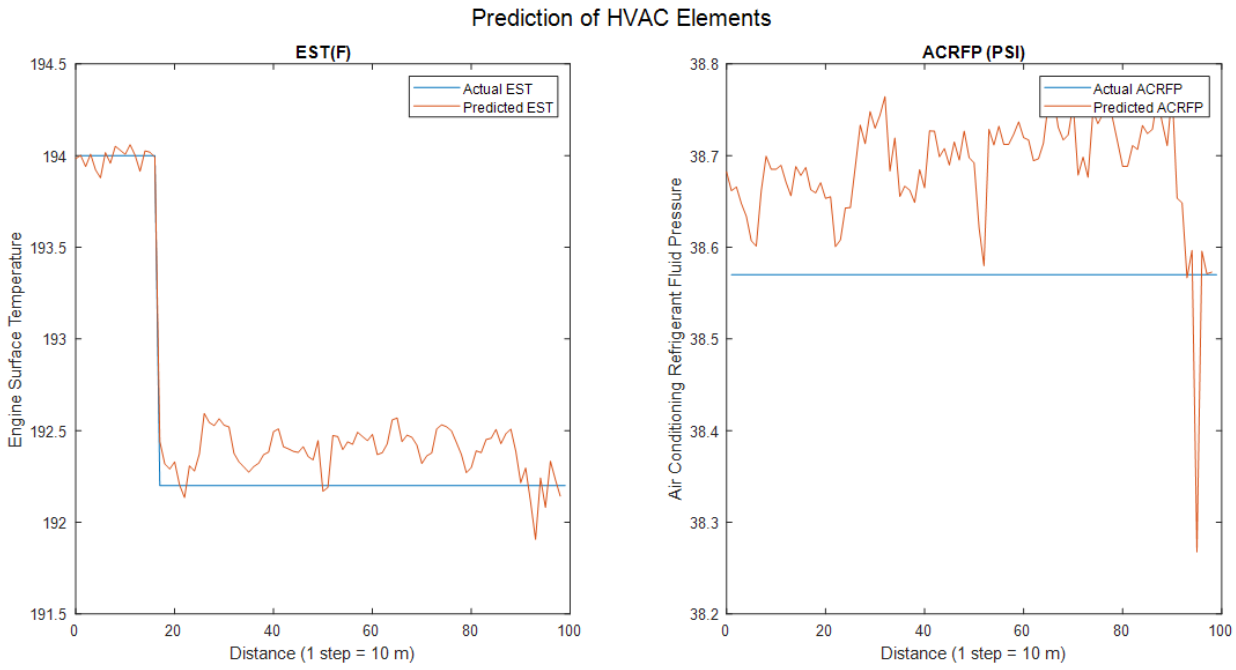

Figure 55: ACCSSP = 55 MPH, CAT = 85 °F, EAT = 34.7 °F

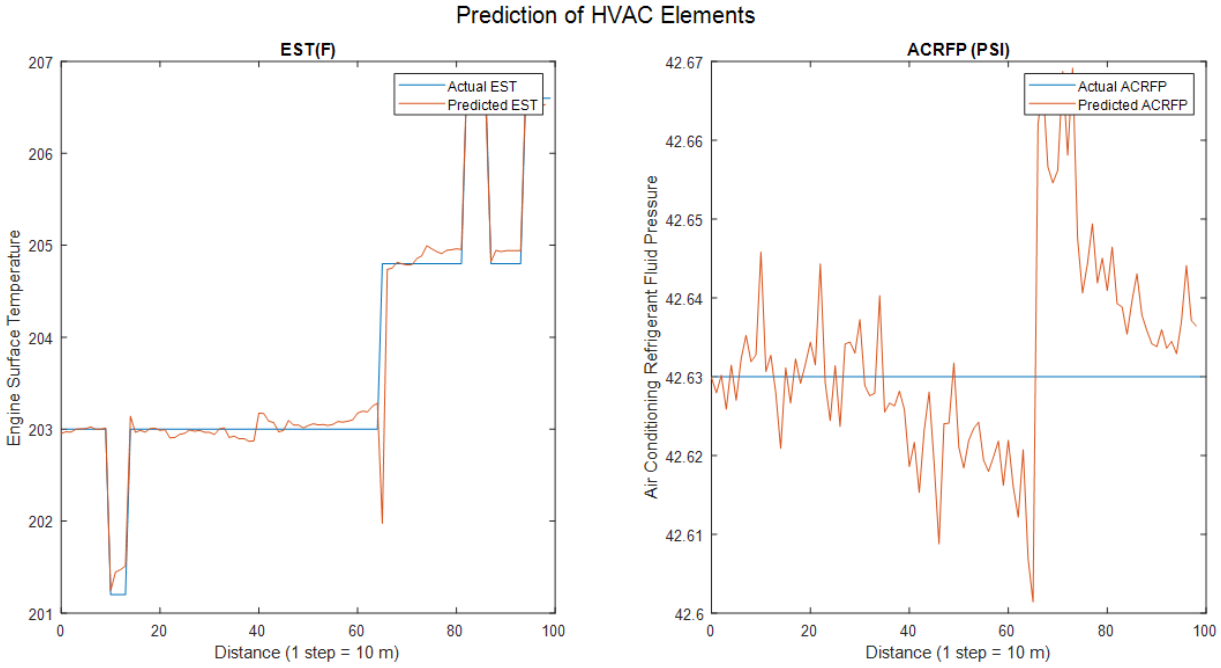

Figure 56: ACCSSP = 65 MPH, CAT = 80 °F, EAT = 38.9 °F

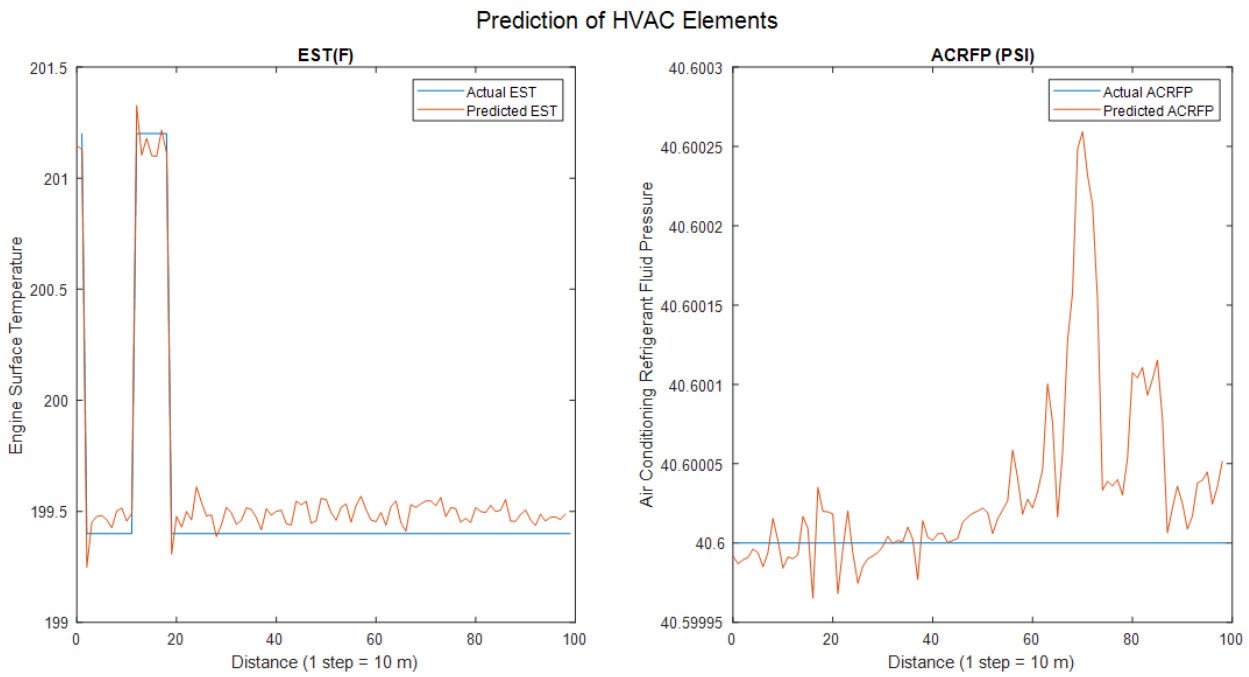

Figure 57: ACCSSP = 75 MPH, CAT = 75 °F, EAT = 37.4 °F

Appendix I

Figures: Prediction of [ACCSSP]—2020 Cadillac CT5

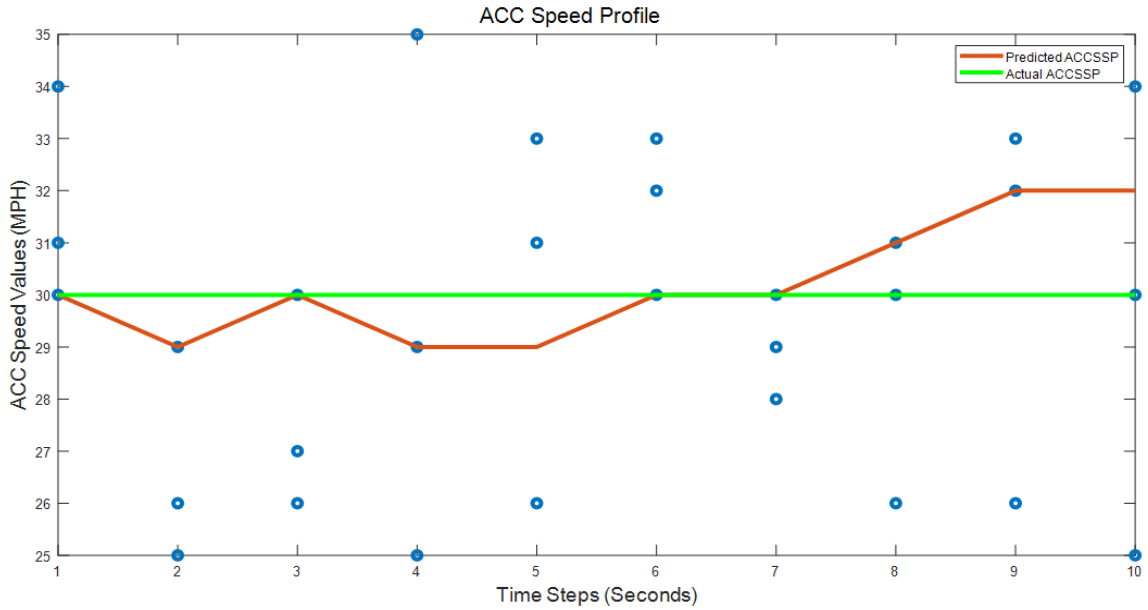

Figure 58: ACCSSP—IAS = 30 MPH.

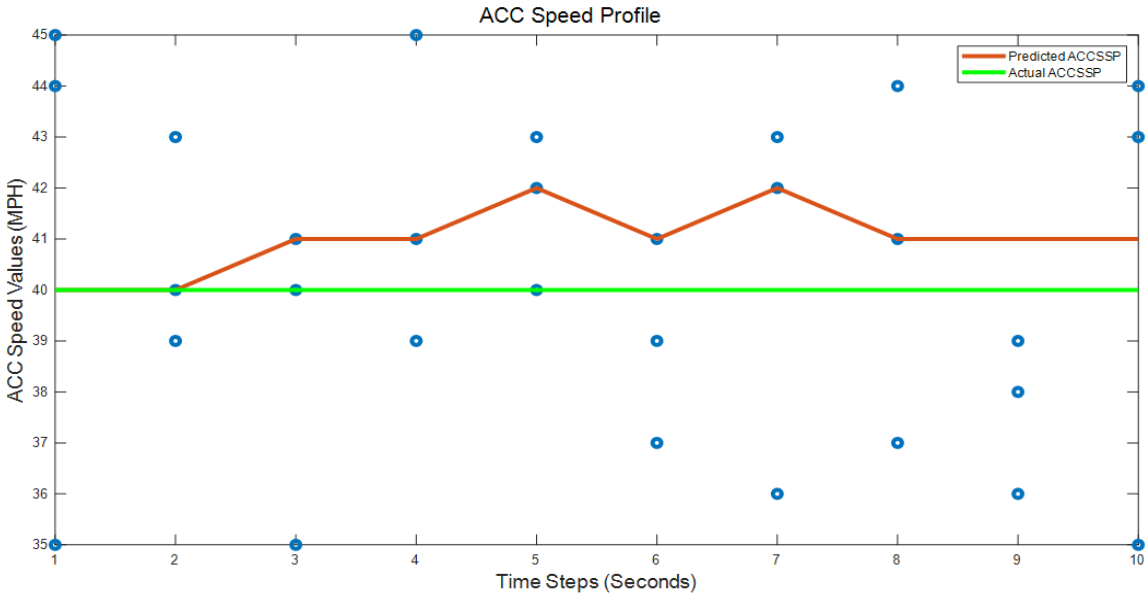

Figure 59: ACCSSP—IAS = 40 MPH.

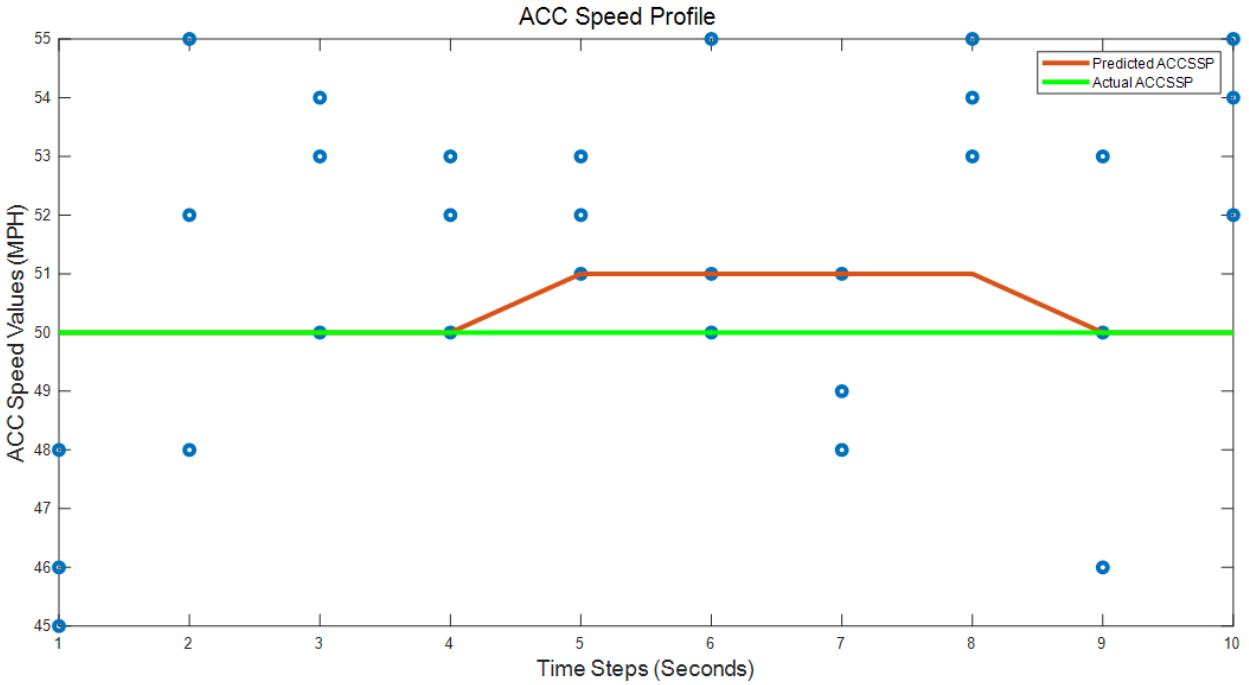

Figure 60: ACCSSP—IAS = 50 MPH.

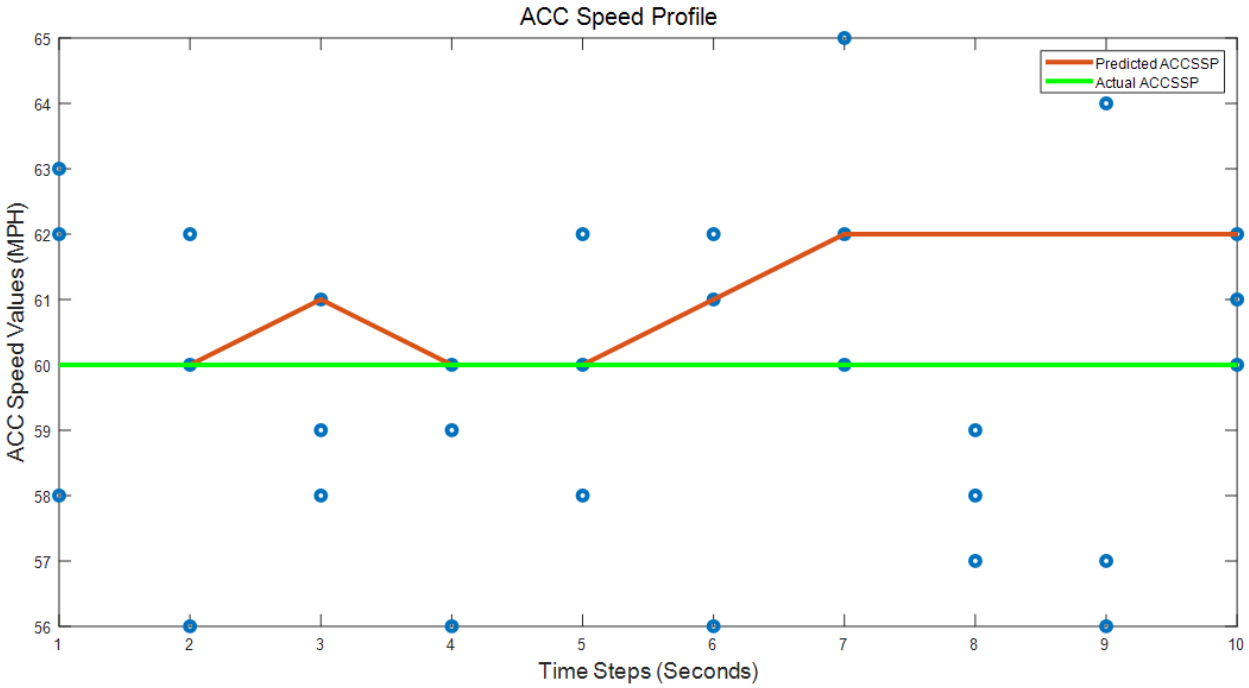

Figure 61: ACCSSP—IAS = 60 MPH.

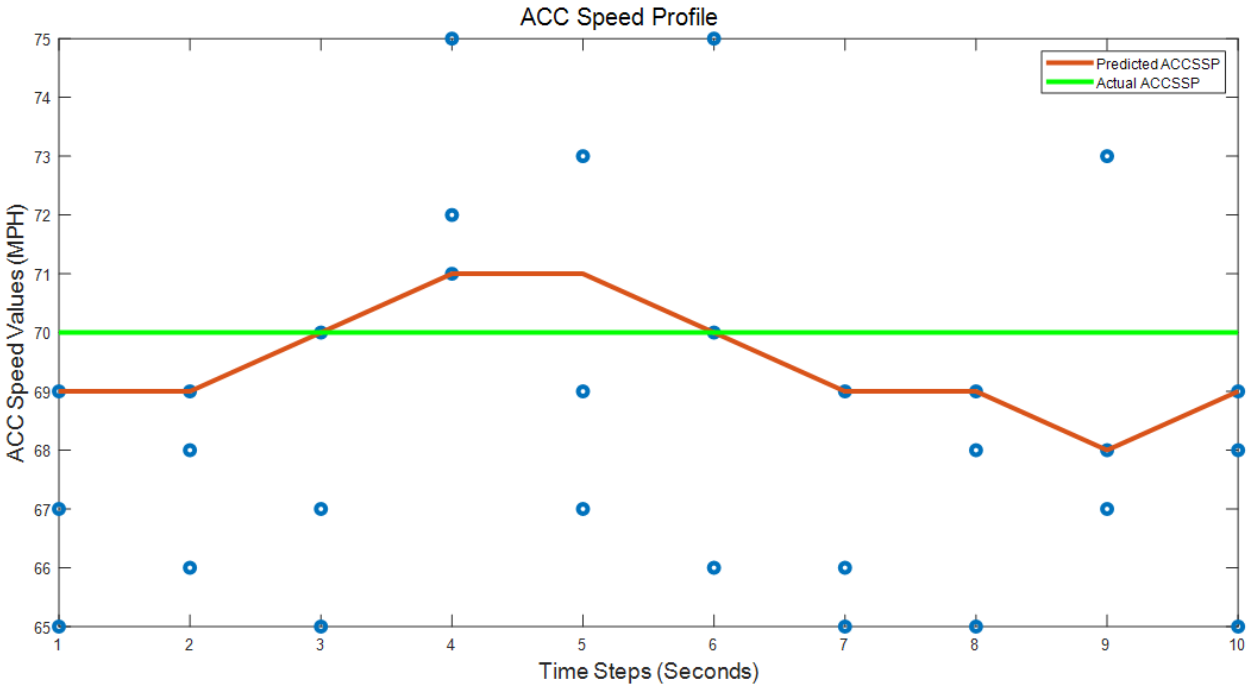

Figure 62: ACCSSP—IAS = 70 MPH.

Appendix J

Figures: Prediction of [CATSP]—2020 Cadillac CT5

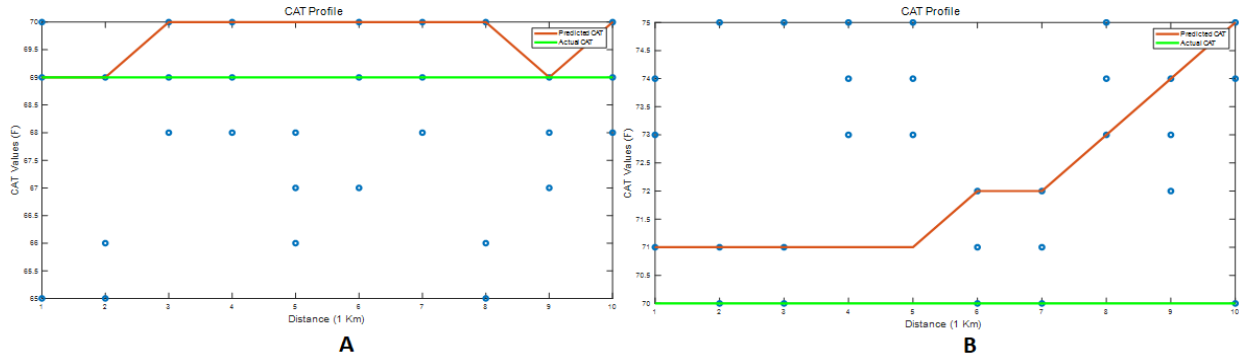

Figure 63: CATSP: (A) ICAT = 69 °F; EAT = 82.07 °F; (B) ICAT = 70 °F; EAT = 38 °F—ACCSSP = 30 MPH.

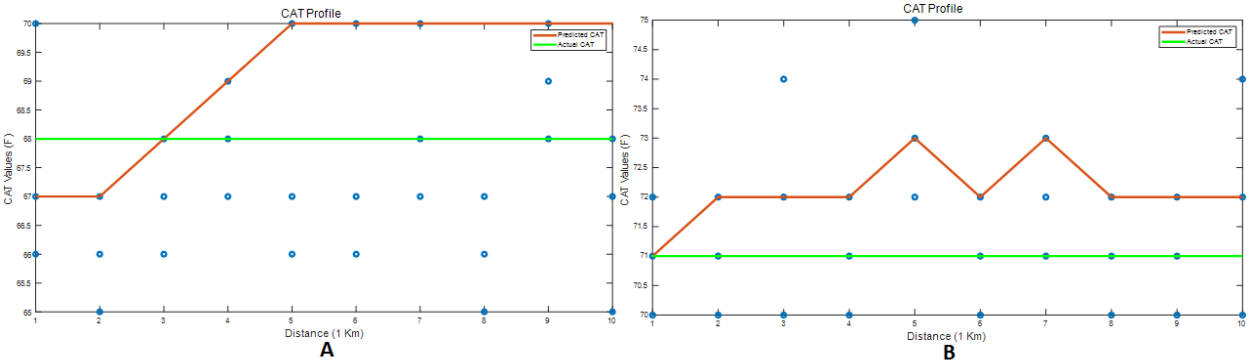

Figure 64: CATSP: (A) ICAT = 68 °F; EAT = 85.3 °F; (B) ICAT = 71 °F; EAT = 37.63 °F—ACCSSP = 40 MPH.

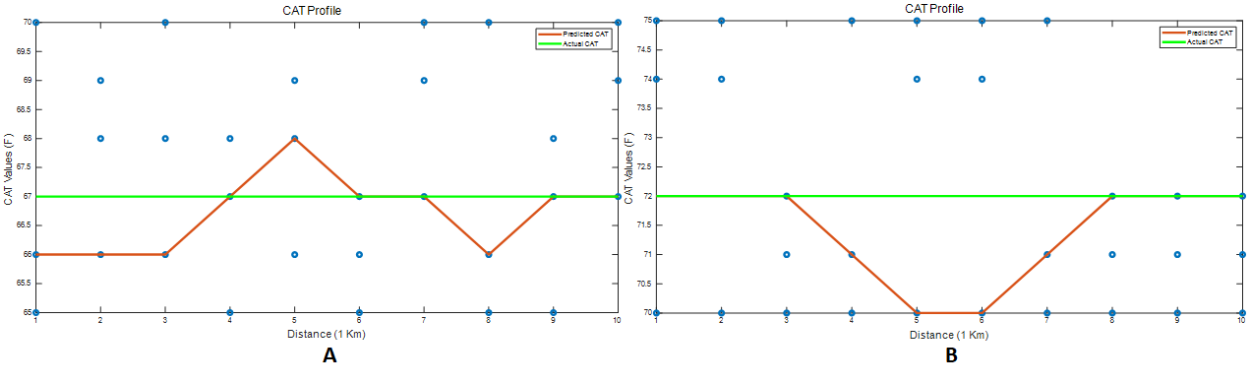

Figure 65: CATSP: (A) ICAT = 66 °F; EAT = 80.73 °F; (B) ICAT = 72 °F; EAT = 40.1 °F—ACCSSP = 50 MPH.

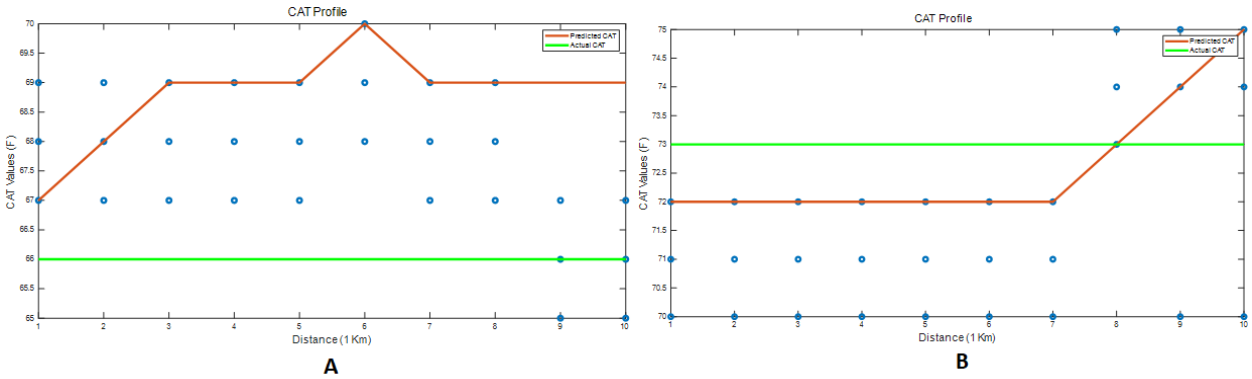

Figure 66: CATSP: (A) ICAT = 66 °F; EAT = 79.5 °F; (B) ICAT = 73 °F; EAT = 38.86 °F—ACCSSP = 60 MPH.

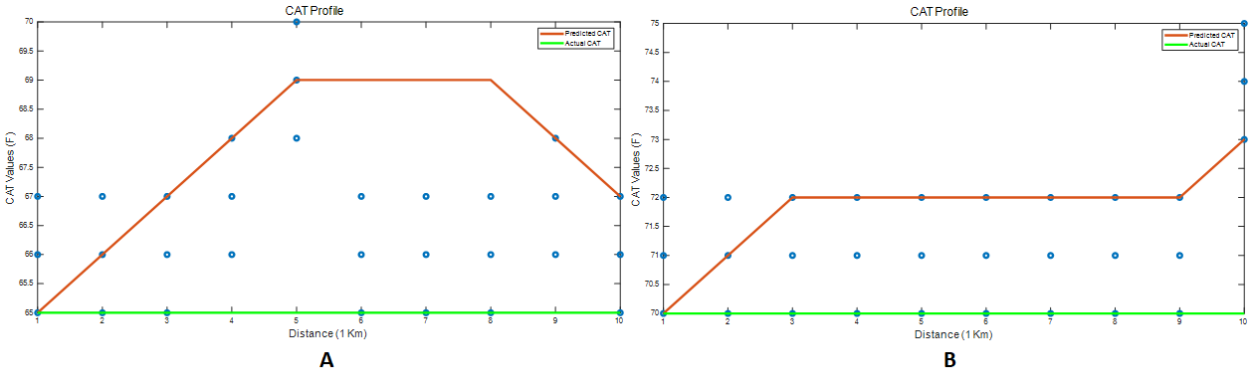

Figure 67: CATSP: (A) ICAT = 65 °F; EAT = 76.1°F; (B) ICAT = 70 °F; EAT = 36.52 °F—ACCSSP = 70 MPH.

Appendix K

Figures: Quantification of IVDM Using [IEE, IEM]—2020 Cadillac CT5

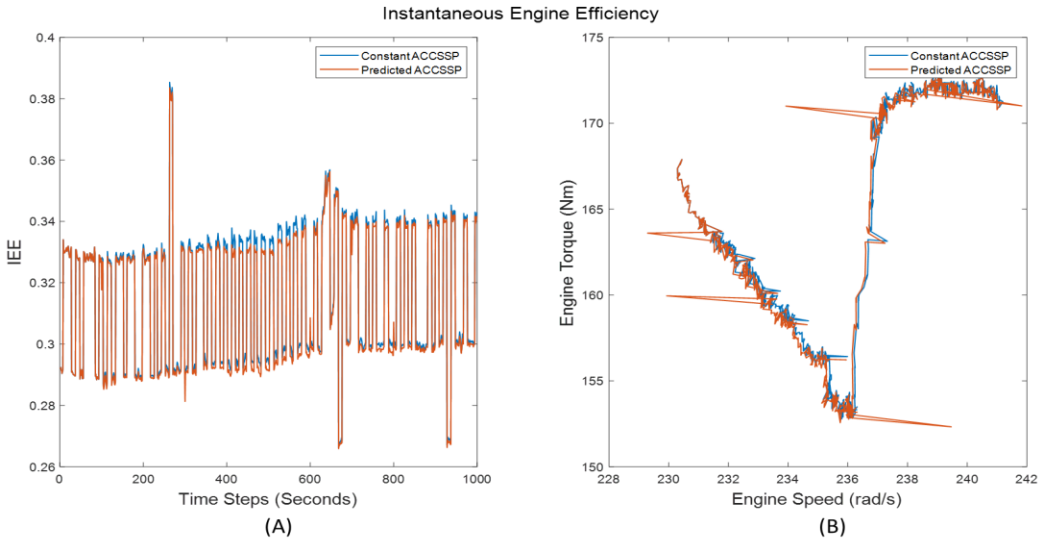

Figure 68: Validation: (A) IEE; (B) IEM—ACCSSP = 70 MPH.

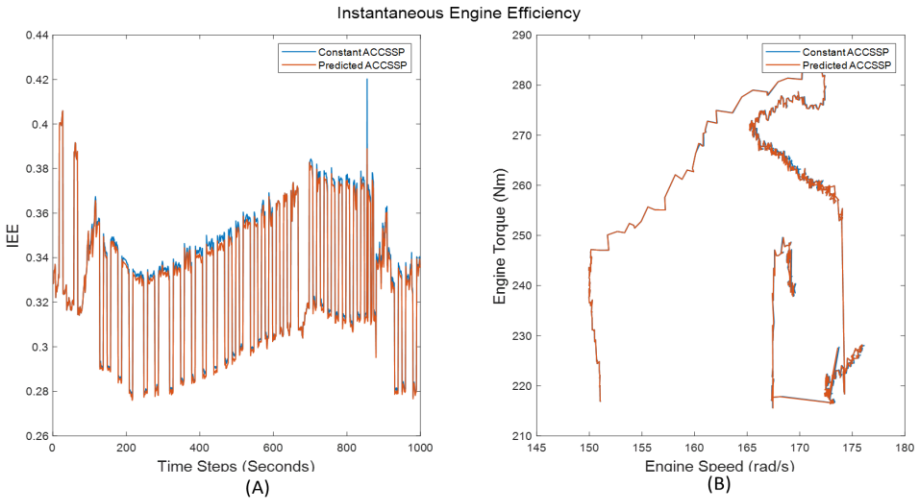

Figure 69: Validation: (A) IEE; (B) IEM—ACCSSP = 60 MPH.

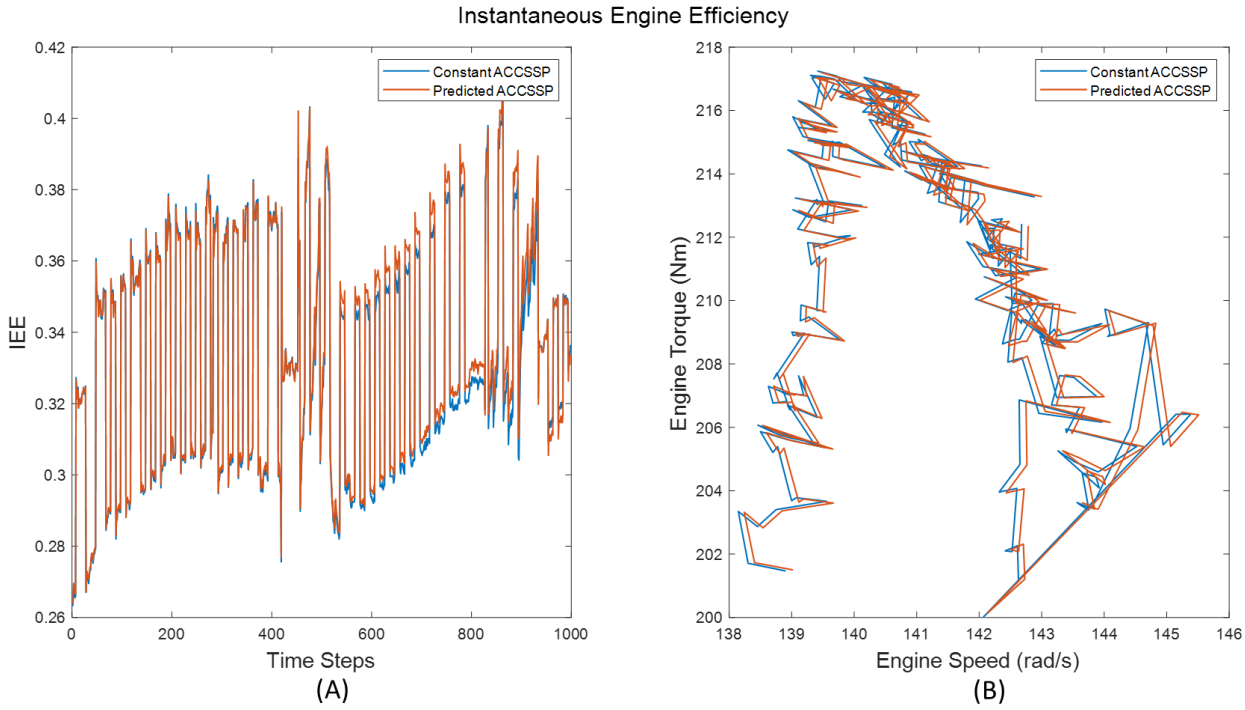

Figure 70: Validation: (A) IEE; (B) IEM—ACCSSP = 50 MPH.

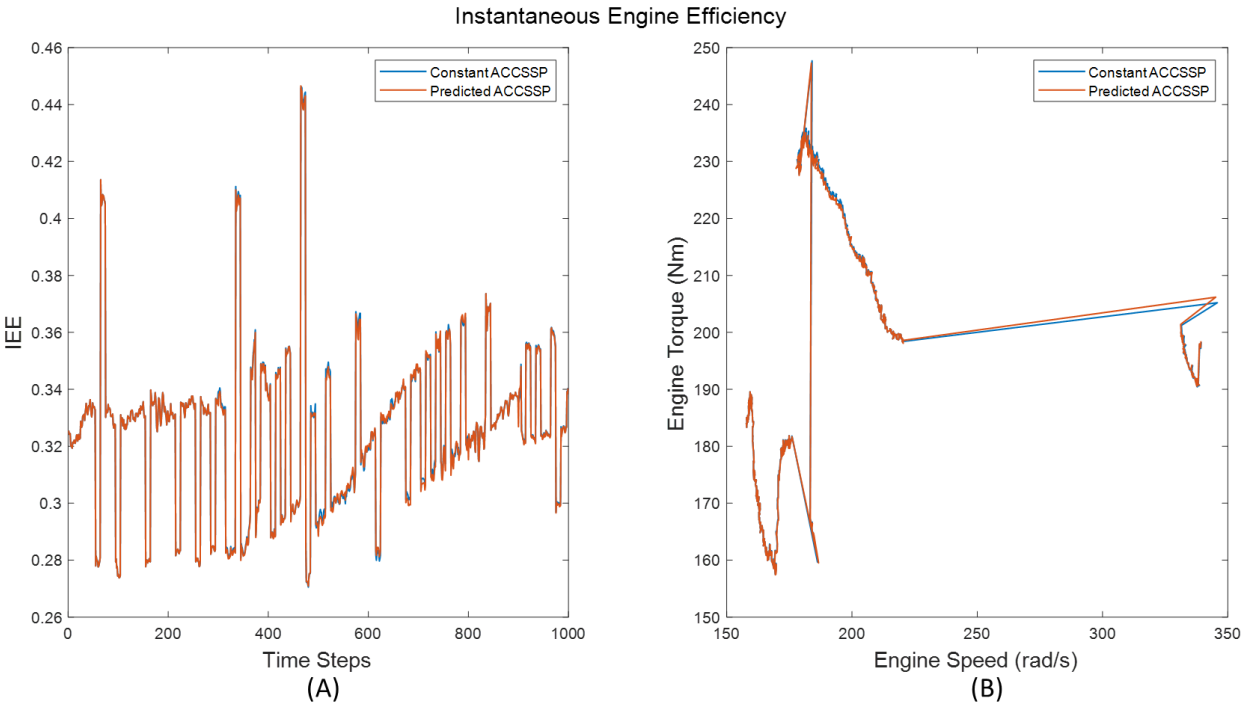

Figure 71: Validation: (A) IEE; (B) IEM—ACCSSP = 40 MPH.

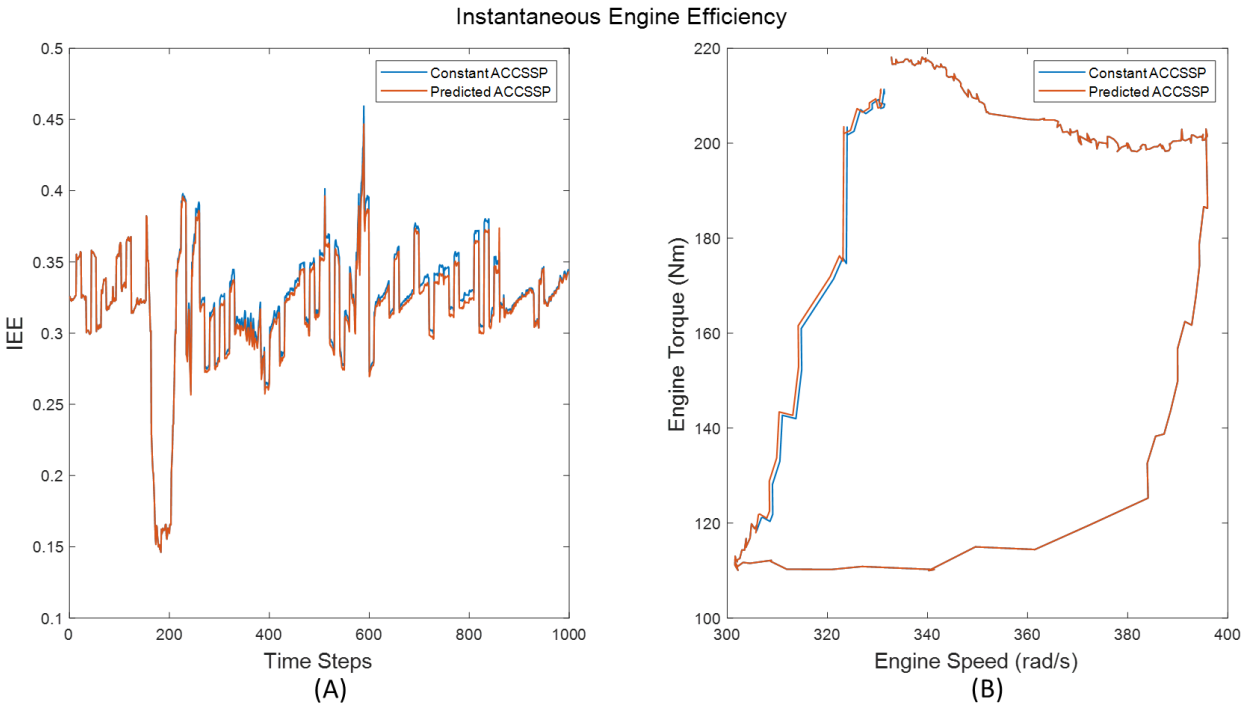

Figure 72: Validation: (A) IEE; (B) IEM—ACCSSP = 30 MPH.

Appendix L

Algorithms: MATLAB Scripts

Basic algorithms were deployed using m-scripts which assist the predictive models and concept of Intelligent Vehicle Drive Mode (IVDM). The developed logic was posted as GitHub repositories discussed in Appendix M.

1. Algorithm: Resolving simultaneous equations—3 Variables; 2 Equations

Result: Unique solution for known boundary conditions
defineProblem = optimproblem('ObjectiveSense','min')
X = optimvar('x',3,1)
defineProblem.Objective = $(X(3) * X(1) - X(2))^2$
Constraint 1: minSpeed ≤ X(1) ≤ maxSpeed
Constraint 2: minLateralAcceleration ≤ X(2) ≤ maxLateralAcceleration
Constraint 3: minYawRate ≤ X(3) ≤ maxYawRate
Constraint 4: $(2R - \frac{X(1)^2}{X(2)} - \frac{X(1)}{X(3)})^2 == 0$
Initial coordinate: X_0 *— Mean value of the boundary values*
Solution = solve(defineProblem,X_0*)*

2. Algorithm: Identifying the “NAN” — Computational analysis

Result: Identifying the replacing “NAN” - MATLAB
while d < numIterations do *[r,c] = find(isnan(cell2mat(tTest)))* *if [r,c] != []* *tTest(r,c) = tTest(r,c-1)* *end* *d+ = 1* *end*

3. Algorithm: Estimating the smooth ACCSSP — Fail safe action

(**Note**: Similar algorithm was adopted to estimate the CATSP)

Result: Estimating speed profile with three eligible values for each second.
$eligibleSpeedValues_k$ = [S_a, S_b, S_c] ; $initialSpeedValue_0$ = [S_0] *diffSpeedMatrix = abs(*$eligibleSpeedValues_k$*-* $initialSpeedValue_0$*)* *indexMinValue = find(diffSpeedMatrix ==min(diffSpeedMatrix))* *if min(diffSpeedMatrix) == 1* $estimatedSpeedValue_k$ = *max(*$eligibleSpeedValues_k$*(*$indexMinValue$*))* *else* $estimatedSpeedValue_k = initialSpeedValue_0$ *end*

4. Algorithm: Estimating the range of allowable CAT (°F) — Correlation with EAT (°F)

Result: The range of CAT based on external air temperature (EAT).
if $EAT_k \geq 65$ *°F*
lowerLimitCAT = 65 °F ; higherLimitCAT = 70 °F ;
else
lowerLimitCAT = 70 °F ; higherLimitCAT = 75 °F ;
end

Appendix M

Source Code: MATLAB Scripts — GitHub repositories

All the computational models were developed using built-in functions of MATLAB, and the scripts were posted as the GitHub repositories (private mode) for reference of this research. The m-scripts developed are available on request.

1. **Estimation of vehicle speed for low curvatures.** Chapter 5 discusses the concept of resolving simultaneous equations to obtain a unique speed for a definite curvature, which represents the ideal steering behavior. [Reference 27: Kolachalama, S., et.al (2022), IDETC/CIE - 88919; ASME].

   https://github.com/skolachalama/NonLinear-Simultaneous-Equations.git

2. **Prediction of EOP using NARX method.** Chapter 6 discusses the NARX deep learning method to predict the EOP using the time-sensitive data retrieved from real-time testing. [Reference 37: Kolachalama, S., et.al (2021), (No. 2021-01-0186). SAE Technical Paper].

   https://github.com/skolachalama/NARX-EOP.git

3. **Prediction of EOP using LSTM method.** Chapter 6 discusses the LSTM deep learning method to predict the EOP using the time-sensitive data retrieved from real-time testing. [Reference 37: Kolachalama, S., et.al (2021), (No. 2021-01-0186). SAE Technical Paper].

   https://github.com/skolachalama/LSTM-EOP.git

4. **Prediction of ACCSSP by optimizing EOP**. Chapter 6 discusses a predictive model of the engine operating point, and Chapter 7 details the process to estimate the optimal ACCSSP for future time steps that enhances engine operating conditions. [Reference 24: Kolachalama, S., & Malik, H. (2021). *Vehicles*, *3*(4), 749-763].

   https://github.com/skolachalama/Prediction-ACCSSP.git

5. **Prediction of CATOP using NARX method.** Chapter 6 details the process to predict CATOP [EST, ACRFP] for the future time steps that affects engine performance. [Reference 29: Kolachalama, S., & Malik, H. (2021). *Vehicles*. 2021; 3(4):872-889].

   https://github.com/skolachalama/NARX-CATOP.git

6. **Prediction of CATSP by optimizing CATOP.** The details of the NARX predictive model and the optimization criteria of HVAC elements were presented in Chapter 7. Based on the developed concept, the optimal CAT set profile was generated challenging the constant set value. [Reference 29: Kolachalama, S., & Malik, H. (2021). *Vehicles*. 2021; 3(4):872-889].

   https://github.com/skolachalama/Prediction-CATSP.git

Bibliography

1. Dietsche, K. H., & Kuhlgatz, D. (2014). History of the automobile. In *Fundamentals of Automotive and Engine Technology* (pp. 1-7). Springer Vieweg, Wiesbaden.

2. Sturgeon, T. J., Memedovic, O., Van Biesebroeck, J., & Gereffi, G. (2009). Globalisation of the automotive industry: main features and trends. *International Journal of Technological learning, innovation and development*, *2*(1-2), 7-24.

3. Zoepf, S. M. (2011). *Automotive features: mass impact and deployment characterization* (Doctoral dissertation, Massachusetts Institute of Technology).

4. Zoepf, S., & Heywood, J. B. (2012). Characterizations of deployment rates in automotive technology. *SAE International Journal of Passenger Cars-Electronic and Electrical Systems*, *5*(2012-01-1057), 541-552.

5. Chau, C. K., Elbassioni, K., & Tseng, C. M. (2017). Drive mode optimization and path planning for plug-in hybrid electric vehicles. *IEEE Transactions on Intelligent Transportation Systems*, *18*(12), 3421-3432.

6. Davis, B. (2019). Teen Driver Support System Technology Transfer.

7. Goodarzi, A., & Esmailzadeh, E. (2007). Design of a VDC system for all-wheel independent drive vehicles. *IEEE/ASME Transactions On Mechatronics*, *12*(6), 632-639.

8. Lairenlakpam, R., Jain, A. K., Gupta, P., Kamei, W., Badola, R., & Singh, Y. (2018). *Effect of Real world driving and different drive modes on vehicle emissions and fuel consumption* (No. 2018-01-5017). SAE Technical Paper.

9. Paul, A., Chauhan, R., Srivastava, R., & Baruah, M. (2016). *Advanced driver assistance systems* (No. 2016-28-0223). SAE Technical Paper.

10. Melman, T., de Winter, J., Mouton, X., Tapus, A., & Abbink, D. (2021). How do driving modes affect the vehicle's dynamic behavior? Comparing Renault's Multi-Sense sport and comfort modes during on-road naturalistic driving. *Vehicle system dynamics*, *59*(4), 485-503.

11. Zhang, X., & Mi, C. (2011). *Vehicle power management: modeling, control and optimization*. Springer Science & Business Media.

12. Onder, C. H., & Geering, H. P. (1995). *Model-based engine calibration for best fuel efficiency* (No. 950983). SAE Technical Paper.

13. Taghavifar, H., & Mardani, A. (2017). Off-road vehicle dynamics. *Studies in Systems, Decision and Control*, *70*, 37.

14. Sharma, A., Singh, J., & Kumar, A. (2015). Optimum design and material selection of Baja vehicle. *International Journal of Current Engineering and Technology*, *5*(3), 2169-2180.

15. Baldacci, R., Battarra, M., & Vigo, D. (2008). Routing a heterogeneous fleet of vehicles. In *The vehicle routing problem: latest advances and new challenges* (pp. 3-27). Springer, Boston, MA.

16. Chen, Z., Li, X., & Zhou, X. (2019). Operational design for shuttle systems with modular vehicles under oversaturated traffic: Discrete modeling method. *Transportation Research Part B: Methodological*, *122*, 1-19.

17. Cariou, C., Lenain, R., Thuilot, B., & Berducat, M. (2008, September). Automatic guidance of a four-wheel steering vehicle. In *66th LandTechnik Conference: Agricultural Engineering* (p. 6). VDI Verlag GmbH.

18. Gao, Z., Smith, D. E., Daw, C. S., Edwards, K. D., Kaul, B. C., Domingo, N., ... & Jones, P. T. (2015). The evaluation of developing vehicle technologies on the fuel economy of long-haul trucks. *Energy Conversion and Management*, *106*, 766-781.

19. Hac, A., Fulk, D., & Chen, H. (2008). Stability and control considerations of vehicle-trailer combination. *SAE International Journal of Passenger Cars-Mechanical Systems*, *1*(2008-01-1228), 925-937.

20. Boggio-Marzet, A., Monzon, A., Rodriguez-Alloza, A. M., & Wang, Y. (2021). Combined influence of traffic conditions, driving behavior, and type of road on fuel consumption. Real driving data from Madrid Area. *International Journal of Sustainable Transportation*, 1-13.

21. Labuhn, P. I., & Chundrlik Jr, W. J. (1995). *U.S. Patent No. 5,454,442*. Washington, DC: U.S. Patent and Trademark Office.

22. Marsden, G., McDonald, M., & Brackstone, M. (2001). Towards an understanding of adaptive cruise control. *Transportation Research Part C: Emerging Technologies*, *9*(1), 33-51.

23. Luo, L. H., Liu, H., Li, P., & Wang, H. (2010). Model predictive control for adaptive cruise control with multi-objectives: comfort, fuel-economy, safety and car-following. *Journal of Zhejiang University SCIENCE A*, *11*(3), 191-201.

24. Kolachalama, S., & Malik, H. (2021). Predictive Model of Adaptive Cruise Control Speed to Enhance Engine Operating Conditions. *Vehicles*, *3*(4), 749-763.

25. S Kolachalama, CL Hay, T Mushtarin, N Todd, J Heitman, S Hermiz, An Algorithm To Estimate Steering Behavior Using Vehicle Radius Of Curvature, 647068, Research Disclosure, Questel Ireland Ltd - March 2018.

26. Wåhlberg, A. E. (2007). Long-term effects of training in economical driving: Fuel consumption, accidents, driver acceleration behavior and technical feedback. *International journal of industrial ergonomics*, *37*(4), 333-343.

27. Kolachalama S, Hay CL, Malik H. (2022). Estimation of Vehicle Speed for Low Curvatures assuming Ideal Steering Behavior. IDETC/CIE 2022 - 88919; ASME.

28. Borman, G., & Nishiwaki, K. (1987). Internal-combustion engine heat transfer. *Progress in energy and combustion science*, *13*(1), 1-46.

29. Kolachalama S, Malik H. A NARX Model to Predict Cabin Air Temperature to Ameliorate HVAC Functionality. *Vehicles*. 2021; 3(4):872-889.

30. Liang, C., Ji, L., Mousavi, H., & Sandu, C. (2019, October). Evaluation of tire traction performance on dry surface based on tire-road contact stress. In *SIAR International Congress of Automotive and Transport Engineering: Science and Management of Automotive and Transportation Engineering* (pp. 138-152). Springer, Cham.

31. Sudin, M. N., Abdullah, M. A., Shamsuddin, S. A., Ramli, °F R., & Tahir, M. M. (2014). Review of research on vehicles aerodynamic drag reduction methods. *International Journal of Mechanical and Mechatronics Engineering*, *14*(02), 37-47.

32. Kolachalama, S., Kuppa, K., Mattam, D., & Shukla, M. (2008, January). Thermal Analysis of Radiator Core in Heavy Duty Automobile. In *Heat Transfer Summer Conference* (Vol. 48487, pp. 123-127).

33. Eathakota, V., Singh, A. K., Kolachalam, S., & Krishna, K. M. (2010, September). Determination of optimally stable posture for force actuator based articulated suspension for rough terrain mobility. In *FIRA RoboWorld Congress* (pp. 154-161). Springer, Berlin, Heidelberg.

34. Eathakota, V. P., Kolachalama, S., Krishna, K. M., & Sanan, S. (2008). Optimal posture control for force actuator based articulated suspension vehicle for rough terrain mobility. In *Advances In Mobile Robotics* (pp. 760-767).

35. Kolachalama, S., & Lakshmanan, S. (2021). *Using Deep Learning to Predict the Engine Operating Point in Real-Time* (No. 2021-01-0186). SAE Technical Paper.

36. Johansson, K. H., Törngren, M., & Nielsen, L. (2005). Vehicle applications of controller area network. In *Handbook of networked and embedded control systems* (pp. 741-765). Birkhäuser Boston.

37. Jaynes, M., Dantu, R., Varriale, R., & Evans, N. (2016, December). Automating ECU identification for vehicle security. In *2016 15th IEEE International Conference on Machine Learning and Applications (ICMLA)* (pp. 632-635). IEEE.

38. Gusev, S. V., Johnson, W., & Miller, J. (1997, June). Active flywheel control based on the method of moment restrictions. In *Proceedings of the 1997 American Control Conference (Cat. No. 97CH36041)* (Vol. 5, pp. 3426-3430). IEEE.

39. Kakaee, A. H., Shojaeefard, M. H., & Zareei, J. (2011). Sensitivity and effect of ignition timing on the performance of a spark ignition engine: an experimental and modeling study. *Journal of Combustion*, *2011*.

40. Chen, X., Chi, R., Wang, J., Pang, C., & Xiao, Q. (2011, October). Driver safe speed model based on BP neural network for rural curved roads. In International Conference on Computer and Computing Technologies in Agriculture (pp. 92-102). Springer, Berlin, Heidelberg.

41. Chowdhury, M. A., Warren, D. L., Bissell, H., & Taori, S. (1998). Are the criteria for setting advisory speeds on curves still relevant? ITE Journal, 68, 32-45.

42. Eboli, L., Mazzulla, G., & Pungillo, G. (2016). Combining speed and acceleration to define car users' safe or unsafe driving behavior. Transportation research part C: emerging technologies, 68, 113-125.

43. Ibrahim, M. °F, Misro, M. Y., Ramli, A., & Ali, J. M. (2017, August). Maximum safe speed estimation using planar quintic Bézier curve with C2 continuity. In AIP Conference Proceedings (Vol. 1870, No. 1, p. 050006). AIP Publishing LLC.

44. Merrit, D. (1988). Safe speeds on curves: a historical perspective of the ball bank indicator. ITE Journal, 58(9), 15-19.

45. Bonneson, J., Pratt, M., Miles, J., & Carlson, P. (2007). Development of guidelines for establishing effective curve advisory speeds. Texas Transportation Institute, CollegeStation, TX, USA.

46. Bonneson, J. A., Pratt, M. P., & Miles, J. (2009). Evaluation of alternative procedures for setting curve advisory speed. Transportation research record, 2122(1), 9-16.

47. Carlson, P. J., Burris, M., Black, K., & Rose, E. R. (2005). Comparison of radius-estimating techniques for horizontal curves. Transportation research record, 1918(1), 76-83.

48. Carlson, P. J., & Mason Jr, J. M. (1999). Relationships between ball bank indicator readings, lateral acceleration rates, and vehicular body-roll rates. Transportation research record, 1658(1), 34-42.

49. Lusetti, B., Nouveliere, L., Glaser, S., & Mammar, S. (2008, June). Experimental strategy for a system-based curve warning system for a safe governed speed of a vehicle. In 2008 IEEE Intelligent Vehicles Symposium (pp. 660-665). IEEE.

50. Glaser, S., Nouveliere, L., & Lusetti, B. (2007, June). Speed limitation based on an advanced curve warning system. In 2007 IEEE Intelligent Vehicles Symposium (pp. 686-691). IEEE.

51. Wang, Q., Yang, B., Tan, G., Xiong, S., & Zhou, X. (2017). Safe Travelling Speed of Commercial Vehicles on Curves Based on Vehicle-Road Collaboration (No. 2017-01-0080). SAE Technical Paper.

52. Donnell, E. T., Kersavage, K., & Tierney, L. F (2018). Self-Enforcing Roadways: A Guidance report (No. FHWA-HRT-17-098). United States. Federal Highway Administration.

53. Harbluk, J. L., Noy, Y. I., Trbovich, P. L., & Eizenman, M. (2007). An on-road assessment of cognitive distraction: Impacts on drivers' visual behavior and braking performance. Accident Analysis & Prevention, 39(2), 372-379.

54. Holweg, M. (2008). The evolution of competition in the automotive industry. In *Build to order* (pp. 13-34). Springer, London.

55. Luckow, A., Cook, M., Ashcraft, N., Weill, E., Djerekarov, E. and Vorster, B., 2016, December. Deep learning in the automotive industry: Applications and tools. In *2016 IEEE International Conference on Big Data (Big Data)* (pp. 3759-3768). IEEE.

56. Malikopoulos, A.A., Papalambros, P.Y. and Assanis, D.N., 2010. Online identification and stochastic control for autonomous internal combustion engines. *Journal of dynamic systems, measurement, and control*, *132*(2).

57. Malikopoulos, A.A., Assanis, D.N. and Papalambros, P.Y., 2009. Real-time self-learning optimization of diesel engine calibration. *Journal of engineering for gas turbines and power*, *131*(2).

58. Farrington, R., & Rugh, J. (2000). *Impact of vehicle air-conditioning on fuel economy, tailpipe emissions, and electric vehicle range* (No. NREL/CP-540-28960). National Renewable Energy Lab., Golden, CO (US).

59. Malikopoulos, A.A., Papalambros, P.Y. and Assanis, D.N., 2007, January. A learning algorithm for optimal internal combustion engine calibration in real time. In *International Design Engineering Technical Conferences and Computers and Information in Engineering Conference* (Vol. 48078, pp. 91-100).

60. Shayler, P.J., Goodman, M. and Ma, T., 2000. The exploitation of neural networks in automotive engine management systems. *Engineering Applications of Artificial Intelligence*, *13*(2), pp.147-157.

61. Turkson, R.°F, Yan, °F, Ali, M.K.A. and Hu, J., 2016. Artificial neural network applications in the calibration of spark-ignition engines: An overview. *Engineering science and technology, an international journal*, *19*(3), pp.1346-1359.

62. Parlak, A., Islamoglu, Y., Yasar, H. and Egrisogut, A., 2006. Application of artificial neural network to predict specific fuel consumption and exhaust temperature for a diesel engine. *Applied Thermal Engineering*, *26*(8-9), pp.824-828.

63. Togun, N.K. and Baysec, S., 2010. Prediction of torque and specific fuel consumption of a gasoline engine by using artificial neural networks. *Applied Energy*, *87*(1), pp.349-355.

64. Rahimi-Ajdadi, F and Abbaspour-Gilandeh, Y., 2011. Artificial neural network and stepwise multiple range regression methods for prediction of tractor fuel consumption. *Measurement*, *44*(10), pp.2104-2111.

65. Wu, J.D. and Liu, J.C., 2012. A forecasting system for car fuel consumption using a radial basis function neural network. *Expert Systems with Applications*, *39*(2), pp.1883-1888.

66. Liu, D., Chen, H., Gao, J., Zhao, J. and Hu, Y., 2020. Predictive coordinated control of fuel consumption and emissions for diesel engine vehicles under intelligent network environments. *Science China Information Sciences*, *64*(9), pp.1-3.

67. Song, K., Li, F, Hu, X., He, L., Niu, W., Lu, S. and Zhang, T., 2018. Multi-mode energy management strategy for fuel cell electric vehicles based on driving pattern identification using learning vector quantization neural network algorithm. *Journal of Power Sources*, *389*, pp.230-239.

68. Zeng, W., Khalid, M.A., Han, X. and Tjong, J., 2020. A Study on Extreme Learning Machine for Gasoline Engine Torque Prediction. *IEEE Access*, *8*, pp.104762-104774.

69. Tasdemir, S., Saritas, I., Ciniviz, M. and Allahverdi, N., 2011. Artificial neural network and fuzzy expert system comparison for prediction of performance and emission parameters on a gasoline engine. *Expert Systems with Applications*, *38*(11), pp.13912-13923.

70. Cirak, B. and Demirtas, S., 2014. An application of artificial neural network for predicting engine torque in a biodiesel engine. *American Journal of Energy Research*, *2*(4), pp.74-80.

71. Cay, Y., 2013. Prediction of a gasoline engine performance with artificial neural network. *Fuel*, *111*, pp.324-331.

72. Harris, H.D., 1992. Prediction of the torque and optimum operating point of diesel engines using engine speed and fuel consumption. *Journal of agricultural engineering research*, *53*, pp.93-101.

73. Sekmen, Y., Gölcü, M., Erduranlı, P. and Pancar, Y., 2006. Prediction of performance and smoke emission using artificial neural network in a diesel engine. *Mathematical and Computational Applications*, *11*(3), pp.205-214.

74. Vong, C.M., Wong, P.K. and Li, Y.P., 2006. Prediction of automotive engine power and torque using least squares support vector machines and Bayesian inference. *Engineering Applications of Artificial Intelligence*, *19*(3), pp.277-287.

75. Khayyam, H., Kouzani, A. Z., Hu, E. J., & Nahavandi, S. (2011). Coordinated energy management of vehicle air conditioning system. *Applied thermal engineering*, *31*(5), 750-764.

76. Johnson, V. H. (2002). *Fuel used for vehicle air conditioning: a state-by-state thermal comfort-based approach* (No. 2002-01-1957). SAE Technical Paper.

77. Lee, J., Kim, J., Park, J., & Bae, C. (2013). Effect of the air-conditioning system on the fuel economy in a gasoline engine vehicle. *Proceedings of the Institution of Mechanical Engineers, Part D: Journal of Automobile Engineering*, *227*(1), 66-77.

78. Lee, J., Kim, J., Park, J., & Bae, C. (2013). Effect of the air-conditioning system on the fuel economy in a gasoline engine vehicle. *Proceedings of the Institution of Mechanical Engineers, Part D: Journal of Automobile Engineering*, *227*(1), 66-77.

79. Khayyam, H. (2013). Adaptive intelligent control of vehicle air conditioning system. *Applied Thermal Engineering*, *51*(1-2), 1154-1161.

80. Nasution, H. (2008). Development of fuzzy logic control for vehicle air conditioning system. *Telkomnika*, *6*(2), 73.

81. Khayyam, H., Abawajy, J., & Jazar, R. N. (2012). Intelligent energy management control of vehicle air conditioning system coupled with engine. *Applied thermal engineering*, *48*, 211-224.

82. Khayyam, H., Kouzani, A. Z., & Hu, E. J. (2009, June). Reducing energy consumption of vehicle air conditioning system by an energy management system. In *2009 IEEE intelligent vehicles symposium* (pp. 752-757). IEEE.

83. Huang, K. D., Tzeng, S. C., Jeng, T. M., & Chiang, W. D. (2006). Air-conditioning system of an intelligent vehicle-cabin. *Applied Energy*, *83*(6), 545-557.

84. Fayazbakhsh, M. A., & Bahrami, M. (2013). Comprehensive modeling of vehicle air conditioning loads using heat balance method. *SAE technical paper*, *2013*, 1507.

85. Cvok, I., Ratkovic, I., & Deur, J. (2020). *Optimization of control parameters of vehicle air-conditioning system for maximum efficiency* (No. 2020-01-1242). SAE Technical Paper.

86. Diaconescu, E., 2008. The use of NARX neural networks to predict chaotic time series. *WSEAS Transactions on Computer Research*, *3*(3), pp.182-191.

87. Siami-Namini, S., Tavakoli, N. and Namin, A.S., 2018, December. A comparison of ARIMA and LSTM in forecasting time series. In *2018 17th IEEE International Conference on Machine Learning and Applications (ICMLA)* (pp. 1394-1401). IEEE.

88. Stanton, N.A. and Young, M.S., 2005. Driver behavior with adaptive cruise control. *Ergonomics*, *48*(10), pp.1294-1313.

89. Hoedemaeker, M. and Brookhuis, K.A., 1998. Behavioural adaptation to driving with an adaptive cruise control (ACC). *Transportation Research Part F: Traffic Psychology and Behaviour*, *1*(2), pp.95-106.

90. Kesting, A., Treiber, M., Schönhof, M. and Helbing, D., 2007. Extending adaptive cruise control to adaptive driving strategies. *Transportation Research Record*, *2000*(1), pp.16-24.

91. Rudin-Brown, C.M. and Parker, H.A., 2004. Behavioural adaptation to adaptive cruise control (ACC): implications for preventive strategies. *Transportation Research Part F: Traffic Psychology and Behaviour*, *7*(2), pp.59-76.

92. Moon, S. and Yi, K., 2008. Human driving data-based design of a vehicle adaptive cruise control algorithm. *Vehicle System Dynamics*, *46*(8), pp.661-690.

93. Rosenfeld, A., Bareket, Z., Goldman, C.V., LeBlanc, D.J. and Tsimhoni, O., 2015. Learning drivers' behavior to improve adaptive cruise control. *Journal of Intelligent Transportation Systems*, *19*(1), pp.18-31.

94. Milanés, V., Shladover, S.E., Spring, J., Nowakowski, C., Kawazoe, H. and Nakamura, M., 2013. Cooperative adaptive cruise control in real traffic situations. *IEEE Transactions on intelligent transportation systems*, *15*(1), pp.296-305.

95. Kesting, A., Treiber, M., Schönhof, M. and Helbing, D., 2008. Adaptive cruise control design for active congestion avoidance. *Transportation Research Part C: Emerging Technologies*, *16*(6), pp.668-683.

96. Milanés, V. and Shladover, S.E., 2014. Modeling cooperative and autonomous adaptive cruise control dynamic responses using experimental data. *Transportation Research Part C: Emerging Technologies*, *48*, pp.285-300.

97. Ploeg, J., Serrarens, A.°F and Heijenk, G.J., 2011. Connect & Drive: design and evaluation of cooperative adaptive cruise control for congestion reduction. *Journal of Modern Transportation*, *19*(3), pp.207-213.

98. Kesting, A., Treiber, M., Schönhof, M., Kranke, °F and Helbing, D., 2007. Jam-avoiding adaptive cruise control (ACC) and its impact on traffic dynamics. In *Traffic and Granular Flow'05* (pp. 633-643). Springer, Berlin, Heidelberg.

99. Li, S.E., Guo, Q., Xu, S., Duan, J., Li, S., Li, C. and Su, K., 2017. Performance enhanced predictive control for adaptive cruise control system considering road elevation information. *IEEE Transactions on Intelligent Vehicles*, *2*(3), pp.150-160.

100. Lu, C., Dong, J. and Hu, L., 2019. Energy-efficient adaptive cruise control for electric connected and autonomous vehicles. *IEEE Intelligent Transportation Systems Magazine*, *11*(3), pp.42-55.

101. Vedam, N., 2015. *Terrain-Adaptive Cruise Control: A Human-Like Approach* (Doctoral dissertation).

102. Kolmanovsky, I.V. and Filev, D.P., 2010. Terrain and traffic optimized vehicle speed control. *IFAC Proceedings Volumes*, *43*(7), pp.378-383.

103. Gáspár, P. and Németh, B., 2014. Design of adaptive cruise control for road vehicles using topographic and traffic information. *IFAC Proceedings Volumes*, *47*(3), pp.4184-4189.

104. Németh, B. and Gáspár, P., 2011. Road inclinations in the design of LPV-based adaptive cruise control⋆. *IFAC Proceedings Volumes*, *44*(1), pp.2202-2207.

105. Ma, J., Hu, J., Leslie, E., Zhou, °F, Huang, P. and Bared, J., 2019. An eco-drive experiment on rolling terrains for fuel consumption optimization with connected automated vehicles. *Transportation Research Part C: Emerging Technologies*, *100*, pp.125-141.

106. Németh, B. and Gáspár, P., 2013. Design of vehicle cruise control using road inclinations. *International Journal of Vehicle Autonomous Systems*, *11*(4), pp.313-333.

107. Kolachalama, S., & Malik, H. (2022). Intelligent vehicle drive mode which predicts the driver behavior vector to augment the engine performance in real-time. *Data-Centric Engineering, 3*, E14.

108. Kolachalama, S., Surti. I, & Malik, H. (2022). Interpretation of Electric Vehicle Operating Point based on the Dynamic State of the Vehicle. *Experimental Results,* (Accepted).